Photonic crystal fibers -
from theory to practice

Libori, Stig E. Barkou

Publication date:
2002

Document Version
Publisher's PDF, also known as Version of record

Photonic Crystal Fibers - From Theory to Practice

Ph.D. Thesis

Stig E. Barkou Libori

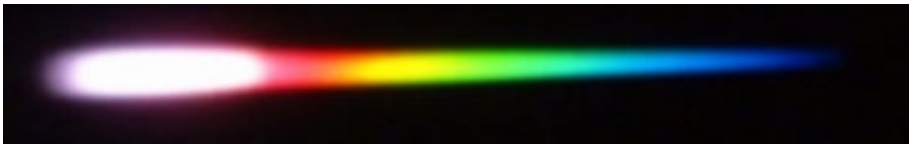

Picture on cover page: The spectrum of a white-light fiber generator, seen through a prism. Experiment performed by Erling Riis, Strathclyde University, Glasgow. The fiber was drawn by Crystal Fibre A/S. Courtesy NKT Research A/S.

Photonic Crystal Fibers - From Theory to Practice

Ph.D thesis Thesis
of
Stig E. Barkou Libori

February 28th, 2002
Research Center COM
Technical University of Denmark
Lyngby, Denmark

The work presented in this thesis was carried out at the Research Center COM (Communications, Optics, and Materials) in partial fulfillment of the requirements for the Ph.D.- degree from the technical University of Denmark.

Supervisor: Professor, Dr. Techn. Anders Bjarklev

Abstract

During this Ph.D. work, attention has been focused on understanding and analyzing the modal behavior of micro-structured fibers. Micro-structured fibers are fibers with a complex dielectric topology, and offer a number of novel possibilities, compared to standard silica based optical fibers.

The thesis focuses on understanding the basic mechanisms controlling the modal properties of micro-structured fibers. One important sub-class of micro-structured fibers are fibers that guide light by index effects similar to those index effects that ensure guidance of light in standard optical fibers. Such micro-structured fibers are the ones most often treated in literature concerning micro-structured fibers. These micro-structured fibers offer a whole range of novel wave guiding characteristics, including the possibility of fibers that guide only one mode irrespective of the frequency of light, and nonlinear fibers with zero dispersion wavelength well below 1300 nm. This thesis describes the functionalities of these fibers, and further point to novel application areas, such as new efficient fiber amplifiers and fibers with new possibilities within dispersion management. When pointing toward novel possibilities, the thesis will attempt to offer a proof of concept, rather than an in-depth analysis, thus reflecting the present state of the art within the area of micro-structured fibers.

Another important sub-class of micro-structured fibers is photonic bandgap fibers. Photonic bandgap fibers are far more complicated to manufacture, compared to micro-structured fibers that guide light by simple index effects, because of stringent requirements concerning the periodicity of the cladding structure of the fibers. The theoretical investigation of these fibers is also more complex, than the investigation of micro-structured fibers that guide light by simple index effects. However, photonic bandgap fibers offer more radical possibilities, such as core regions with an effective index that is lower than the surrounding effective cladding index- one may guide light in air- and dispersion qualities that differ from both those of index guiding micro-structured fibers as well as from the dispersion properties of standard optical fibers.

Sammenfatning

Igennem dette Ph.D arbejde har opmærksomheden været fokuseret på at forstå og analysere de modale sammenhænge i mikrostrukturerede fibre. Mikrostrukturerede fibre er fibre med en kompleks dielektrisk topologi, og tilbyder et antal nye muligheder, sammenlignet med almindelige step index fibre.

Rapporten fokuserer på at forstå de basale mekanismer, som kontrollerer mikrostrukturerede fibres modale egenskaber. En vigtig undergruppe af mikrostrukturerede fibre er fibre, som leder lys via index effekter meget lig de index effekter, der sikrer bølgeledning af lys i almindelige optiske fibre. Sådanne mikrostrukturerede fibre er de, som oftest bliver beskrevet i litteratur angående mikrostrukturerede fibre. Sådanne mikrostrukturerede fibre tilbyder en lang række nye bølgeledende karakteristika, inklusive muligheden for fibre, som kun understøtter en bunden tilstand (mode) uanset lysets bølgelængde, samt ulineære fibre med nul dispersion ved en lysbølgelængde et godt stykke under 1300 nm. Denne afhandling beskriver egenskaberne ved sådanne fibre og peger endvidere imod nye anvendelses områder indenfor området dispersions kontrol. Når der i afhandlingen peges på nye muligheder vil det tilstræbes at tilbyde en beskrivelse af muligheden, snarere end en dybdegående analyse, således at det nuværende stade indenfor området mikrostrukturerede fibre herved reflekteres.

En anden vigtig undergruppe af mikrostrukturerede fibre er fotoniske båndgabs fibre. Fotoniske båndgabs fibre er langt mere komplicerede at fremstille end mikrostrukturerede fibre, der leder lys ved simple index effekter, grundet kravet om en stringent periodisk kappe struktur i disse fibre. Den teoretiske undersøgelse af disse fibre er også mere kompliceret end undersøgelserne af mikrostrukturerede fibre, der leder lys ved simple index effekter. Imidlertid tilbyder fotoniske båndgabs fibre mere radikale muligheder, såsom kerneområder med et effektivt index som er lavere end det omgivende effective kappe index- man kan lede lys i luft- og dispersions egenskaber som afviger både fra det man finder i index bølgeledende mikrostrukturede fibre såvel som fra dispersions egenskaberne i standard optiske fibre.

Acknowledgements

Although the present author takes full responsibility of the work presented in this thesis, there are some people whom the author would like to express special gratitude towards. First and foremost prof. Anders Bjarklev, without whom this work would not have been possible. Over the years, I have come to increasingly respect your ability to recognize the potential of people, rather than just look at their present level of accomplishments. Also, your ability to inspire people in your group to reach their potential has been important to the way I have felt about working in the group (I have felt good).

I would also like to express my appreciation to Jes Broeng, who has always been an inspiration due to his great excitement and enthusiasm concerning the topic of photonic crystal fibers.

Part of the work in the group has been participating in the work with students. I have met a large number of students, who have been an inspiration with their excitement and curiosity concerning micro-structured fibers.

Finally, I would like to express gratitude to the people who have taken part in the caring of my children while I have been doing my PH.D. work. It is reassuring to know, that the children are taken care of, when e.g. traveling abroad. Special gratitude is directed toward my former wife and Marianne Bruhn and Magali Grant as well as toward my childrens grand parents. It is nice to live in a time and age, where it is possible for a single parent to do scientific research.

Publications

Journal papers

S.E.Barkou, J.Broeng and A.Bjarklev 'Silica-air photonic crystal fiber design that permits waveguiding by a true photonic bandgap effect', Optics Letters, Vol.24, No.1, pp.46-48, january 1999

S.E.Barkou, J.Broeng and A.Bjarklev 'Guidance of light along an air column in a new class of optical fibers', DOPSNYT, 14. 1-1999,pp.16-21, 1999

J.Broeng, S.E.Barkou, A.Bjarklev, J.Knight, T.Birks and P.St.J.Russell 'Highly Increased Photonic Band Gaps in Silica/Air Structures' Optics Communications, Vol.156, pp240-44, 1998

T.Søndergaard, J.Broeng, A.Bjarklev, K.Dridi and S.E.Barkou 'Suppression of spontaneus emission for a two-dimensional honeycomb photonic band gap structure estimated using a new effective-index model', IEEE Journal of 'Quantum Electronics, Vol.34, No.12,pp2308-13, Dec. 1998

J.Broeng, D.Mogilevstev, S.E.Barkou and A.Bjarklev 'Photonic Crystal Fibres: A New Class of optical Waveguides', Optical Fiber Technology (Invited Paper), Vol.5, pp.305-30, 1999

J.Broeng, T.Søndergaard, S.E.Barkou, P.M.Barbeito and A.Bjarklev 'Waveguidance by the photonic bandgap effect in optical fibers', J.Opt.A: Pure Appl. Opt., Vol.1, pp.477-82, 1999

J.B.Nielsen, T.Søndergaard, S.E.Barkou, A.Bjarklev, J.Broeng and M.B.Nielsen 'Two-dimensional Kagomé Structure, Fundamental Hexagonal Photonic Crystal Configuration', IEEE Electronics Letters, Vol.35, No.20, pp.1736-37, September 1999

J.Broeng, S.E.Barkou, T.Søndergaard and A.Bjarklev 'Analysis of air-guiding photonic bandgap fibers', Optics Letters, Vol.25, No.2, pp.96-98, Jan. 15, 2000

T.W.Berg, A.Bjarklev, J.Broeng, S.E.Barkou Libori, E.Knudsen, T.Søndergaard and M.G.Dyndgaard 'Polarization properties of honeycomb-structured photonic bandgap fibres', J.Opt.A: Pure Appl. Opt., Vol.2, pp.584-99, 2000

J.B.Nielsen, T.Søndergaard, S.E.Barkou, A.Bjarklev and J.Broeng 'Two-dimensional Kagomé Photonic Bandgap Waveguide', IEEE photonics Technology Letters, Vol.12, No.6, pp.630-32, June 2000

A. Bjarklev, J.Broeng and S.E.Barkou 'New developments in photonic crystal fibres' Northern Optics 2000, Uppsala, Sweden, 6-8 june, 2000, invited paper IN1, p.31, and DOPSNYT 2-2000, p.7, 2000

J.Broeng, S.E.Barkou, A.Bjarklev, T.Søndergaard and E.Knudsen 'Crystal Fibre Technology', DOPSNYT, 2-2000, pp.22-28, 2000

T.P.Hansen, J.Broeng, S.E.Barkou Libori, E.Knudsen, A.Bjarklev, J.Riis Jensen and H.Simonsen 'Highly birefringent index-guiding photonic crystal fibers', IEEE Photonics Technology Letters, Vol.13, No.6, pp.588-90, 2001

K.P.Hansen, M.Dybendal Nielsen, T.P.Hansen, T.Sørensen, J.Broeng, S.Barkou Libori, H.Simonsen, J.Riis Jensen and A.Bjarklev 'Novel design properties of photonic crystal fibres', DOPSNYT 2-2001, pp16-21, 2001

T. Sørensen, J. Broeng, A. Bjarklev, E. Knudsen and S.E. Barkou libori 'Macro-bending loss properties of photonic crystal fibre', IEEE Electronics Letters, Vol.37, No.5, pp.287-89, 2001

Conference papers:

S.E.Barkou, J.Broeng and A.Bjarklev 'Dispersion properties of photonic bandgap guiding fibers', Optical Fiber Communication Conference OFC'99, San Diego, Ca, USA, paper FG5, pp.117-9, Feb.21-26, 1999

S.Barkou, J.Broeng and A.Bjarklev 'Photonic Bandgap Fibers', LEOS'99, San Francisco, CA, USA, paper WAA1, pp.615-16, Nov.8-11, 1999, Invited

S.E.Barkou, J.Broeng and A.Bjarklev 'Leakage-free, guidance of light in hollow core optical fibers', CLEO'2000, San Francisco, CA, USA, paper CWK40, pp.319-21, May 7-12, 2000

S.E.Barkou, J.Broeng and A.Bjarklev 'Modal control in photonic crystal fibres' Northern Optics 2000, Uppsala, Sweden, Poster PO14, p.82, 6-8 june, 2000

S.E.Barkou Libori, J.Broeng, E.Knudsen, A.Bjarklev and H.R.Simonsen 'High-birefringent photonic crystal fiber', Optical fiber Communications, paper no. TuM2-1, Anaheim, CA, USA, 2001

S.E.Barkou Libori and A.Bjarklev 'Photonic Crystal Fibres - Theory and Practice' To be presented at LEOS Benelux 'Photonic Crystal Workshop', Het Pand, Ghent, Belgium, 29 may, 2002, Invited

J.Broeng, S.E.Barkou and A.Bjarklev 'Waveguiding by the Photonic Band Gap Effect', 19th Topical Meeting of the EOS, Marseilles, France, Sept. 1998

A.Bjarklev, J.Broeng, K.Dridi and S.E.Barkou 'Dispersion properties of Photonic Crystal Fibres', 24th European Conference on Optical Communication, ECOC'98, Madrid, Spain, Vol.1, pp135-6, Sept.20-24, 1998

A.Bjarklev, J.Broeng, S.Barkou and T.Søndergaard 'Fundamentally new microstructured fiber waveguides for potential sensor applications', Light For Life 99, Cancun Q.R., Mexico, paper W4.4, July 27-30, 1999

J.Broeng, S.Barkou, T.Søndergaard and A.Bjarklev 'Dispersion properties of photonic bandgap fibres', COST 268 meeting in Stockholm, March 15-17, 1999

A.Bjarklev, J.Broeng and S.E.Barkou 'Modelling of photonic crystal fibres', European Conference on Optical Communication ECOC'99, Nice, France, pp.16-19, Sept.26-30, 1999, Invited

A.Bjarklev, J.Broeng and S.Barkou 'Novel electromagnetic waveguides using photonic crystals' PIERS 2000, Cambridge, MA, USA, pp.182, July 2000

E.Knudsen, A.Bjarklev, J.Broeng and S.E.Barkou 'Waveguiding properties of photonic crystal fibres' Photonic Crystals and Light Localization, NATO Advanced Study Institute, Crete, Greece, June 19-30, 2000

E.Knudsen, A.Bjarklev, J.Broeng and S.E.Barkou 'Macro-bending loss estimation for air-guiding photonic crystal fibres', OFS'2000, vol.4185, pp.904-7, 2000

A.Bjarklev, J.Broeng and S.E.Barkou 'Photonic Bandgap Fibers: Theory and Experiments', IEEE Lasers and Electro-Optics Society 2000 Annual meeting, vol. 1, pp, 336-7, Puerto Rico

J.Broeng, S.E.Barkou, A.Bjarklev, T.Søndergaard and E.Knudsen 'Crystal Fiber Technology', Optical Society of America Annual Meeting, paper TUC3, p.69, Rhode island, USA, 2000

A.Bjarklev, J.Broeng, S.E.Barkou Libori, E.Knudsen and H.R.Simonsen 'Photonic crystal fiber modelling and applications', Invited paper for optical Fiber Communications Conference, paper no. TuC1-1, Anaheim, CA, USA, 2001

J.Broeng, D.Mogilevtsev, S.E.Barkou Libori and A.Bjarklev 'Polarization-preserving holey fibers', Conference on Lasers and Electro-Optics - Pacific rim, paper no. Ma1-3, Tokyo, Japan, July 2001

J.Broeng, T.P.Hansen, S.E.Barkou libori, E.Knudsen, A.Bjarklev and J.R.Jensen 'Birefringence in photonic crystal fibers', OECC/IOOC'2001, paper no. TuG-3, Sydney, Australia, july 1-5, 2001

J.Riishede, S.E.Barkou Libori, A.Bjarklev, J.Broeng and E.Knudsen 'Photonic crystal fibres and effective index approaches', European Conference on Optical Communications, ECOC'2001, paper no. Th.A.1.5, 2001

A.Bjarklev, T.P.Hansen, K.Hougaard, S.E.Barkou Libori, E.Knudsen and J.Broeng 'Microbending in photonic crustal fibres - An ultimate loss limit?', European Conference on Optical Communications, ECOC'2001, paper no.We.L.2.4, 2001

T.Sørensen, J.Broeng, A.Bjarklev, E.Knudsen, S.E.Barkou Libori, H.Simonsen and J.R.Jensen 'Macrobending loss properties of photonic crystal fibres with different air filling fractions', European Conference on optical Communication, ECOC'2001, paper no. We.P.1, 2001

Patents:

S.E.Barkou, A.Bjarklev and J.Broeng 'Optical fibers used in optical communications, sensor technology, spectroscopy and medicine', Patent no. WO9964903, Published 2000

S.E.Barkou, A.Bjarklev and J.Broeng 'Photonic band gap fiber for communication purposes and for fiber laser or fiber amplifier applications', Patent no. WO9964904, Published 2000

S.E.Barkou, A.Bjarklev and J.Broeng 'Micro-structured optical fiber, such as polarization maintaining fiber for optical communication, has a cladding region comprising primary elongated elements having non-circular cross-section', Patent no. WO200060390, Published 2001

Contents

Chapter 1

Introduction

For decades most optical fibers have relied on the physical effect termed total internal reflection for the guidance of light. Total internal reflection allows light to be guided along a dielectric core region of an optical fiber, provided the optical core is surrounded by a dielectric cladding with a lower refractive index than the refractive index of the core. Low-loss optical fibers guiding light by total internal reflection, is the backbone of the information society, due to the vast amounts of information that may be distributed through networks of optical fibers. Optical fibers today find extensive use within areas such as telecommunications, medicine, sensor technology and spectroscopy [1, 2, 3, 4, 5].

Since 1987 [6, 7] extensive research has revealed that compound dielectric materials, deliberately created with a structural size on the same order of magnitude as the wavelength of light, give the possibility of a new phenomenon termed photonic bandgaps. Photonic bandgaps may be seen as an optical analogue to the electronic bandgaps of semiconductors, and may lead to a whole new series of optical products in the future since they allow light to be localized and guided within cavities and waveguides [8, 9, 10, 11, 12, 13]. Particularly interesting to the field of optical fibers, is the possibility of guiding light along core regions with a low refractive index (such as hollow air cores), [14, 15, 16, 17, 18, 19, 20, 21].

Photonic bandgaps were discovered independently by Yablonovich and John [6, 7], when they were studying spontaneous emission control and localization of light in novel periodic materials. These novel periodic dielectric structures were termed photonic crystals to emphasize their periodic nature, and termed photonic bandgap materials to describe the purpose build periodic dielectric materials exhibiting frequency intervals where no extended

field solutions existed. Light incident on a photonic bandgap material with a frequency within the photonic bandgap would be reflected away from the material, since it would not be allowed to propagate through the material. Originally this led to the notion that one should be able to inhibit spontaneous emission, since radiative relaxation of an exited atom, or a recombination of an electron-hole pair would be physically impossible if the energy released or absorbed by the transition was within the photon energy level of a photonic bandgap. This has generated quite a large interest in photonic crystals and photonic bandgap technology, due to the apparent resemblance with the control of electrons made possible by the electronic bandgaps of semi conductors [10, 11, 22, 23, 24, 25, 26, 27, 28, 29].

The complete inhibition of particular photon energy levels depend on a full three-dimensional photonic bandgap. Such dielectric materials do not exist in nature, most likely because they require a large contrast between the dielectrics involved, however, one-dimensional photonic bandgaps are often seen as the metallic colors on insects and butterfly wings we so admire. Such metallic colors in nature change their color as one turns ones head, since the color of the photonic bandgaps depend on the viewing angle. In this sense they closely resemble the one-dimensional mirrors often used in e.g. lasers today. Correspondingly, the demand that a photonic bandgap should be a complete three-dimensional bandgap, prohibiting photon transmission ferom any angle has been relaxed. Rather one speak of one-dimensional bandgaps (such as Bragg-stacks or dielectric mirrors), two-dimensional bandgaps [15, 16, 17, 18, 19, 21, 30, 31, 32, 33, 34] or full three-dimensional bandgaps [10, 29, 35, 36, 37, 38, 39, 40].

A one-dimensional mirror displays one-dimensional photonic bandgaps as soon as a dielectric contrast exist between the different dielectric layers [10]. On the other hand a significant dielectric contrast is needed for the formation of a two-dimensional bandgap [10]. Even higher dielectric contrast is needed to ensure a three-dimensional photonic bandgap [10]. Combined with a significantly increased complexity when manufacturing higher order photonic bandgap materials it is understandable, why only the one-dimensional dielectric mirror had been exploited before 1987.

Photonic crystal fibers guiding light by the photonic bandgap effect have a two-dimensional periodic dielectric structure in the cross-section of the fiber. The dielectric structure is, however, invariant in the longitudinal direction of the fiber. Compared to planar structures based on two-dimensional photonic bandgap materials this offers the advantage of providing a structure of infinite height. Furthermore, photonic crystal fibers are not produced directly with a structural size near the wavelength of light to be guided by

the fiber, rather the fiber is stacked from circular silica tubes and rods, and then drawn to the final size in a manner comparable to the drawing of standard step index fibers [18, 41, 42]. It is, therefore, not surprising that the first experimental verification of the photonic bandgap effect at optical wavelengths was made with a photonic bandgap fiber [20].

Photonic bandgap fibers have one further advantage compared to planar two-dimensional photonic crystals. Since light is to be guided along the fiber, rather than being reflected from normal incidence, the demands on the dielectric contrast are less stringent. It is relatively simple to design silica-air structures that will provide a two-dimensional photonic bandgap, while the index contrast between silica and air is insufficient to ensure a two-dimensional photonic bandgap for use in planar structures. Also, the demands on the structural size are more readily accomplished, since the structural size can be made larger for optical fibers than for planar structures.

The field of photonic crystal fibers was founded by Russell and co-workers [17, 41]. [17] shoved that it was theoretically possible to design silica-air based photonic bandgap structures for use in photonic bandgap fibers. [41] was the realization of a micro-structured fiber that guided light. This fiber did, however, not guide light by the photonic bandgap effect. This led to the realization that micro-structured fibers could also be designed to guide light by utilizing an effect very similar to total internal reflection. Such fibers did not merely represent a novel way of producing fibers with a performance similar to traditional step index fibers, since it was realized that these fibers offered a whole new range of opportunities, including the possibility of fibers that would only support a single mode irrespective of the wavelength of light [15, 42] and fibers with powerful nonlinear functionalities [43, 44, 45]. The main part of this thesis is devoted to investigating the possibilities of micro-structured fibers that do not rely on the photonic bandgap effect to guide light. Fibers guiding light by the photonic bandgap effect are significantly more difficult to manufacture. This is because such a photonic bandgap fiber must have a near perfect periodic geometry in the cross-section for photonic bandgaps to appear, whereas micro-structured fibers guiding light by an effect similar to total internal reflection do not need very accurate periodicity to function [46]. This is reflected in the literature concerning micro-structured fibers, since far more papers have been published on the functionalities of photonic crystal fibers that do not exhibit photonic bandgaps.

The author of this thesis has worked with the theoretical investigation of photonic crystal fibers since 1996. An important milestone was reached

in the year 2000 when the the present author was a co-founder of the company Crystal Fibre A/S. Crystal Fibre A/S is devoted to the development and manufacturing of photonic crystal fibers and currently produce and sell numerous types of microstructured fibers. None of the current products available from Crystal Fibre A/S are based on the photonic bandgap effect, thus reflecting the current emphasis on fibers that guide light by index effects in a solid core region.

The remainder of this thesis is organized as follows:

Chapter 2 describes the physical plane wave model that is the basis of the calculations presented in this thesis. The development of a full-vectorial model, capable of analyzing dielectric structures with high complexity was an important step to the investigation of photonic crystal fibers. Although the present author did not develop the model described here, he was one of two people that analyzed photonic bandgap fibers using a full-vectorial model [16, 47]. The basis of this model was developed during the authors Master Thesis. The chapter also describes the method used to investigate photonic crystal fibers, and offers insight to the modal behavior of microstructured fibers.

Chapter 3 investigates basic properties of periodic dielectric structures. It is described how one can introduce an effective index to a photonic crystal intended as a cladding structure of a photonic crystal fiber. The chapter also introduces structures with photonic bandgaps.

In chapter 4, fibers with an effective step index analogy are investigated. The special cut-off properties and the qualitative behavior of the macrobending losses are investigated. It is shown that the fibers may be used for nonlinear processes, such as e.g. white light generation, as well as for non linear purposes. The possibility of designing fibers with a mode field cross section that is almost invariant as a function of the wavelength is shown for the first time.

Chapter 5 discusses photonic bandgap fibers. The honeycomb photonic bandgap honeycomb fiber designs are shown to be able to exhibit strong positive group velocity dispersion. It is shown that this is related to the special behavior of the fraction of the energy of the guided mode that is propagating in air.

In chapter 6, microstructured fibers suitable for group velocity dispersion compensation are discussed. The presentation will emphasize the principles underlying photonic crystal fibers designed for dispersion compensating purposes, as well as introduce numerical examples of such structures.

In chapter 7, a summary is given along with some of the concluding remarks to this thesis.

Chapter 2

Modelling Photonic Crystal Fibers

Micro-structured fibers are fibers with a rich topology in the refractive index of the cladding structure [48]. Typically, a micro-structured fiber consist of a large number of air-holes embedded within a silica background host material, while the core-region is topologically more simple [41, 49]. Still, the computational demands for calculating the characteristics of a micro-structured fiber accurately, are far greater than the corresponding demands when calculating the characteristics of standard step index fibers, because of the dielectric complexity of micro-structured fibers. One type of micro-structured fibers is Photonic Bandgap fibers, that guide light by an effect that may be seen as an optical analogue to the electronic bandgaps of semi conductors [17, 47]. It is particularly demanding to make calculations on such Photonic Bandgap fibers, since the guided modes are not represented by the lowest eigenvalue solutions to the eigenvalue problem [19].

Many methods have been suggested for calculating aspects of micro-structured fibers, including a Transfer Matrix method [17], a Step Index Fiber analogy [50, 51] where the micro-structured fiber is treated as a step index fiber with a strongly wavelength dependent refractive index of the cladding, a localized function method where the electromagnetic field is expanded in localized basis functions such as Hermite-Gaussian functions [46, 52], the plane wave method [47] that will be treated in this chapter and a Finite Element method [53]. One possible method, that have not been addressed in the literature, for investigating micro-structured fibers, is the Finite Difference Time domain methods, particularly with periodic boundary conditions.

The present chapter describes the plane-wave method used for the calculations within this thesis. The chapter does not claim, however, that this is the best method for analyzing micro-structured fibers theoretically. Each of the above mentioned methods for investigating micro-structured fibers has specific advantages when analyzing micro-structured fibers. Some specific reasons that the plane wave method is preferred in this thesis may be listed as: 1) Unlike the Transfer Matrix method, the Finite Difference Time Domain method or the finite Element Method the plane wave method is a modal method, implying that the modal nature of the solutions to Maxwell's equations is given directly. 2) No particular knowledge about the solution is required, whereas a characteristic width and center of each basis function must be chosen with the localized function approach. 3) Unlike the step index fiber analogy it is a fully vectorial method that is applied directly to the fiber design in question. Further a step index fiber analogy cannot be used to solve problems involving fibers that guide light by the Photonic Bandgap effect. 4) An optimized method (the Fast Fourier Transform) exist for calculating the overlap integrals of the plane wave method. Therefore, the plane wave method may be cast in a way that scales favorably with the complexity of the fiber design.

2.1 Some Necessary Properties of a Suitable Model

To make calculations of micro-structured fibers, one must be able to calculate both the characteristics of the guided modes, and of the cladding modes. Guided modes are most often modes that are well localized, while cladding modes typically exist in most of the cladding structure. This is not different from the situation in standard optical fibers , however, the complexity of the cladding structure in micro-structured optical fibers cause the demand of a model that is able to describe cladding modes with a complex geometry.

At the fundamental level one may distinguish between modal models (such as the plane-wave method or models using localized functions), and propagating models (such as Finite-Difference Time-Domain methods, Finite element methods or Transfer Matrix methods). Modal methods offer good understanding of the modal nature of the propagation, while propagating models may more readily be implemented to include non-modal characteristics, such as complex dielectric constants. At the present level of investigation, the author favors modal methods, however, in the future the analysis of micro-structured fibers may reach a level, that would necessitate the inclusion of non-modal methods.

Modal methods involve the expansion of the field as superpositions of basis functions, such as plane waves. Plane waves are very efficient for modeling periodic dielectric structures, since the basis functions (cosines) are spatially extended as are the modes of periodic dielectric structures. However, plane waves are not especially efficient at describing localized modes, such as the guided modes of micro-structured optical fibers, since guided modes are not periodic solutions. One may partly resolve this weakness of the plane-wave method, by imposing an artificial periodicity to the problem. This is done by repeating the core-region periodically within the infinite dielectric cladding structure, thus in effect creating a 'supercell' (see **Figure 2.1**) that may be analyzed using the plane-wave method . If the periodic 'cores' are spaced sufficiently far apart to ensure that the different core-regions do not affect each other significantly (the size of the supercell should be significantly larger than the effective mode area of the guided modes), such a supercell method may yield correct field solutions for the guided modes. However, isolating the core-regions from each other, often demands a large supercell and, therefore, enforces the need of a large number of field expansion terms, to ensure sufficiently detailed representation of the field solutions and of the dielectric structure. Fortunately, an optimized plane wave method exist that allows a large number of plane waves to be included in the calculations [54], since some of the calculations shown in this thesis have demanded the use of more than 4 million plane waves.

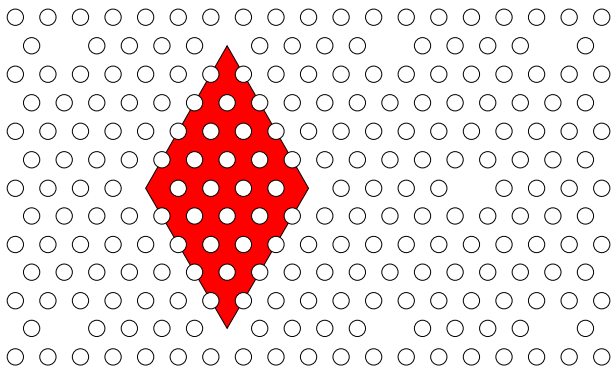

Figure 2.1: The supercell approximation. The core-region is repeated to create a periodic dielectric problem that may be solved using the plane wave method

2.2 The Plane-Wave Method

The plane-wave method is a periodic method in that it calculates periodic field solutions within periodic dielectric structures. The field solutions need to satisfy Maxwell's equations:

$$\begin{aligned} \nabla \cdot \mathbf{B} &= 0 \\ \nabla \times \mathbf{E} + \frac{1}{c}\frac{\partial \mathbf{B}}{\partial t} &= 0 \\ \nabla \cdot \mathbf{D} &= 4\pi\rho \\ \nabla \times \mathbf{H} - \frac{1}{c}\frac{\partial \mathbf{D}}{\partial t} &= \frac{4\pi}{c}\mathbf{J} \end{aligned} \tag{2.1}$$

Here $\mathbf{E}$ and $\mathbf{H}$ are the macroscopic electric and magnetic fields, $\mathbf{D}$ and $\mathbf{B}$ are the displacement and magnetic induction fields, while ρ and $\mathbf{J}$ are the free charges and currents. For the optical fibers we will calculate upon, we will assume that the fiber consist of well defined regions of homogeneous dielectric material, and that no sources of light exist inside the fiber, so that no free charges or currents exist inside the fiber.

We further ignore nonlinear effects- that is we assume that $\mathbf{E}$ and $\mathbf{D}$ are linearly related, and that the materials within the fiber (typically silica and air) are isotropic and macroscopic, thus ensuring that $\mathbf{E}(\mathbf{r},\omega)$ and $\mathbf{D}(\mathbf{r},\omega)$ are related by a scalar dielectric constant $\epsilon(\mathbf{r},\omega)$. Last it is assumed that the dielectrics may be described by real numbers, that is we ignore losses. These (quite usual) assumptions make it possible to reduce Maxwell's equations to:

$$\begin{aligned} \nabla \cdot \mathbf{H}(\mathbf{r},t) &= 0 \\ \nabla \times \mathbf{E}(\mathbf{r},t) + \frac{1}{c}\frac{\partial \mathbf{H}(\mathbf{r},t)}{\partial t} &= 0 \\ \nabla \cdot \epsilon(\mathbf{r})\mathbf{E}(\mathbf{r},t) &= 0 \\ \nabla \times \mathbf{H}(\mathbf{r},t) - \frac{\epsilon(\mathbf{r})}{c}\frac{\partial \mathbf{E}(\mathbf{r},t)}{\partial t} &= 0 \end{aligned} \tag{2.2}$$

Since Maxwell's equations are linear, we may describe the time dependence of the field solutions, by expanding the fields into a set of harmonic modes. Then the diffentiations with time in (2.2) simplifies, thus making it possible to describe each modal field solution by an operator equation in

either the electric or the magnetic field (2.3), with the condition that the divergence of either the magnetic or the displacement field must be zero.

$$\begin{aligned} \nabla \times \nabla \times \mathbf{E}(\mathbf{r}) &= (\frac{\omega}{c})^2 \epsilon(\mathbf{r}) \mathbf{E}(\mathbf{r}) \\ \nabla \times (\frac{1}{\epsilon(\mathbf{r})} \nabla \times \mathbf{H}(\mathbf{r})) &= (\frac{\omega}{c})^2 \mathbf{H}(\mathbf{r}) \end{aligned} \tag{2.3}$$

The **H**-field operator is a simple Hermitian operator, while the **E**-field operator is a generalized Hermitian operator. Furthermore, the magnetic field is transverse, which reduces the size of the eigenvalue-problem. One may recast the **E**-field operator into a simple eigenvalue operator in the **D**-field. The D-field is also transverse, however, unfortunately the **D**-field operator is not Hermitian. Therefore, it appears to be computationally most efficient to cast the eigenvalue-problem as an eigenvalue problem in the magnetic field [10].

According to Bloch's theorem, the field solutions allowed in a periodic dielectric structure can be described as a plane wave multiplied by a Bloch solution, with the same periodicity as the lattice structure:

$$\begin{aligned} \mathbf{H}(\mathbf{r}) &= e^{i\mathbf{k}\cdot\mathbf{r}} \mathbf{u}(\mathbf{k}, \mathbf{r}) \\ \mathbf{u}(\mathbf{k}, \mathbf{r}) &= \mathbf{u}(\mathbf{k}, \mathbf{r} + \mathbf{R}) \end{aligned} \tag{2.4}$$

Here $\mathbf{R}$ represents a lattice vector of the periodic dielectric structure, that is $\mathbf{R} = n\mathbf{R}_1 + m\mathbf{R}_2$, where $\mathbf{R}_1$ and $\mathbf{R}_2$ are primitive lattice-vectors and m and n are whole numbers. Taking the Fourier transform of the Bloch solution gives:

$$\begin{aligned} \mathbf{u}(\mathbf{k}, \mathbf{r}) &= \int h(\mathbf{G}) e^{i\mathbf{G}\cdot\mathbf{r}} \mathbf{e}(\mathbf{k}) d\mathbf{G} \\ \mathbf{u}(\mathbf{k}, \mathbf{r} + \mathbf{R}) &= \int h(\mathbf{G}) e^{i\mathbf{G}\cdot(\mathbf{r}+\mathbf{R})} \mathbf{e}(\mathbf{k}) d\mathbf{G} \end{aligned} \tag{2.5}$$

(2.5) shows that $h(\mathbf{G}) = h(\mathbf{G}) e^{i\mathbf{G}\cdot\mathbf{R}}$, or correspondingly:

$$\mathbf{G} \cdot \mathbf{R} = n2\pi \tag{2.6}$$

Again n represents a whole number. Clearly the **G**-vectors define a new lattice with primitive lattice vectors $\mathbf{G}_1$, $\mathbf{G}_2$, such that $\mathbf{R}_i \cdot \mathbf{G}_j = 2\pi\delta_{ij}$, i,j= 1,2, and such that a reciprocal lattice-vector is given as $\mathbf{G} = n\mathbf{G}_1 + m\mathbf{G}_2$. Because of the periodic dielectric structure we may, therefore, replace the integral in (2.5) with a summation over all possible reciprocal lattice-vectors, and insert the summation into (2.4) to obtain an expression for the magnetic field.

$$\mathbf{H}(\mathbf{k},\mathbf{r}) = \sum_{all\ \mathbf{G}} \sum_{l=1}^{2} h_l(\mathbf{k},\mathbf{G})\mathbf{e}_l(\mathbf{k}+\mathbf{G})e^{i(\mathbf{k}+\mathbf{G})\cdot\mathbf{r}} \tag{2.7}$$

(2.7) shows why this method is commonly termed the plane-wave method. Each mode (or frequency component) is described as an infinite sum of plane waves, with wavevectors $\mathbf{k}+\mathbf{G}$. Before (2.7) is inserted in the operator equation (2.3) one must ensure that the calculated solutions are transverse ($\nabla \cdot \mathbf{H} = 0$). This is ensured by choosing the unit-vectors such that: $\mathbf{k}+\mathbf{G}$, $\mathbf{e}_1(\mathbf{k}+\mathbf{G})$ and $\mathbf{e}_2(\mathbf{k}+\mathbf{G})$ form a triad (are orthogonal to each other).

$$\begin{aligned} \mathbf{e_1}(\mathbf{k}+\mathbf{G}) \cdot (\mathbf{k}+\mathbf{G}) &= 0 \\ \mathbf{e_2}(\mathbf{k}+\mathbf{G}) \cdot (\mathbf{k}+\mathbf{G}) &= 0 \\ \mathbf{e_1}(\mathbf{k}+\mathbf{G}) \cdot \mathbf{e_2}(\mathbf{k}+\mathbf{G}) &= 0 \end{aligned} \tag{2.8}$$

The dielectric structure and the Bloch-solution share the same periodicity, so we can Fourier-transform the dielectric constant as:

$$\begin{aligned} \frac{1}{\epsilon(\mathbf{r})} &= \sum_{all\ \mathbf{G}} \epsilon_{\mathbf{G}}^{-1} e^{i\mathbf{G}\cdot\mathbf{r}} \\ \epsilon_{\mathbf{G}}^{-1} &= \frac{1}{a_c}\int_{a_c} \frac{1}{\epsilon(\mathbf{r})} e^{-i\mathbf{G}\cdot\mathbf{r}} d^2\mathbf{r} \end{aligned} \tag{2.9}$$

Here a_c is the area spanned by the unit-cell, defined by $\mathbf{R}_1$ and $\mathbf{R}_2$. Having expanded the magnetic field as well as the dielectric structure, the eigenvalue equation (2.3) may be solved by casting the problem as a matrix problem or as an operator problem.

2.2.1 The First Brillouin Zone, and the Calculation of Guided Modes

In this section it will be shown, how one should vary the **k**-vector, introduced in the preceding section, to calculate the photonic bandgaps of a periodic dielectric structure, and to calculate guided modes in periodic dielectric structures. As a starting point, we will consider the illustration shown in **Figure 2.2**. To the left is illustrated a periodic dielectric structure with air-holes placed on a triangular lattice within a dielectric background. The figure defines the inter-hole distance, Λ, the hole-diameter, d, the primitive lattice vectors, $\mathbf{R}_1$ and $\mathbf{R}_2$, and a unit-cell spanned by the two primitive lattice-vectors. To the right of **Figure 2.2** is shown the primitive reciprocal lattice-vectors, $\mathbf{G}_1$ and $\mathbf{G}_2$, and the Brillouin-zone (shown as a blue hexagonal).

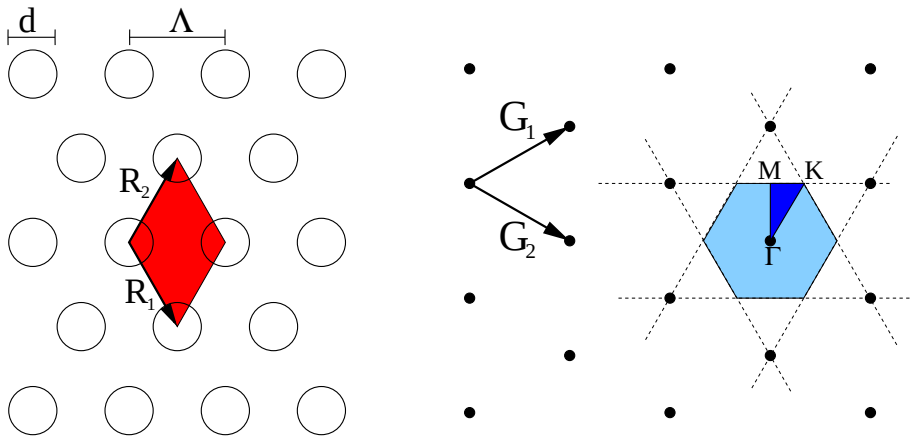

Figure 2.2: The closed-packed dielectric structure, with air-holes placed on a triangular lattice within a silica background material. The lattice-vectors, R_1 and R_2, define the unit cell. The reciprocal lattice-vectors, G_1 and G_2, define the reciprocal lattice, the first Brillouin-zone, and the first irreducible Brillouin-zone. The symmetry points, Γ, M, K are also defined.

For a triangular structure, the primitive lattice-vectors are defined as [55]:

$$\mathbf{R}_1 = \frac{\Lambda}{2}(\mathbf{x} + \mathbf{y}\sqrt{3})$$

$$\mathbf{R}_2 = \frac{\Lambda}{2}(\mathbf{x} - \mathbf{y}\sqrt{3}) \tag{2.10}$$

$$\tag{2.11}$$

The primitive reciprocal lattice-vectors are correspondingly given as:

$$\begin{aligned} \mathbf{G}_1 &= \frac{2\pi}{\Lambda}(\mathbf{x} - \mathbf{y}\frac{\sqrt{3}}{3}) \\ \mathbf{G}_2 &= \frac{2\pi}{\Lambda}(\mathbf{x} + \mathbf{y}\frac{\sqrt{3}}{3}) \end{aligned} \tag{2.12}$$

$$\tag{2.13}$$

Because of the periodic dielectric structure one only need to vary the **k**-vectors within the first Brillouin-zone [56] to find all the frequency solutions to the eigenvalue-problem (2.3). The Brillouin-zone is defined as the area in reciprocal space (**k**-space), that is closer to the central reciprocal lattice-point (shown as a black dot at the center of the Brillouin-zone), than to any other reciprocal lattice-points, as is suggested by the dashed lines used to define the Brillouin-zone [10]. Any point in **k**-space belongs to a Brillouin-zone, however, once the central reciprocal lattice-point is chosen, we will refer to the Brillouin-zone depicted as the first Brillouin-zone.

Often, one does not need to vary **k** within all of the first Brillouin zone either [10]. The triangular dielectric structure depicted in **Figure 2.2** is seen to have 60-degrees rotational symmetry, as well as inversion symmetry. It can be shown that the field-solutions have the same symmetries in **k**-space as the symmetries of the dielectric structure investigated [10]. One therefore only need to vary the **k**-vectors within the so-called irreducible first Brillouin zone, defined in **Figure 2.2** by the symmetry-point, $\mathbf{\Gamma}, \mathbf{M}, \mathbf{K}$.

It is customarily assumed (I have never seen a paper with calculations on Photonic Crystals that did not assume this, actually it is rarely even mentioned) that varying **k** along the boundary of the irreducible first Brillouin-zone will yield the correct photonic bandgaps, though this has (to the authors knowledge) never been stringently proved. Assuming this is correct one may, therefore, find the band-structure (and the Photonic bandgaps) of a periodic dielectric structure by varying **k** along $\mathbf{\Gamma M K \Gamma}$.

Interesting insight about the field solutions is gained, if one rewrites (2.7) as:

$$\mathbf{H}(\mathbf{k}, \mathbf{r}) = e^{i\mathbf{k}_\pi \cdot \mathbf{r}_\pi}[e^{ik_z z} \sum_{all\ \mathbf{G}} \sum_{l=1}^{2} h_l(\mathbf{k}, \mathbf{G}) \mathbf{e}_l(\mathbf{k} + \mathbf{G}) e^{i\mathbf{G}\cdot\mathbf{r}}] \tag{2.14}$$

Here k_z is the magnitude of the $\mathbf{k}$-component along the invariant direction of the dielectric material, $\mathbf{z}$, while π denotes the plane perpendicular to the invariant direction of the crystal. The term inside the square brackets have the same periodicity as the dielectric material. In the $\mathbf{\Gamma}$-point $\mathbf{k}_\pi = 0$, and we therefore conclude (since $e^{i\mathbf{k}_\pi \cdot \mathbf{r}_\pi} = 1$) that the field-solutions to the eigenvalue-problem have the same periodicity as the periodic structure (that is periodicity $\mathbf{R}_1$ and $\mathbf{R}_2$). $\mathbf{M}$ is equal to $\frac{1}{2}(\mathbf{G}_1 - \mathbf{G}_2)$, so choosing $\mathbf{k}_\pi = \mathbf{M}$ one find field solutions with the periodicity $\mathbf{R}_1 - \mathbf{R}_2$ and $2\mathbf{R}_1$. $\mathbf{K} = \frac{1}{3}(2\mathbf{G}_1 - \mathbf{G}_2)$, so the field-solutions have the periodicity $2\mathbf{R}_1 - \mathbf{R}_2$ and $\mathbf{R}_1 - \mathbf{R}_2$ when $\mathbf{k}_\pi = \mathbf{K}$. Only $\mathbf{k} = \mathbf{\Gamma}$ yield field-solutions with the same periodicity as the dielectric structure.

This is important to consider when making calculations on guided modes, by using the supercell method (where one treat the structure as a periodic structure). Different choices of $\mathbf{k}_\pi$ will generally yield different eigenvalue solutions, $(\frac{\omega}{c})^2$, thus leading to the natural question which solution best represents the actual mode guided by the fiber. However, only the solution with $\mathbf{k}_\pi = \mathbf{\Gamma}$ represents a mode with no net-energy flow between the different supercells, and therefore $\mathbf{k}_\pi = \mathbf{\Gamma}$ is always chosen to represent the guided modes in this thesis.

As opposed to quantum physics no fundamental length scale exist in Maxwell's equations. Therefore, it is customary to formulate the plane wave method with normalized units [56]. In particular the normalized eigenfrequencies are $\frac{\omega\Lambda}{2\pi c}$, where Λ is the interhole distance (as in this thesis) or alternatively the lattice constant (as in planar photonic crystal technology). We choose to let Λ represent the interhole distance, since Λ then may be interpreted as one of the measures defining how difficult it is to manufacture a given fiber. Also, we will in this thesis write the normalized frequencies in a form that more readily shows the structural size for a given wavelength, namely $\frac{\Lambda}{\lambda}$. Often the inverse of the normalized frequency, $\frac{\lambda}{\Lambda}$, which we will in this thesis term the normalized wavelength, is shown.

Not only the eigenvalues, but also the wave-vectors, $\mathbf{k} + \mathbf{G}$ are normalized. This gives the normalized wave-vectors, $\frac{\mathbf{k}\Lambda}{2\pi} + \frac{\mathbf{G}\Lambda}{2\pi}$. In particular the wave-vector component, k_z in the invariant direction of the two-dimensional photonic crystal fibers will be expressed by the normalized propagation constant, $\frac{\beta\Lambda}{2\pi}$. Using these normalized units, the mode index is given by the normalized propagation constant divided by the normalized frequency, while the group index of a guided mode, $c\frac{\partial\beta}{\partial k}$ is given by $\frac{\partial(\frac{\beta\Lambda}{2\pi})}{\partial(\frac{\Lambda}{\lambda})}$.

2.2.2 An Optimized Plane Wave Method

As mentioned in the preceding subsection, one may cast the eigenvalue-problem as a Matrix eigenvalue-problem. Choosing to work with the Hermitian **H**-field operator, one then obtains a Hermitian matrix eigenvalue problem. For TM or TE electromagnetic problems (corresponding to field-solutions where the energy does not travel along the invariant direction of the two-dimensional photonic crystal- that is the **k**-vector from the preceding section is zero along the invariant direction), this means diagonalization of a simple $N \times N$ matrix problem, where N is the number of plane waves, as well as the number of resolution points of the dielectric structure in reciprocal space.

For calculations on micro-structured fibers with a propagation constant, β different from zero, however, the field expansions with the directional unit-vectors $\mathbf{e_1}$ and $\mathbf{e_2}$ from (2.8) begin to couple to each other, and one must therefore diagonalize a simple $2N \times 2N$ eigenvalue problem [57]. Since the computational load for eigenvalue problems increases with N^3, and the demands on memory increases with N^2 this implies, that one cannot solve large micro-structured fiber problems by using this approach, with the present state of computer technology.

For most fiber-problems, however, one is not interested in a complete solution to the eigenvalue problem. Typically, one is interested in knowing the specifics of a few guided modes, while one is not interested in knowing the solutions to non-guided modes. By casting the eigenvalue problem as an operator problem [54] and then searching for solutions with the lowest eigenvalues (using e.g. a conjugate-gradient minimization of the Rayleigh quotient), the demands on computer memory scales linearly with N, while the computational demands scales with N^2. By employing a Fast Fourier Transform (FFT), the computational demands may even scale as favorably as NlogN [54]. In this section such a method will be sketched. Further, it will be shown how one can change this method, so that it is optimized for calculating photonic bandgap guided modes. We again start by employing Maxwell's equation for the magnetic field with the usual assumptions (we consider dielectrics with no sources, and only consider solutions with a periodic time-dependency).

$$\nabla \times (\frac{1}{\epsilon(\mathbf{r})} \nabla \times \mathbf{H}(\mathbf{r})) = (\frac{\omega}{c})^2 \mathbf{H}(\mathbf{r}) \tag{2.15}$$

Since we wish to solve this eigenvalue equation by using conjugate-gradient minimization of the Rayleigh quotient, the basic way to solve the

problem is as follows: Use an arbitrary eigenvalue-trial vector, $\mathbf{h}$ (such as the one expressed by the h_l-components in (2.7). Then compare the left side and the right side of (2.15) using this trial $\mathbf{h}$-vector, and repeat this process while iteratively improving the guess of the eigenvector. This will yield the lowest eigenvalue and eigenvector for the specific choice of $\mathbf{k}$-vector.

More specifically, the smallest eigenvalue, λ_0, and the corresponding eigenvector, $\mathbf{h}_0$ of a simple eigenvalue problem, with matrix $\mathbf{A}$ is also the minimization of the Rayleigh quotient:

$$\lambda_0 = min \frac{\mathbf{h}_0^* \mathbf{A} \mathbf{h}_0}{\mathbf{h}_0^* \mathbf{B} \mathbf{h}_0} \tag{2.16}$$

Therefore one may compute the fundamental eigenvalue-pair, $\lambda_0, \mathbf{h}_0$, by performing an unconstrained minimization of the Rayleigh quotient ($\mathbf{B}$ is the unit matrix when finding the lowest order eigenvalue solution) by using e.g. a conjugate-gradient method. To find the subsequent eigenvalue-pairs, one repeats the minimization while ensuring that the present eigenvector is orthogonal (since the operator is Hermitian) to all prior eigenvectors through the matrix $\mathbf{B}$ [54, 10]. It is important to notice, that one never need to calculate the matrix $\mathbf{A}$ itself, but only the product $\mathbf{A}\mathbf{h}_0$, that is the left hand side of (2.15).

The time consumption for finding the eigenvalue-pairs is therefore proportional to the time it takes to calculate the left hand side of (2.15)- at least when only a few eigenvalue pairs are needed. Taking the curl scales linearly with the size of the eigenvector (the number of basis functions used), however, finding the product of $\frac{1}{\epsilon(\mathbf{r})}$ and $\nabla \times \mathbf{H}(\mathbf{r})$ scales as the number of basis-functions squared, since this is a folding of the two functions in Fourier space. To speed up the evaluation time for problems where a large number of basis functions are used, one instead takes a Fast Fourier Transform (FFT) of $\nabla \times \mathbf{H}(\mathbf{r})$ and then multiplies with $\frac{1}{\epsilon(\mathbf{r})}$ in Real space (since the time used for multiplication scales linearly with the number of basis functions in Real space). To calculate the last curl one then takes a FFT back to Fourier space, before the last curl is taken [54]. The genius of this is, that an optimized algorithm exist for FFT, such that the evaluation of the left hand side of (2.15) now scales as NLogN, where N is the number of basis functions (plane waves) used in the expansion.

A fundamental problem with a Fourier expansion of the dielectric material is the poor representation of the dielectric function, when the dielectric material has discontinuities (as it always does in micro-structured fibers). This may be partly circumvented by expressing the dielectric function $\frac{1}{\epsilon(\mathbf{r})}$ in each point as a tensor, rather than as a scalar. From effective-medium

theory, it is known that one may average the dielectric in two different ways, depending upon the polarization of the incident light, relative to the unit-normal vector, $\hat{\mathbf{n}}$. If $\mathbf{E}(\mathbf{r}) \| \hat{\mathbf{n}}(\mathbf{r})$, one averages $\frac{1}{\epsilon(\mathbf{r})}$. If, instead, $\mathbf{E}(\mathbf{r}) \perp \hat{\mathbf{n}}(\mathbf{r})$, one takes the inverse of the average of $\epsilon(\mathbf{r})$. In general this lead to the tensor elements:

$$\epsilon_{\mathbf{ij}} = \epsilon_{\perp} \mathbf{n_i n_j} + \epsilon_{\|}(\hat{\mathbf{i}} \cdot \hat{\mathbf{j}} - \mathbf{n_i n_j}) \qquad ; \qquad \mathbf{i,j} = \mathbf{x,y,z} \tag{2.17}$$

$$\tag{2.18}$$

For a dielectric structure that is periodic in two dimensions this lead to the following expression for the inverse tensor:

$$\epsilon^{-1} = \begin{pmatrix} \frac{n_y^2}{\epsilon_{\|}} + \frac{n_x^2}{\epsilon_{\perp}} & n_x n_y (\frac{1}{\epsilon_{\perp}} - \frac{1}{\epsilon_{\|}}) & 0 \\ n_x n_y (\frac{1}{\epsilon_{\perp}} - \frac{1}{\epsilon_{\|}}) & \frac{n_x^2}{\epsilon_{\|}} + \frac{n_y^2}{\epsilon_{\perp}} & 0 \\ 0 & 0 & \frac{1}{\epsilon_{\|}} \end{pmatrix} \tag{2.19}$$

In [54] it was shown, that the inclusion of this tensor formulation of the dielectric index, greatly reduces the number of plane waves required to obtain a required accuracy for the calculated solutions.

It is a disadvantage of this method, that one needs to calculate the eigenvalues beginning with the fundamental eigenvalues ('from the bottom'). This is not a disadvantage when calculating e.g. guided modes in a fiber where the guided modes have the lowest energy (such as usual index-guiding step-index fibers), however, for so-called bandgap-guiding fibers this becomes a severe disadvantage.

If we denote the operator $\nabla \times \frac{1}{\epsilon} \nabla \times$, A, then we may remedy this problem by using the operator $(A - (\frac{\omega_0}{c})^2)^2$. This corresponds to the new eigenvalue-problem:

$$[\nabla \times \frac{1}{\epsilon} \nabla \times \nabla \times \frac{1}{\epsilon} \nabla \times -2(\frac{\omega_0}{c})^2 \nabla \times \frac{1}{\epsilon} \nabla \times + (\frac{\omega_0}{c})^4] \mathbf{h} = ((\frac{\omega}{c})^2 - (\frac{\omega_0}{c})^2)^2 \mathbf{h} \tag{2.20}$$

where the eigenfrequencies are frequency shifted to $((\frac{\omega}{c})^2 - (\frac{\omega_0}{c})^2)^2$. By choosing ω_0 to be at the mid-gap frequency of the bandgap, any guided modes within the photonic bandgap will have the lowest shifted frequency, and will therefore be the modes first found by this operator. By shifting between Real space and Fourier space, the calculation of the left hand side of this eigenvalue operator equation still scales as NLogN, where N is the number of basis functions used.

2.3 Summary of chapter 2

No single wave vector exist for the solutions to periodic dielectric structures. Rather each mode is described by a large number of wave vectors by the truncated plane wave method. However, for two-dimensional periodic dielectric structures the wave vector component in the invariant direction of the dielectric crystal is well defined.

The photonic bandgaps of periodic dielectric structures are found by varying the wavevectors along the boundary of the irreducible Brillouin zone. For guided solutions, however, we always choose the central point in the first Brillouin zone with the same symmetry as the supercell.

The plane wave method used for the work presented in this thesis is an optimized version, scaling almost linearly with the number of plane waves used to describe the problem. The method may be formulated to calculate interior eigenstates first, making it a very suitable method for photonic bandgap problems.

Chapter 3

Basic Properties of Photonic Crystal Fibers

In the formulation, that was suggested in [17], the cladding structure of Photonic Crystal Fibers (PCFs) consisted of a large number of air-holes placed two-dimensionally periodically on a silica background. The air-holes therefore defined a perfect two-dimensional lattice, which offered the possibility of Photonic Band Gaps (PBGs). PBGs will be introduced in section 3.4. It was suggested in [17], that optical fibers with a cladding structure exhibiting PBGs, could guide light by the PBG-effect, if light was allowed in a central core-region due to a transverse resonance condition, while this guided light was not allowed in the cladding region, because of the PBG-effect.

Early PCFs did in fact guide light in a pure silica core region [41], even though the cladding structure showed no evidence of PBGs. This led to the realization, that these fibers guided light by a mechanism similar to total internal reflection [15, 58]. Such micro-structured fibers have aspects that have important analogies in common step-index fibers. They will be introduced in section 3.3.

3.1 Total Internal Reflection and Multiple Reflections

The concept of total internal reflection is vital to the functioning of traditional silica-based optical fibers, such as step-index fibers (SIF) [59]. Imagine a SIF, typically consisting of a germanium-doped (Ge) silica core, surrounded by a silica cladding. The traditional purpose of doping the core with Ge, is to raise the effective refractive index of the silica, thus effec-

tively creating a core-region with a refractive index, that is higher than the refractive index of the cladding.

For a given finite core-size and wavelength, one or more modes of light may be able to propagate along the core-region of the fiber, without escaping out through the cladding of the fiber, because of total internal reflection.

Since the core is finite-sized, only a finite number of modes will be allowed to propagate through a step-index fiber. For a bend-less fiber, the energy carried by each of these modes will in principle propagate losslessly (ignoring e.g. dissipation) along the direction of the core-region, as they are not allowed to escape to the cladding region, because of the refractive index step between the core and the cladding. In a simplified ray analogy, the guiding mechanism is explained by the photons being reflected back to the core, by the core-cladding interface, thus the name total internal reflection (TIR).

Though such a simplified ray analogy may lead to conclusions that are not completely true (for instance the erroneous conclusion that no energy propagates outside the core-cladding interface), it does provide a good understanding of the basic guiding mechanism involved in the guidance of light in traditional optical fibers. Particularly, it describes how light may be confined by a simple circular core-cladding interface.

In micro-structured fibers, such a well defined core-cladding interface does not usually exist [51]. Typically the cladding consists of a large number of air-holes distributed within a silica background material. Since air has a considerably lower refractive index than silica (1.0 compared to 1.444 at 1550 nm wavelength), the air-holes lower the effective index of the cladding region. If one places the air-holes periodically in the cladding region, and then removes one of the central air-holes (thus creating a central core-region with relatively less air compared to the cladding region), it is perhaps not surprising that light can be guided along this silica core region by a mechanism similar to total internal reflection [58].

However, distributing such air-holes within a high-index background material is not simply a novel way of lowering the effective refractive index of the cladding region. If the size of the atoms or the distance between the atoms is comparable to the wavelength of light to be guided by the fiber, novel phenomena related to constructive and destructive interference may appear. In particular, if one places the air-hole atoms periodically one may find propagation constant intervals that are not allowed to exist in the cladding region at a particular wavelength- an effect similar to the electronic bandgaps found in semi-conductors. It is common to refer to such forbidden frequency regions as Photonic Band Gaps (PBG) [55, 17, 10].

PBGs appear because of multiple reflections at the 'atom'-background interfaces. Micro-structured fibers may exploit either the lowering of the effective index of the cladding region [15], or the strong scattering phenomena (such as PBGs) [20, 21, 47] or both [60]. Either way, the multiple reflections within the cladding region, open up the possibility of cladding modes behaving quite different from the cladding modes found in SIFs.

3.2 Properties of Periodic Dielectric Materials

The periodic dielectric materials that are used as the cladding material of the micro-structured fibers analyzed in this thesis, share a number of common characteristics. These will be exemplified in this section, by analyzing closed-packed periodic dielectric structures. The structures consist of a background material with a refractive index of 1.45 (close to the refractive index of silica), and circular air-holes placed on a triangular lattice (see **Figure 2.2**).

First to be able to make some comparison with the homogeneous cladding material of SIFs, we need to define an analogue to the refractive index of the cladding material [17, 47]. It should be stressed at this point, that the modes allowed within a periodic material cannot be described by the usage of a simple wavevector. Instead, one way of interpreting the modes of a periodic dielectric structure is offered by the plane wave description [56]. Here each cladding mode can be seen as a superposition of an infinite number of plane waves, each with a different wavevector, $\mathbf{k}+\mathbf{G}$, where $\mathbf{G}$ is a reciprocal lattice vector. As an example, the magnetic field may be expanded as:

$$\mathbf{H}(\mathbf{k},\mathbf{r}) = \sum_{all\ \mathbf{G}} \sum_{l=1}^{2} h_l(\mathbf{k},\mathbf{G})\mathbf{e}_l(\mathbf{k}+\mathbf{G})e^{i(\mathbf{k}+\mathbf{G})\cdot\mathbf{r}} \tag{2.7}$$

Without loss of generality one may term the invariant direction of a two-dimensional periodic dielectric structure the $\mathbf{z}$-direction. Then we can reformulate the expression of the magnetic field as:

$$\mathbf{H}(\mathbf{k},\mathbf{r}) = e^{i\beta z} \sum_{all\ \mathbf{G}} \sum_{l=1}^{2} h_l(\mathbf{k},\mathbf{G})\mathbf{e}_l(\mathbf{k}+\mathbf{G})e^{i(\mathbf{k}_\pi+\mathbf{G})\cdot\mathbf{r}_\pi}$$

Here β denotes the magnitude of the $\mathbf{z}$-component of $\mathbf{k}$, while π denotes projection into the $\mathbf{xy}$-plane. It is seen that the variation along the $\mathbf{z}$-direction is now defined solely by the magnitude of the $\mathbf{z}$-component of $\mathbf{k}$, β, [55].

In a micro-structured optical fiber light is to be guided along the **z**-direction. The guided light will, therefore, not couple to the periodic cladding material, if the propagation constant of the guided mode is larger than β_{max} of the periodic cladding material at the particular wavelength, since the micro-structured fiber is invariant in the **z**-direction. For usage in optical fibers (this is not a general definition of the effective index of a photonic crystal), it is correspondingly possible to calculate the effective index, or the cladding index, of the fundamental cladding mode as $\frac{\beta}{k}$, where the wavenumber $k = \frac{2\pi}{\lambda}$ and λ is the free space wavelength. Therefore, this report will not make any nominal distinction between the propagation constant, β, of a guided mode, or the **z**-component, β, of the wavevectors of cladding modes in a micro-structured dielectric material.

The calculated cladding indices for a number of closed-packed dielectric structures, are shown in **Figure 3.1** and **Figure 3.2**. Since material dispersion is not included in the calculation of these cladding indices, the effective index of the fundamental cladding mode, $\frac{\beta}{k}$, is shown as a function of the normalized wavelength $\frac{\lambda}{\Lambda}$, or the normalized frequency $\frac{\Lambda}{\lambda}$, where Λ is the the distance between the center of neighboring cladding holes, or the lattice constant.

Figure 3.1 and **Figure 3.2** show that the cladding index may be lowered by increasing the fraction of air in the periodic dielectric structure, which is explained by more energy of the fundamental cladding being located in the air-holes. For a given air-filling fraction (or normalized hole-diameter, $\frac{D}{\Lambda}$, where D is the airhole diameter, the cladding index is seen to behave as follows: If the wavelength, λ is significantly shorter than the structure size, Λ, the cladding index is close to the refractive index of the background material (the refractive index of the background silica is 1.45 in the examples in **Figure 3.1**). As $\frac{\lambda}{\Lambda}$ is increased (by e.g. increasing the wavelength λ) the effective cladding index is lowered until it ultimately reaches a minimum value, where the effective index is relatively independent of the wavelength. At these long normalized wavelength regions, the micro-structured material is perceived as a homogeneous material by the fundamental cladding mode. Analytical expressions for the effective index is given for various types of dielectrics in [61]. For a triangular arrangement of air holes (with the dielectric constant ϵ_{air}) within a silica background with dielectric constant ϵ_{si}, such that the air-filling fraction of the air holes is f, the effective cladding index is given as:

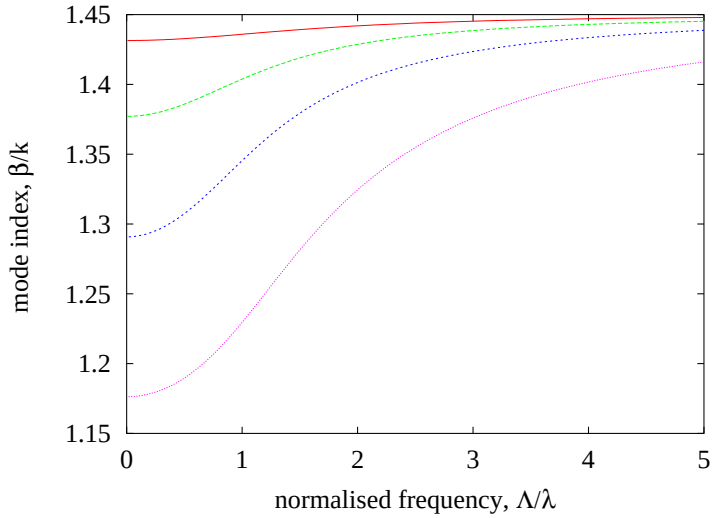

Figure 3.1: The effective cladding index for a closed-packed dielectric structure, with air-holes placed on a triangular lattice within a silica background material. The cladding index is depicted as a function of the normalized frequency, with the cladding air hole size as a parameter. $\frac{D}{Lambda} = 0.2$ (red curve), $\frac{D}{Lambda} = 0.4$ (green curve), $\frac{D}{Lambda} = 0.6$ (blue curve), $\frac{D}{Lambda} = 0.8$ (purple curve) are depicted.

$$n_{eff} = \sqrt{\epsilon_{si} \frac{[1 - f\frac{\epsilon_{si}-\epsilon_{air}}{\epsilon_{si}+\epsilon_{air}}]}{[1 + f\frac{\epsilon_{si}-\epsilon_{air}}{\epsilon_{si}+\epsilon_{air}}]}} \tag{3.1}$$

Using the effective index $\frac{\beta}{k}$, a micro-structured dielectric material may reflect light incident from an adjacent material with an effective index (or a refractive index) that is larger than the effective index of the micro-structured material- assuming that the light is incident at a sufficiently small angle. It is, therefore, possible to use micro-structured periodic dielectric materials to guide light in e.g. a solid silica core region. This is not only a novel interesting alternative to standard optical fibers, it furthermore offers the possibility of utilizing the novel wavelength-dependence of the effective cladding index, as well as exploiting the very low cladding index levels that becomes possible by employing fibers with large air-filling fractions in the cladding region (for e.g. High-Δ fibers, where Δ [59, 62] is the relative refractive index difference between the core and the cladding).

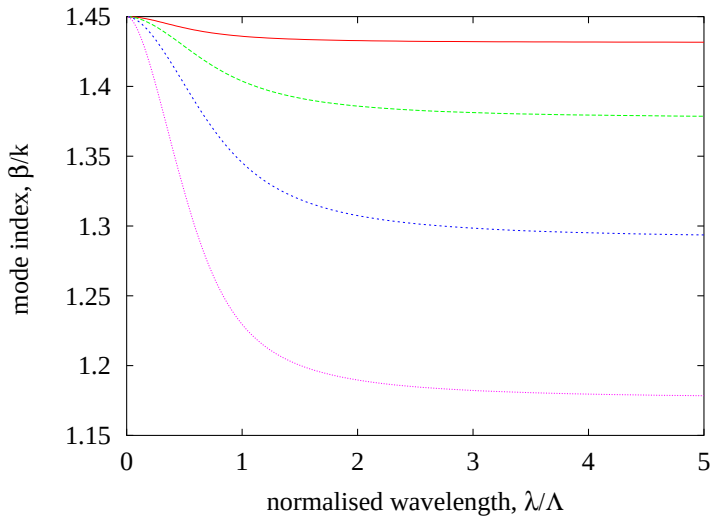

Figure 3.2: The effective cladding index for a closed-packed dielectric structure, with air-holes placed on a triangular lattice within a silica background material. The cladding index is depicted as a function of the normalized wavelength, with the cladding air hole size as a parameter.. $\frac{D}{Lambda} = 0.2$ (red curve), $\frac{D}{Lambda} = 0.4$ (green curve), $\frac{D}{Lambda} = 0.6$ (blue curve), $\frac{D}{Lambda} = 0.8$ (purple curve) are depicted.

Since the demand that the effective core index should be larger than the effective cladding index, to ensure guidance of light we will say that such micro-structured fibers guide light by modified total internal reflection suggesting the strong resemblance to standard step index fibers that guide light by total internal reflection.

3.3 Photonic Crystal Fibers with a Step-Index Analogy

We will now consider micro-structured fibers where the cladding air-hole 'atoms' are distributed periodically within the cladding region. We will, however, restrict ourselves to investigating guided modes that are not guided by the PBG-effect. We will say that such fibers have a step-index analogy and point out some important characteristics of the guided mode(s). This will provide valuable information about some of the novel possibilities that

are possible with these fibers.

Since the cladding air-hole 'atoms' are distributed periodically, we will refer to these fibers as Photonic Crystal Fibers (PCF). However, the cladding structure does not need to be strictly periodic to ensure guidance of light [63, 64]. For a non-periodic cladding structure, the cladding structure should not allow modes with a mode-index that is equal to the mode-index of the guided modes to exist anywhere in the cladding structure.

3.3.1 Photonic Crystal Fibers with small air-holes

Consider a PCF with cladding air-holes placed on a triangular lattice (a closed packed structure), such as the PCF shown schematically in **Figure 3.3**. We will assume a diameter of the air-holes of 20% of the center to center spacing between neighboring cladding air-holes (i.e. $D = 0.2\Lambda$). The core-region is formed by the omission of a single central air-hole.

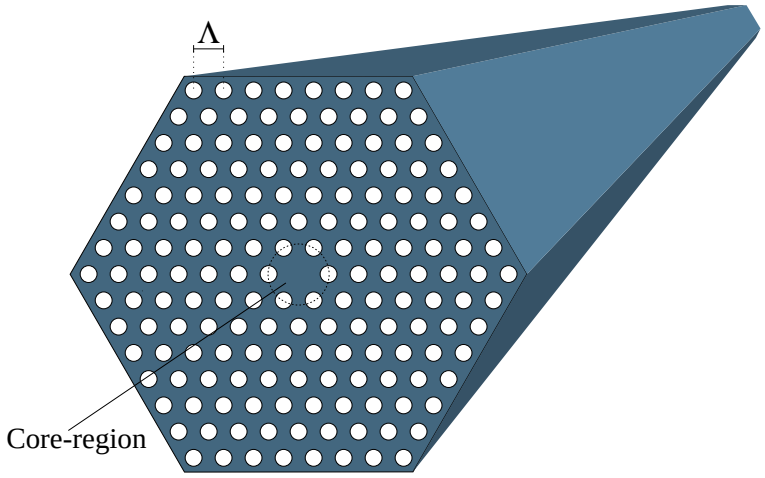

Figure 3.3: The transverse structure of a closed-packed PCF. The interhole distance (the center to center distance between neighboring air holes) is defined by the Figure as Λ.

We will further assume that the fiber is made of pure silica glass with a refractive index of 1.45 at all wavelengths of light, and air-holes with a refractive index of 1.0 (these simplifications are made for reasons of clarity).

To support the claim that this fiber in many ways resembles more traditional step-index fibers, the calculated effective index of the fundamental cladding mode is shown in **Figure 3.4**. We will refer to the effective index

of the fundamental cladding mode as the effective cladding index, since it corresponds to the refractive index of the cladding in a step-index fiber.

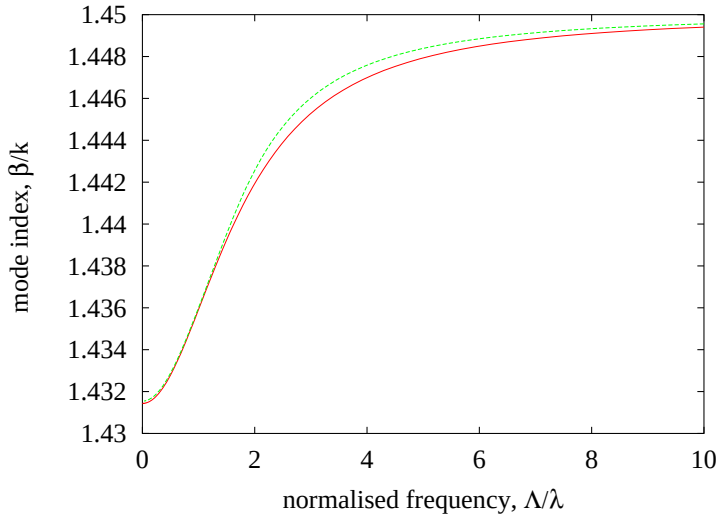

Figure 3.4: The mode index of the guided mode (green curve) and the effective cladding index (red curve) as a function of the normalized frequency. Only one mode is guided by the fiber, irrespective of the wavelength.

In **Figure 3.4** the horizontal axis depicts the normalized frequency, $\frac{\Lambda}{\lambda}$. Here λ is the usual free-space wavelength of the light, while Λ is the inter-hole distance or in this case, the lattice constant. The vertical axis depicts, $\frac{\beta}{k}$, where β is the longitudinal component of the wavevector (along the fiber length axis), and k is the free-space wavenumber. For a guided mode, β is equal to the propagation constant (since all the energy flows along the longitudinal direction of the optical fiber), wherefore $\frac{\beta}{k}$ is also termed the mode-index in this thesis, since the ultimate goal of this study is to understand the modal behavior of guided modes.

If one choose to ignore the influence of material dispersion, one would find that the cladding index of a traditional step-index fiber is independent of the wavelength, λ. However, as was described in the preceding section, the cladding index varies significantly with the normalized wavelength in micro-structured fibers, even when ignoring material dispersion.

In step-index fibers, a core-mode is considered to be guided, at a given wavelength, if the mode-index of the guided mode lies above the refractive

index of the cladding. This is a sound principle, since only such core-modes will not be allowed to couple to cladding modes and thereby leak to the cladding. Likewise, we will in this thesis, consider core-modes with a mode-index above the effective cladding index to be guided modes, even for micro-structured fibers with a step-index analogy.

Figure 3.4 also depicts the mode-index of the fundamental guided mode as a function of $\frac{\lambda}{\Lambda}$. Qualitatively we observe a behavior quite similar to the behavior of the effective cladding index. At short (normalized) frequencies the fiber does not appear to guide light, since the mode-index of the complete fiber is equal to the effective cladding index. At higher normalized frequencies, the mode-index of the fundamental mode rises sufficiently above the effective cladding index, and the fundamental core-mode becomes a guided (and well localized) mode.

The mode-index of the fundamental core-mode rises above the effective cladding index, because the core-region is formed by the omission of one of the cladding air-holes. This creates a relatively large area of silica at the center of the PCF (cf. **Figure 3.3**). The fundamental core-mode is therefore able to avoid the air-holes at a longer wavelength than the fundamental cladding mode.

At short normalized wavelengths, the mode-index of the fundamental core-mode approaches the largest refractive index of the core-region (silica), however, the mode-index of the fundamental core-mode remains below the effective index of silica and above the effective cladding index at all wavelengths [49]. The calculations show that this fiber has a fundamental core-mode that should in principle not couple to any of the cladding modes, despite the fact that no clearly defined core-cladding boundary exist. This may seem surprising from a ray-point of view: Why does the light guided by the core not escape to the cladding, while still avoiding the cladding air-holes, especially at short wavelengths? The answer is that a ray model is to simplistic because it assumes that the mode can be viewed as a set of rays that act independently of each other. Instead the mode should be viewed as a whole, such that a PCF is able to support a guided mode, if it allows the mode to have a propagation constant that is higher than the longitudinal component of the wave-vector of any of the cladding modes in the surrounding cladding structure.

Figure 3.4 only depicts the behavior of the mode-index of the fundamental core-mode. One may ask if the behavior of the mode-index of the guided higher order core-modes behave similarly. However, the calculations reveal that this fiber does not guide any higher order modes, irrespective of the wavelength. This is clearly a fundamental difference from even low-

Δ step index fibers (Δ is defined as $\frac{n_{core}-n_{cladding}}{n_{core}}$ [59, 62], where n_{core} is the refractive index of the core, while $n_{cladding}$ is the refractive index of the cladding). This difference is fundamentally linked to the difference in the way the cladding and the core indices behave. In basic PCFs, the effective core-index and the effective cladding index have the same asymptotic value at short normalized wavelengths, which is the refractive index of the background material (typically fused silica). The cladding index approaches the index of silica in a way which ensures, that only a finite number of modes can be guided by the fiber, irrespective of the frequency. This is one of the qualities of PCFs that have attracted quite some attention. At the end of the next subsection, this quality will be investigated further.

3.3.2 Photonic Crystal Fibers with large air-holes

If one adopt the design from the preceding subsection and enlarges the cladding air-holes to $D = 0.8\Lambda$ a different picture emerges (see **Figure 3.5**). At long normalized wavelengths only a single fundamental guided mode is supported by the fiber. However, at shorter wavelengths more modes become guided by the fiber. It is interesting to note that still, only a finite number of modes are guided by the fiber, irrespective of the wavelength.

To investigate this phenomenon of only a finite number of guided modes further, the effective or normalized frequency, V_{eff} may be investigated. For a standard optical fiber (a simple step-index fiber), V_{eff} is defined as [59, 62]:

$$V_{eff} = k\rho\sqrt{n_{co}^2 - n_{cl}^2} \tag{3.2}$$

where n_{co}^2 and n_{cl}^2 are the wavelength independent refractive index (apart from material dispersion which we ignore for reasons of clarity) of the core and the cladding, respectively. ρ is the radius of the fiber core. To generalize this definition of V_{eff} to micro-structured fibers with a periodic cladding index, we replace n_{cl} with $\frac{\beta}{k}$ for the fundamental cladding mode, [49], $\frac{\beta_{fsm}}{k}$ (fsm refers to the fundamental space filling mode). Some ambiguity of the radius of the core exist in PCFs [51], since no well defined boundary exist between the core and the cladding. One obvious choice is to choose a core radius of the inter-hole distance, Λ [51, 65]. Irrespective of the choice of the core radius, it should be noticed that V_{eff} scales linearly with the choice of the core-radius, leading to the conclusion that the exact choice of core-radius will not qualitatively alter the results of the investigation. One possible choice of V_{eff} is [51]:

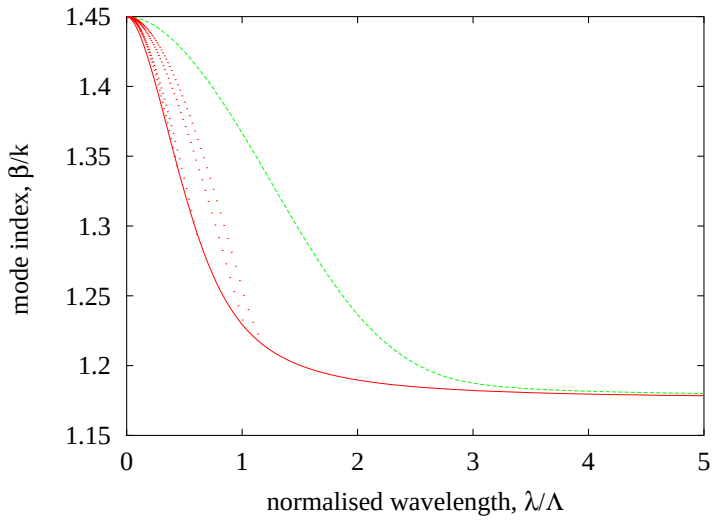

Figure 3.5: The effective cladding index and the mode index of the guided modes supported by a photonic crystal fiber with large cladding air holes ($\frac{D}{\Lambda} = 0.8$). The fundamental mode is shown in green, while the effective cladding index is shown with red. The higher order guided modes are shown with dots.

$$V_{eff} = k0.6\Lambda\sqrt{n_{co}^2 - (\frac{\beta_{fsm}}{k})^2} \tag{3.3}$$

From (3.2) it is seen that V_{eff} scales linearly with k (or inversely with the wavelength), since we ignore material dispersion. However, for PCFs $\frac{\beta_{fsm}}{k}$ approaches n_{co}, as the frequency is increased. As a result the calculated behavior of V_{eff} in PCFs behave as depicted in **Figure 3.6**. At long wavelengths V_{eff} scales inversely with the normalized frequency, since the cladding index is constant in this region. As the energy in the fundamental cladding modes begin to escape the cladding air-holes at higher frequencies, the rise in V_{eff} is slower and eventually V_{eff} reaches a near-constant value [49]. From standard fiber technology [59] it is well-known that V_{eff} is a measure of the number of modes that is guided by the fiber. Therefore a PCF will only guide a finite number of modes, irrespective of the normalized wavelength, since only finite values of V_{eff} are reached. Or stated differently: At short normalized wavelengths the rising of the effective cladding index as the frequency is increased is able to ensure that V_{eff} does not rise

with the frequency. This behavior of the cladding index is ultimately linked to the way the field escapes the cladding air-holes. In the next chapter, a very similar behavior is found, when it is investigated how large a fraction of the power of the guided modes of PCFs that is propagating in air.

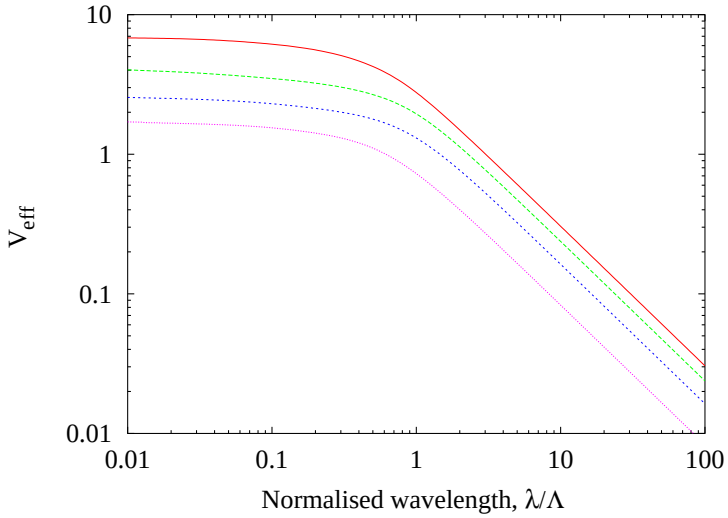

Figure 3.6: The behavior of V_{eff} as a function of the normalized wavelength. The parameter is the cladding air hole size: $D = 0.2\Lambda$ (purple curve), $D = 0.4\Lambda$ (blue curve), $D = 0.6\Lambda$ (green curve), $D = 0.8\Lambda$ (red curve),

3.4 Bragg Reflections and Photonic Bandgap Guiding Fibers

If the dielectric material that constitutes the cladding of the micro-structured fiber is two-dimensionally periodic, we refer to it as a two-dimensional photonic crystal [10]. Photonic crystals may be seen as dielectric materials with periodic scatters, and are in some cases able to exhibit forbidden frequency regions, photonic bandgaps (PBGs). The typical definition of a PBG is a frequency region where no extended field solutions exist to Maxwell's equation, assuming that no longitudinal component of the wavevectors exist (β is assumed to be zero). In the case of fibers guiding light by the PBG-effect, it is more correct to state that a PBG is an interval of combinations of the propagation constant, β and the wavelength of light where no extended

solutions exist to Maxwell's equations. This definition acknowledges that the forbidden frequency intervals depend on the propagation constant of the guided mode(s) [55]. Light incident on a photonic crystal with a frequency within a PBG of the photonic crystal will not be allowed to propagate through the crystal and will therefore be reflected away from the photonic crystal. Therefore, photonic bandgap materials are sometimes referred to as dielectric mirrors.

Such PBGs are the optical equivalent to the electronic bandgaps of solid state physics. PBGs typically occur when the wavelength of the light is of the same order of magnitude as the structural size- the periodicity of the photonic crystal. Much research is directed towards the exploitation of PBGs in dielectric structures that are periodic in one, two or three dimensions. Generally PBGs can have only as high periodicity as the periodicity of the dielectric material involved [10].

Periodic dielectric structures with a two-dimensional PBG can be of use in micro-structured optical fibers, since they prohibit energy from radiating away from the core-region, while allowing light to propagate along the invariant direction of the fiber. A schematic representation of a PBG fiber is shown in **Figure 3.7**.

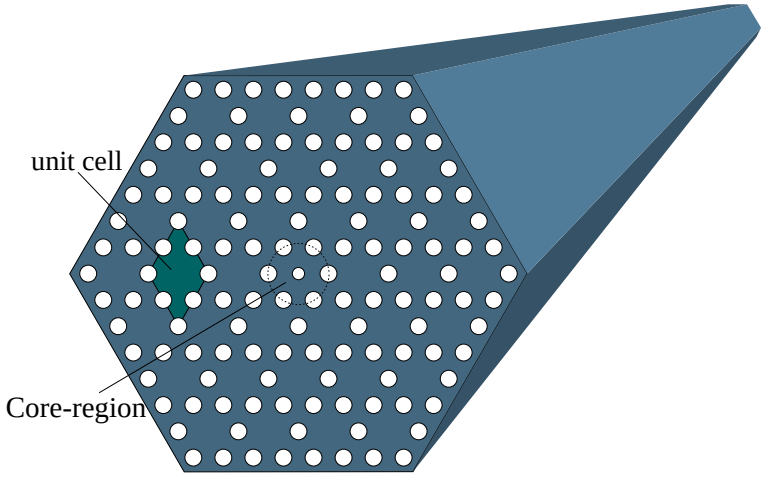

Figure 3.7: A fiber that is guiding light by the Photonic Bandgap effect may be designed with a core-region that is created by adding an extra air-hole to the cladding structure

To perform calculations on PBG structures or even PBG fibers with the plane wave method, a method very similar to the one used for calculating

the fundamental cladding mode is used. First it is noticed, that according to the derivation of Maxwell's equation for periodic structures, the variation of the field of a mode along the invariant direction of the dielectric material may be expressed by a simple propagation constant, β:

$$\mathbf{H}(\mathbf{k},\mathbf{r}) = e^{i\beta z} \sum_{all\ \mathbf{G}} \sum_{l=1}^{2} h_l(\mathbf{k},\mathbf{G}) \mathbf{e}_l(\mathbf{k}+\mathbf{G}) e^{i(\mathbf{k}_\pi+\mathbf{G})\cdot\mathbf{r}_\pi}$$

From a mathematical point of view the only difference to the calculations that must be performed to find the modes guided by PBG effects, or alternatively the fundamental guided mode in a fiber guiding the light by simple index effects, is that now we are not particularly interested in the fundamental mode. Instead we wish to find the modes that define the boundaries of the photonic bandgap, or the modes that correspond to guided solutions within a photonic bandgap. For identifying the photonic bandgaps of a cladding structure using a given propagation constant, β, one varies $\mathbf{k}_\pi$ along the boundary of the irreducible Brillouin zone for a desired number of eigenvalues (e.g. for silica with airholes placed periodically on a honeycomb lattice, it is known that PBGs tend to appear between bands number 2 and 3, and between eigensolutions number 6 and 7. Therefore, one will need to calculate at least 7 bands to correctly identify both of these PBGs, for a given choice of β.

Figure 3.8 illustrates the band-structure for a periodic dielectric material. The structure has circular air holes placed on a honeycomb lattice. Each air hole has the diameter $D = 0.6\Lambda$, where Λ is the interhole distance. For each band the normalized wavelength, $\frac{\lambda}{\Lambda}$ is shown as $\mathbf{k}_\pi$ is varied along the boundary of the irreducible Brillouin zone. The normalized value of the wavevector along the invariant direction is $\frac{\beta\Lambda}{2\pi} = 2.0$.

In this plot, the eigenvalue of the fundamental eigenstate appear at the top, while higher order eigenvalues appear below the fundamental eigenvalue for a given value of $\mathbf{k}_\pi$. Notice that between bands 2 and 3 (as well as between bands number 6 and 7) there are frequency intervals where no extended solutions are found to Maxwell's equations. These are the photonic bandgaps for this particular value of $\frac{\beta\Lambda}{2\pi}$.

For PBG fibers also, the invariant structure in the **z**-direction implies that the wavevector cannot change in this direction. Therefore, if a localized mode has a frequency within a PBG of the surrounding cladding structure (for a given value of β), then this localized mode cannot escape through the cladding and is correspondingly a guided mode. This explanation of a guided PBG mode strictly follows the logic of the plane-wave method

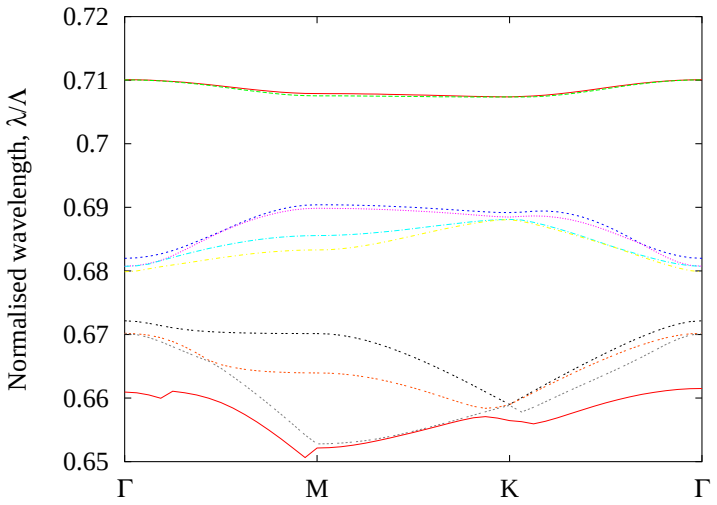

Figure 3.8: The dispersion relation of a periodic dielectric structure with the air holes placed on a honeycomb lattice structure. The symmetry points Γ, M, K are shown on the first axis. The second axis gives the normalized wavelength, $\frac{\lambda}{\Lambda}$, as the **k**-vector traverses the boundary of the irreducible Brillouin zone. The normalized propagation constant, $\frac{\beta\Lambda}{2\pi}$, is 2.0

since this method calculates the eigenfrequencies for a given choice of β. Physically, it may be more meaningful to say that if β of the localized mode is within a forbidden β-interval of the cladding at the particular wavelength, then the guided mode cannot couple to any cladding modes, and the mode must be a guided mode.

In **Figure 3.9** is shown the effective index, $\frac{\beta}{k}$ as a function of the normalized wavelength, $\frac{\lambda}{\Lambda}$ for a structure with air holes on a honeycomb lattice. The diameter of the cladding air holes is 0.6Λ. The behavior of the fundamental space filling mode (The effective cladding index), and the boundary of the lowest order photonic bandgap (above band 2) is shown. It is noticed that the effective index ranges of the photonic bandgap (for a given frequency) is below the effective cladding index, as a result of the photonic bandgap boundaries being the frequencies of higher order eigenvalues. This has the important effect that one may guide light within core-regions with an effective index below the effective cladding index [17].

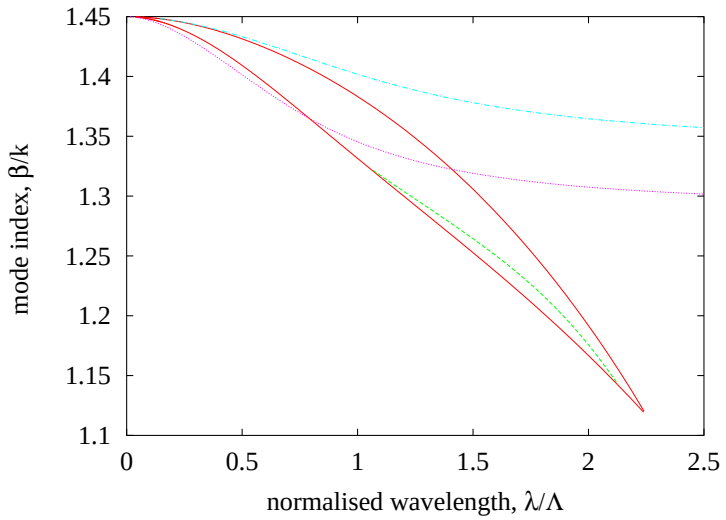

Figure 3.9: The effective cladding index (blue), the PBG boundaries of the fundamental photonic bandgap between bands 2 and 3 (red).

3.5 Summary of chapter 3

One important aspect of micro-structured dielectric materials to be used as cladding structures in optical fibers, is that an effective cladding index may be defined. The effective cladding index was found to be strongly wavelength dependent, a quality that lead to the possibility of micro-structured fibers that support only a finite number of guided modes, irrespective of the wavelength of the light. These fibers are said to guide light by modified total internal reflection. Even more radical is the possibility of photonic bandgaps in a periodic dielectric structure. This makes it possible to guide light in a core-region with a lower refractive index, than the effective cladding index.

Chapter 4

Properties of Photonic Crystal Fibers With a Step-Index Analogy

In the preceding chapter, some basic properties of periodic dielectric materials were described. It was shown that periodic dielectric materials may be used as cladding regions in photonic crystal fibers. In this chapter such fibers will be investigated further, with emphasis on fibers that guide light by modified total internal reflection, an effect very similar to the well-known guiding principle of Total Internal reflection.

4.1 A Step-Index Analogy

As shown previously, PCFs in many respects resemble standard step-index fibers. One may define an effective cladding index, corresponding to the refractive index of the cladding structure of a step-index fiber, and much of the intuition known from step-index fibers still hold, e.g. a large step-index between the core and the cladding leads to multi-mode fibers if the core is sufficiently large, as is the case for small values of $\frac{\lambda}{\Lambda}$ combined with large values of $\frac{D}{\Lambda}$. It has, therefore, been suggested that one can estimate basic fiber parameters by investigating a suitable step-index fiber with a refractive index of the cladding that varies in the same way that the effective index of the cladding varies for the PCF in question [49, 51, 50] (see **Figure 4.1**).

Different schemes have been applied [51, 66], however, it is generally agreed that the best correspondence is obtained by choosing the refractive index of silica to be the refractive index of the core and choosing the radius of

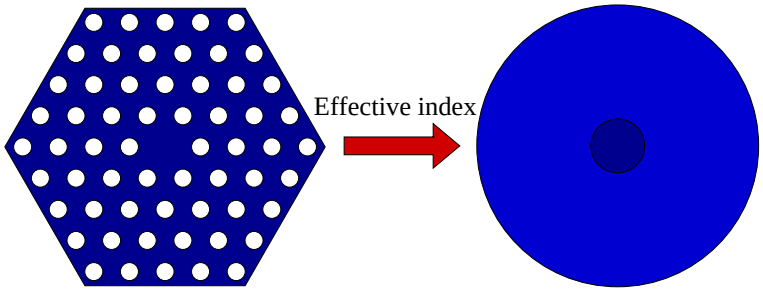

Figure 4.1: A micro-structured fiber with air holes on a triangular cladding structure, and a solid core-region created by the omission of the central air hole, resembles a step index fiber with a wavelength dependent cladding index.

the core, ρ, as approximately 0.6Λ [51, 66]. Using this value of ρ the cut-off properties of the PCF resemble those of step-index fibers, that is a second order cut-off at a V_{eff}-value of approximately 2.4. It is interesting that this analogy is reasonably independent of $\frac{D}{\Lambda}$- this suggests that the guided modes of PCFs resemble Gaussian profiles as do the modes of standard step-index fibers.

This was investigated in [67], by calculating the overlap between the guided mode of the PCF and an optimized Gaussian profile. It was found that the modes of PCFs do in fact resemble Gaussians- typically the overlap is better than 95%. This is evidence, that index guiding micro-structured fibers do in fact resemble step index fibers, when discussing basic modal characteristics. However, it should be noticed that the cross-sections of the cladding modes of PCFs are very much affected by the influence of the cladding air holes. When discussing more advanced topics, such as the leakage losses through the cladding structure of PCFs one should therefore, ideally, not attempt to employ simple step index analogies.

In this thesis, the step index analogy is underlying the calculations on bending losses, and is further often referred to, when discussing the qualitative behavior of PCFs.

4.2 The Fraction of Energy Propagating in Air

Designing optical fibers with a large number of cladding air-holes does provide a number of novel possibilities, even when restricting oneself to fibers that guide light by modified total internal reflection. As shown earlier this

may give fibers that only guide light in a single mode, irrespective of the wavelength [49]. One may also design fibers with a large numerical aperture, since the effective cladding index may be lowered significantly, compared to the refractive index of the core material, silica.

However, the possibility of having optical fibers, with a fraction of the energy of the guided mode being guided in air, in itself offers a number of interesting possibilities. This opens up the possibility of introducing materials into the cladding air-holes, that may interact with the electromagnetic field, and thereby create the possibility of e.g. novel gas sensors. Also the large refractive index difference between silica and air, gives a number of novel characteristics, concerning the behavior of the group velocity, as a function of the wavelength of light.

In this section, we will investigate the fraction, μ, of the fundamental guided mode that is propagating in air. Though some results have been presented on the issue (such as the possibility of having up to 40% of the field propagating in air, [68]), no systematic investigation of the amount of energy propagating in air has been presented.

The starting point of the analysis is the expression for the group velocity [62]:

$$v_g = c\frac{\beta}{k}\frac{\int_A(\mathbf{H}\times\mathbf{E}^*\cdot\mathbf{z}dA}{\int_A \epsilon\mathbf{H}\times\mathbf{E}^*\cdot\mathbf{z}dA} \tag{4.1}$$

This expression is valid for a guided mode, where the integration should be over the cross-section where the field is non-zero. For a PCF with only two dielectrics involved (which we will term ϵ_{air} and ϵ_{si} this may be rewritten as:

$$v_g = c\frac{\beta}{k}\frac{\int_A(\mathbf{H}\times\mathbf{E}^*)\cdot\mathbf{z}dA}{\epsilon_{si}\int_{silica}\mathbf{H}\times\mathbf{E}^*\cdot\mathbf{z}dA + \epsilon_{air}\int_{air}\mathbf{H}\times\mathbf{E}^*\cdot\mathbf{z}dA} \tag{4.2}$$

Introducing the fraction of the field propagating in air, μ we obtain:

$$v_g = c\frac{\beta}{k}\frac{\int_A(\mathbf{H}\times\mathbf{E}^*)\cdot\mathbf{z}dA}{[\epsilon_{si}(1-\mu)+\epsilon_{air}\mu]\int_A\mathbf{H}\times\mathbf{E}^*\cdot\mathbf{z}dA} \tag{4.3}$$

or:

$$\mu = \frac{\epsilon_{si} - \frac{\beta}{k}\frac{c}{v_g}}{\epsilon_{si}-\epsilon_{air}} \tag{4.4}$$

Since $\frac{c}{v_g}$ is the group index of the mode we conclude that

$$\mu = \frac{\epsilon_{si} - n_f n_g}{\epsilon_{si} - \epsilon_{air}} \tag{4.5}$$

Here n_f is the modal phase index, while n_g is the modal group index (defined by e.g. $v_g = \frac{c}{n_f - \lambda \frac{\partial n_f}{\partial \lambda}}$). We may therefore estimate the fraction of the field propagating in air, using only one numerical differentiation. This method is preferred in this thesis, since the method of evaluating the fraction of the power propagating in air, directly from the wave-vectors poses some problems by itself (the purpose of introducing the effective tensor into the plane-wave method is to be able to obtain correct eigenvalues using a limited number of basis functions [54]. This, on the other hand, makes it ambiguous to evaluate how much of the field is propagating in air, since the plane-wave mesh used to describe the dielectric structure is in effect to small).

The resulting calculations is depicted in **Figure 4.2**. It is noticed that the value is independent of the wavelength at long wavelengths. This is the region where the fiber is not truly guiding a confined mode. However, as the frequency is increased and the fundamental mode becomes truly guided, the field gradually escapes the air-holes. Again one finds a clear power law of the way the field escapes the air-holes-, this may be generalized to illustrate the way the fundamental mode behaves in periodic dielectric structures. At short wavelengths the amount of the field that is propagating in air is with good accuracy proportional to the square of the wavelength. As one would expect it is further seen that larger air-holes tend to imply that a larger portion of the electromagnetic energy is propagating in air.

The maximum fraction of the field propagating in air that may be obtained depends on the values of $\frac{D}{\Lambda}$ and Λ that is considered feasible, however, it appears that the suggested value of 40% of the field propagating in air is not an unrealistic value, though it will require small structures with large air-filling fractions.

4.3 The Core Size of Large-Core Fibers

Since PCFs reaches only finite V_{eff}-values, only a finite number of modes are guided by these fibers, irrespective of the wavelength. Still, one may obtain a very large index step, compared to traditional step-index fibers, since the effective cladding index may be as low as approximately 1.1. In some aspects a constant V_{eff}-value may be seen as ideal. It offers the possibility of a fiber with a mode-field area, that is almost independent of the wavelength. Such a fiber may be seen as a low-Δ fiber at long wavelengths and as a high-Δ fiber

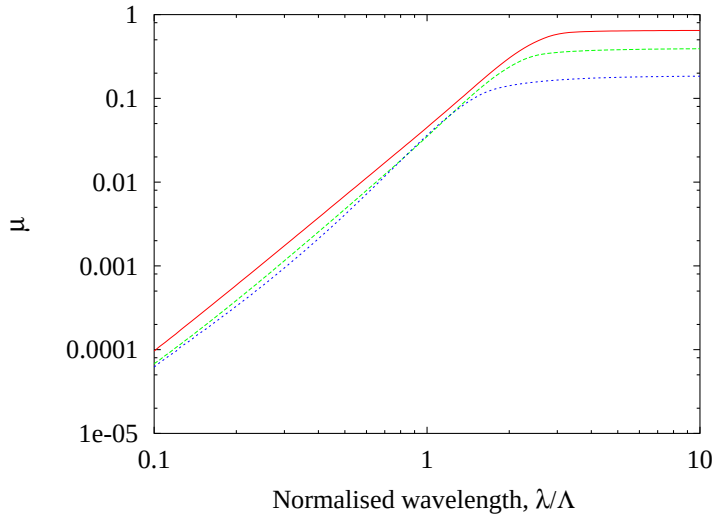

Figure 4.2: The fraction, μ, of the power of the electromagnetic field, that is propagating in air, as a function of the normalized wavelength, $\frac{\lambda}{\Lambda}$. The design is cladding air-holes on a triangular lattice, with air-hole diameters (from the bottom at large normalized wavelengths) $D = 0.4\Lambda$, $D = 0.6\Lambda$, $D = 0.8\Lambda$ respectively. The core-region is formed by omitting the central air-hole

(relatively) at short wavelengths. The numerical aperture will, therefore, be wavelength dependent, as will the bending losses.

Still, in many situations it is attractive to have a fiber with a constant effective mode-field area. As an example one would like a good modal overlap between the pump wavelength (typically 980 nm wavelength) and the signal wavelength (typically 1550 nm wavelength) in an Erbium fiber amplifier, in order to obtain a good conversion of pump power to signal power. This is possible by using a fiber with a constant V_{eff}-value.

Since V_{eff} of micro-structured cladding structures does not become independent of the wavelength at short normalized wavelengths, $\frac{\lambda}{\Lambda}$ such a fiber will have a large structure size, Λ, compared to the wavelength, and therefore the effective mode-field area will be large. This may be of interest for high-power applications, however, the issues of cut-off properties and bending losses should be addressed to obtain efficient fiber designs.

It has already be shown that large air-filling fractions in the cladding lead to PCFs that eventually become multimode. However, large cladding air-

holes also provide large V_{eff}-values because of a larger numerical aperture. It would, therefore, be ideal to have a cladding air-filling fraction that is just small enough to ensure that the fiber is single-mode at all frequencies, since this would give the most bending resistant PCF at all frequencies. However, since V_{eff} only varies very little with the wavelength, it is quite difficult to determine whether the fiber is single-mode or multi-mode at a given wavelength, when the air-filling fraction is near this critical size. Numerical simulations suggest that the fiber is singlemode when $\frac{D}{\Lambda} = 0.45$ but multimode when $\frac{D}{\Lambda} = 0.5$. Measurements on real PCFs drawn at Crystal Fibre A/S confirm these estimates, however, it is equally difficult for the experimentalists to decide exactly at which wavelength a PCF with e.g. $\frac{D}{\Lambda} = 0.5$ becomes multimode, since V_{eff} varies only slowly with the wavelength. For safety, one may state that PCFs with $\frac{D}{\Lambda} \leq 0.45$ are single-mode at all wavelengths.

Different schemes may be used to evaluate the bending losses. One may calculate or measure a critical bending radius, or one may use a step-index fiber analogy and calculate the bending losses of the corresponding step-index fiber. Since it is known that the guided modes resemble Gaussian profiles, this is expected to give good indications of the bending losses of PCFs. In [50], the power loss coefficient, α, due to macro-bending was calculated from a well-known formula from standard fiber optics:

$$\alpha = \frac{\sqrt{\pi} A_e^2 \rho exp(R\frac{-4\Delta W^3}{3\rho V_{eff}^2})}{4PW\sqrt{(\frac{WR}{\rho} + \frac{V_{eff}^2}{2\Delta W})}} \tag{4.6}$$

where Δ is the relative index difference between the refractive index of the core and the cladding, ρ is the core radius, W is the normalized decay parameter in the cladding, A_e is the amplitude coefficient of the cladding electric field, P is the propagating power carried by the fundamental guided mode and R is the curvature radius. Using this method one finds that the macrobending losses become excessive at 1550 nm wavelength (larger than 1 dB/km) for $\frac{D}{\Lambda} = 0.45$, if Λ exceeds approximately $10\mu m$. Fibers drawn at Crystal Fibre A/S suggest that this is indeed the limit where macro-bending losses become a limitation to the performance of the fiber.

In a standard step index fiber, the bending losses are large at long wavelengths, but decreases as the frequency (and V_{eff}) is increased. PCFs also have large bending losses at long wavelengths, since the effective cladding is constant at long wavelengths. At short wavelengths, however, Δ decreases with the square of the wavelength, while V_{eff} is independent of

the wavelength in PCFs. Therefore, α eventually begins to increase with the frequency in PCFs (see **Figure 4.3**) or the structural size, Λ since the structure size scales linearly with the normalized frequency, **Figure 4.4**, [50]- the bending losses at short wavelengths in micro-structured fibers is a result of the same effect that ultimately ensures that PCFs may be made single-mode at all frequencies, namely the increasing effective cladding index as the frequency is increased. In [69, 70] it was shown that the bending losses predicted from this model fits experimental measurements on bending losses. It should be mentioned that the micro-bending losses of photonic crystal fibers have been predicted to be of comparable magnitude to those of step index fibers [71].

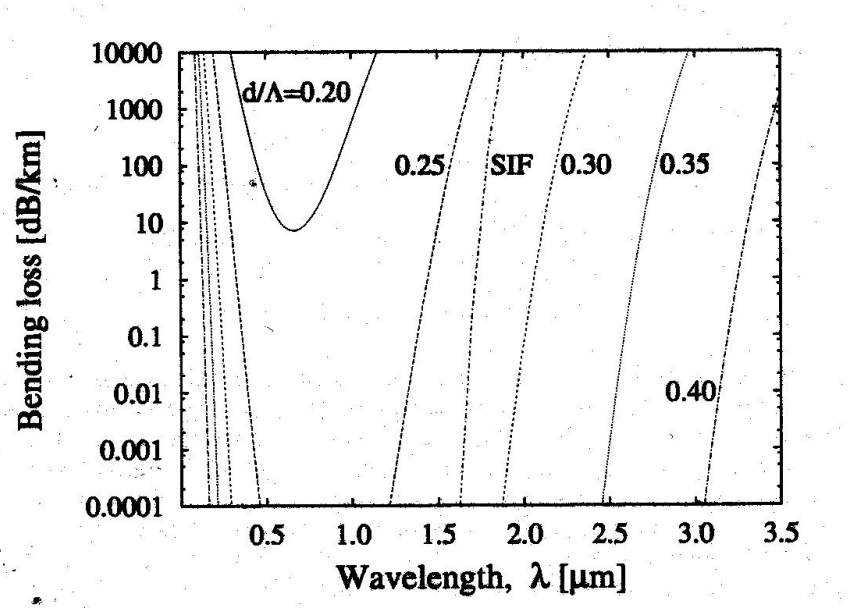

Figure 4.3: Bending losses as a function of the wavelength for PCFs with the interhole distance, $\Lambda = 2.3\mu$m. The normalized hole diameter, $\frac{D}{\Lambda}$ is parameter. The curve labeled 'SIF' shows the bending losses of a standard step index fiber with a core radius of 1.45μm and a refractive index difference of 0.01 at 1.3 μm wavelength. Kindly borrowed from [65]

In single-mode step index fibers, the core cannot be made too large because the doping levels become too small to be able to control. Also the bending losses eventually become excessive. In PCFs, the limitation on the

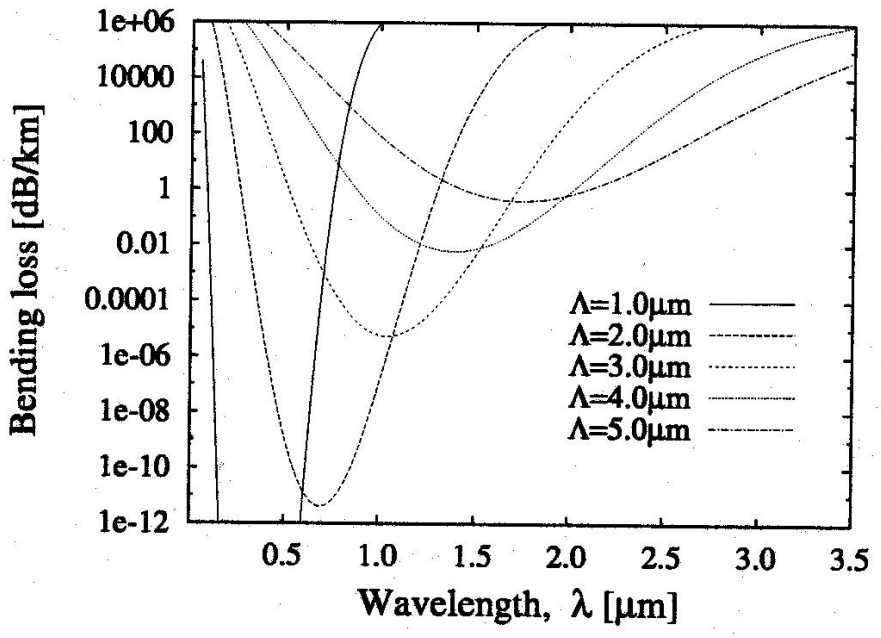

Figure 4.4: Bending losses as a function of the wavelength for PCFs with normalized hole diameter, $\frac{D}{\Lambda} = 0.25$. The interhole distance, Λ is parameter. Kindly borrowed from [65]

maximum core-size that may be employed depends on the control of the air-holes, and is ultimately limited by bending losses. Still, as will be shown, large core PCFs have significant advantages, compared to large core step index fibers.

Even though the bending losses is the ultimate limitation to the core size that is possible to obtain in single-mode fibers (this holds true for both PCFs and step-index fibers), one important difference is the different way the fibers behave with the wavelength. As an example, consider again an erbium fiber amplifier. We will assume the fiber is designed to have as low bending losses as possible at the pump wavelength (980 nm), that is we will assume that V_{eff} is approximately 2.4 at the pump wavelength. Since bending losses increase with the wavelength in step-index fibers, the bending losses at the signal wavelength (1550 nm) are higher than the bending losses at the pump wavelength for the step-index fiber. The limitation on the core-size (linked to the bending losses, which is the ultimate limitation to the core-size), is therefore the combined demand that the bending losses

must be acceptable at 1550 nm wavelength, while the core-size must be sufficiently small to ensure the fiber is singlemode at 980 nm wavelength.

Designing the erbium fiber amplifier as a PCF this changes dramatically. Now one may have $V_{eff} \approx 2.4$ at both the pump and the signal wavelengths. This would give a PCF with an effective mode-area, that is almost equally large at both wavelengths. Further, the bending losses at the signal wavelength would be lower than the bending losses at the pump wavelength, since the bending losses of PCFs decrease with the wavelength in the region where V_{eff} is almost independent of the wavelength. The relevant demands on the PCF is, therefore, a fiber that is singlemode at the pump wavelength, and which also has acceptable bending losses at the pump wavelength. It is correspondingly possible to design the PCF with a larger core-region than the corresponding step-index fiber, since one does not need to design for acceptable bending losses at the signal wavelength. Furthermore, one may obtain a better overlap between the pump and the signal, since the constant V_{eff}-value corresponds to an almost constant effective mode-area. It should be noticed that these possible advantages for erbium amplifier PCFs come at the cost of a lower numerical aperture at the pump wavelength, since the larger core is made possible by a smaller relative effective index step, Δ between the core and the cladding.

I have chosen to stress this point since it has, at times, been described as if PCFs offer a way of relieving the bond between core-size and bending losses [49]. This is not so, since the mode-shape is near Gaussian in both PCFs and step-index fibers the bending loss limitation makes almost equal effective mode-areas possible, rather the advantages on core-size of PCFs are linked to avoiding the problems of very small dopant levels (thereby avoiding possible clustering phenomena). Also PCFs have novel wavelength dependencies that in some cases may offer significantly larger core-sizes. This is linked to the possibility of a near wavelength independent V_{eff}-value, and further gives the possibility of a good modal overlap between e.g. pump and signal in fiber amplifiers, since the effective mode-area is ultimately linked to the combination of the core-size and V_{eff}.

One further advantage of using PCFs as large-core single-mode fibers, is that the waveguide group velocity dispersion of large-core PCFs is positive, while the waveguide group velocity dispersion of large-core step-index fibers is negative. Since the material dispersion at 1550 nm wavelength is positive, this implies that the group velocity dispersion of large-core PCFs will be more positive (and have a more positive slope) than the group velocity dispersion of large-core step-index fibers. This gives the possibility of reducing nonlinear effects related to a near zero dispersion even further with PCFs.

Also, nonlinearities related to dopant materials may be avoided in PCFs, since PCFs may be made without the usage of any dopant materials.

In **Figure 4.5** is depicted the cross-section of a Photonic Crystal Fiber designed to have a large core while remaining single-mode. The core-size is approximately 15μm, while the effective mode-area is estimated to be approximately $100\mu\text{m}^2$. Impressive figures, that reveal the skill of Crystal Fibre A/S- the limitation on the core-size is the bending losses and not difficulties with the control of dopant levels, since the fiber is manufactured without the introduction of any dopant material.

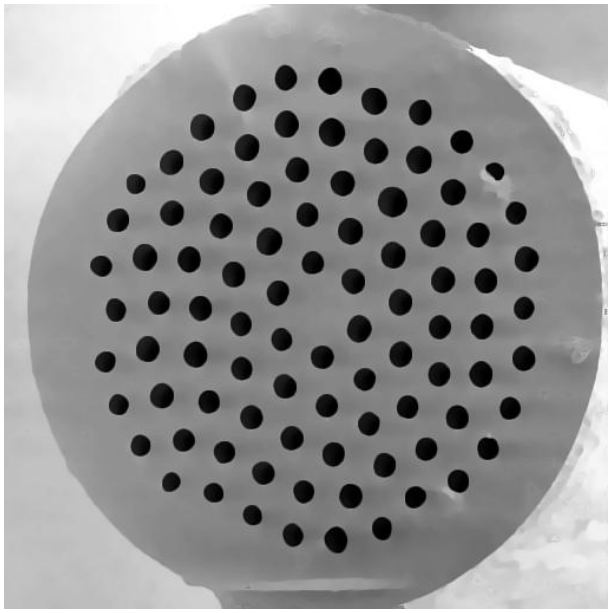

Figure 4.5: A picture of a large core micro-structured fiber produced at Crystal Fibre A/S. The core diameter is approximately 15μm. The fiber is produced using a stack and pull technique [18]. Kindly borrowed from Crystal Fibre A/S

The topic of dopants in micro-structured fibers has mainly been addressed because of the possibility of a fundamental mode cut-off [72],[73]. In **Figure 4.6** is shown the effect of doping the core region for a fiber with a cladding air hole diameter of $D = 0.6\Lambda$. The purple curve shows V_{eff} as a function of the normalized wavelength for the case where no doping material is introduced to the core region. Introducing e.g., Germanium to raise the core index by 0.01 the light blue curve is obtained. As an effect V_{eff} no

longer approaches a constant value, corresponding to a fiber that will guide an arbitrary large number of modes as the wavelength moves approaches zero. However, introducing e.g. fluorine to lower the core index by 0.002 (blue curve), 0.005 (red curve) or 0.01 (green) curve the fiber obtains a first order cutoff at short wavelengths, since V_{eff} drops below zero. However, notice that a plateau of almost constant V_{eff} values exist in these fibers.

A V_{eff} value that is independent of the wavelength corresponds to a mode field cross-section that is almost independent of the wavelength (apart from the energy leaving the air holes at shorter wavelengths). A theoretical test fiber was, therefore, calculated upon to see if a good overlap could be found for such a fiber between the pump wavelength (980 nm) and the signal wavelength (1550 nm) of an Erbium amplifier. The only difference from the standard design was a decreased index of the background material near the core region (lowered by 0.05). The calculated overlap was found to be better than 99.87%, showing the potential of these fibers for Erbium amplifiers. Also it is noticed that the wavelength regions where a plateau of almost constant V_{eff}-values depend on the doping level. Therefore, one may tune the core size by tuning the doping levels. Work is underway to investigate these structures further.

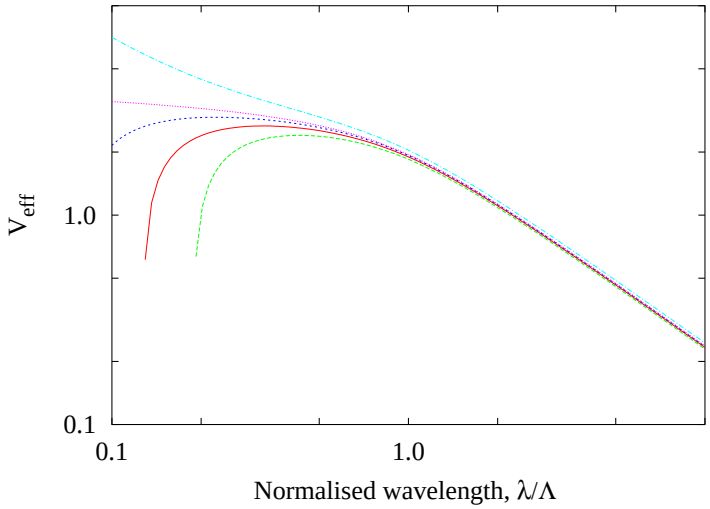

Figure 4.6: The influence of doping the core region. V_{eff} is seen to have an almost constant value before it drops toward zero when the core is doped to a lower refractive index. This is almost ideal for amplifier purposes.

4.4 Group Velocity Dispersion

The group velocity dispersion is given as:

$$GVD = -\frac{\lambda}{c_0}\frac{d^2(\frac{\beta}{k})}{d\lambda^2} \tag{4.7}$$

Therefore if $\frac{d^2(\frac{\beta}{k})}{d\lambda^2} > 0$ then the group velocity dispersion is negative, while the group velocity dispersion is positive if $\frac{d^2(\frac{\beta}{k})}{d\lambda^2} < 0$.

In **Figure 4.7** is shown the cladding index and the mode index of the fundamental guided mode of a PCF with $\frac{D}{\Lambda} = 0.6$. The abrupt rising of the mode index of the guided mode is associated with an upward curvature, corresponding to a negative group velocity dispersion. This is in agreement with the field being localized to the high index silica core, according to the expression for the group velocity of a guided mode, since this corresponds to a lower group velocity:

$$v_g = c_0\frac{\beta}{k}\frac{\int_A(\mathbf{H}\times\mathbf{E}^*)\cdot\mathbf{z}dA}{\int_A \epsilon\mathbf{H}\times\mathbf{E}^*dA} \tag{4.8}$$

By comparing **Figure 4.2** with **Figure 4.7** it is seen that the guided mode only has a significant portion of the energy flowing in the air-regions when the waveguide group velocity dispersion is negative. At shorter wavelengths the group velocity, therefore, becomes almost proportional to the mode index, $v_g \approx \frac{c}{n_{si}^2}\frac{\beta}{k}$ of the guided mode, corresponding to a positive group velocity dispersion. This is in agreement with the downward curvature of the mode index seen in **Figure 4.7** and further ensures that the mode index does not increase to values above the refractive index of the background material, silica. It can be shown that $n_g - n_{si} \approx n_{si} - \frac{\beta}{k}$ in the limit where the normalized wavelength approaches the refractive index of silica. Here n_g denotes the group index of the guided mode. This is illustrated in **Figure 4.7**, but may also be realized by considering the following expressions:

$$\begin{aligned} v_f &= \frac{c}{\frac{\beta}{k}} \\ v_g &\approx \frac{c}{n_{si}^2}\frac{\beta}{k} \\ \frac{d(v_f)}{d(\frac{\beta}{k})} &= -\frac{c}{(\frac{\beta}{k})^2} \end{aligned}$$

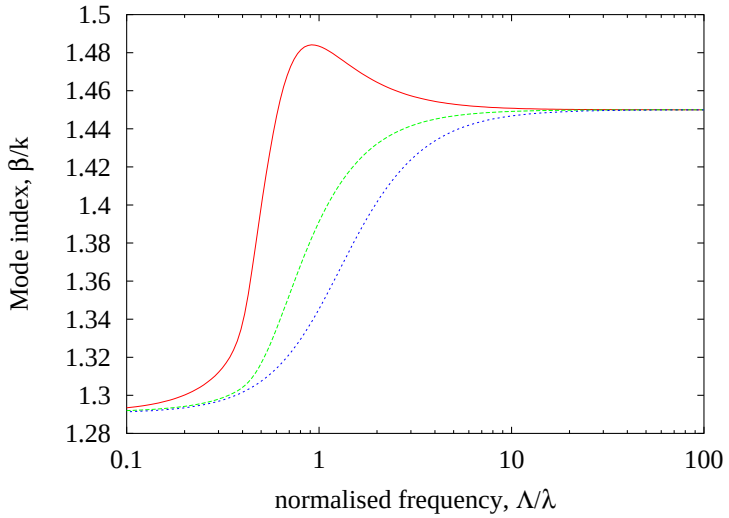

Figure 4.7: The modal index of the fundamental mode of a PCF with a cladding air hole diameter of 0.6Λ. The phase index of the guided mode (green curve), the group index of the guided mode (red curve) and the fundamental cladding index is shown as a function of the normalized frequency, $\frac{\Lambda}{\lambda}$.

$$\frac{d(v_g)}{d(\frac{\beta}{k})} \approx \frac{c}{n_{si}^2} \tag{4.9}$$

(4.10)

$\frac{\beta}{k}$ eventually approaches n_{si}. Therefore, also $\frac{d(v_f)}{d(\frac{\beta}{k})}$ eventually approaches $-\frac{d(v_g)}{d(\frac{\beta}{k})}$. Since both the group index and the phase index approaches n_{si} at short normalized wavelengths we are led to the above stated conclusion that $n_g - n_{si} \approx n_{si} - \frac{\beta}{k}$ at short normalized wavelengths.

For a step index fiber, the fundamental guided mode will also display anomalous waveguide dispersion, however, the fiber will be multimode when the fundamental mode has anomalous waveguide dispersion. The fundamental mode in a step index fiber must display anomalous waveguide dispersion when the normalized propagation constant, B, approaches 1:

$$B = \frac{\frac{\beta}{k} - n_{cl}}{n_{co} - n_{cl}} \tag{4.11}$$

When B approaches 1, however, the fiber is multimode. In a PCF, the

anomalous waveguide dispersion is not directly linked to B approaching 1, rather it is the result of the mode index, $\frac{\beta}{k}$ approaching the refractive index of the core-region. Actually, calculations show that B never approaches 1 in PCFs that are singlemode at all wavelengths [66], leading to the conclusion that a step index analogy may be used even to explain how PCFs may display anomalous waveguide dispersion in singlemode fibers.

That B never approaches 1 may be seen from **Figure 4.8** and **Figure 4.9**. In **Figure 4.8** is shown the cladding index (green curve), the mode index of the fundamental guided mode (blue curve) and the effective index of a honeycomb structure corresponding to the core region (red curve). One may wonder, if the red curve or the refractive index of silica gives the best approximation of the core region, since the mode index tend toward the honeycomb index as the frequency is increased (it also tend toward the refractive index of silica, as discussed earlier).

This is investigated in **Figure 4.9**, where the normalized propagation constant B is shown as a function of the effective frequency, V_{eff}. The red curve shows the values found for the micro-structured fiber when assuming $n_{co} = n_{si}$ and the core radius $\rho = \Lambda$. The agreement with the step index fiber with a refractive cladding index that varies as the effective cladding index of the PCF (green curve) is rather poor. However, choosing $\rho = 0.58\Lambda$ for the photonic crystal fiber (black curve) a good agreement is found with the step index fiber analogy (green).

Since V_{eff} only reaches finite values in PCFs, B does not increase to one as the frequency of light is increased, as it would in a step index fiber analogy. This is possible since both the cladding index and the mode index tend toward n_{si} as the wavelength tends toward zero, and therefore the value of B may tend to any value between 0 and 1. **Figure 4.9** shows that by choosing the proper core radius B tend to the value expected from standard step index technology.

Choosing the honeycomb index as the core index ($\rho = \Lambda$) the blue curve is obtained. The value of B now tend toward 1 for smaller values of V_{eff}, however, one cannot remedy the curve to fit a step index analogy by choosing a larger core radius. We are forced to conclude that the best representation of the effective core index is indeed the refractive index of silica in agreement with the observation that the modal energy is situated in the central silica region at short wavelengths. This is again in agreement with the finding that PCFs can display positive waveguide dispersion while being single mode- both the values of B and V_{eff} are sufficiently limited to make this possible.

This novel possibility of anomalous waveguide dispersion in single mode fibers has important implications. A single mode step index silica based fiber

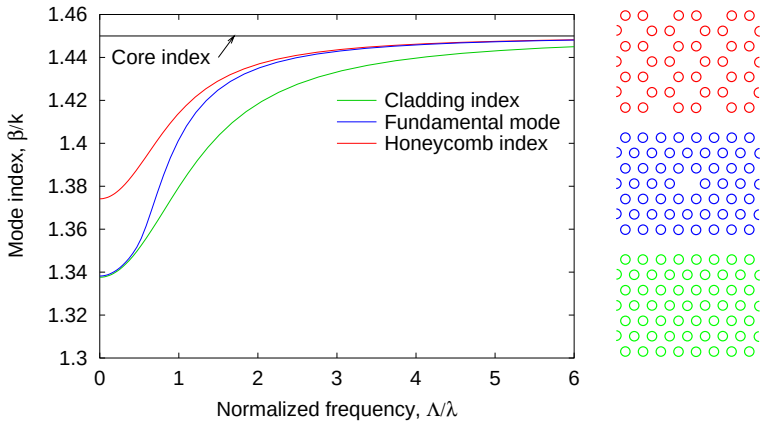

Figure 4.8: The modal index of the cladding structure, the guided mode and the central honeycomb analogy as a function of the normalized frequency. Kindly borrowed from [74]

will always have a negative group velocity dispersion for wavelengths below $1.3\mu m$, since both the material dispersion and the waveguide dispersion is negative. Using a PCF, it becomes possible to design a fiber with positive waveguide dispersion that may be used to counteract the negative material dispersion, thus offering the possibility of fibers with near-zero dispersion at short wavelengths [43]. This is interesting, because a near zero group velocity dispersion is an advantage for numerous nonlinear processes such as Four Wave Mixing and soliton formation. Non-linear processes are most efficient when the core-sizes are small (corresponding to small effective mode areas). It is, therefore, important to understand the way the group velocity waveguide dispersion is linked to the core-size of PCFs.

4.5 The Core Size of PCFs

In this section, the possibility of designing PCFs with very large numerical aperture will be considered. Such fibers may be used for e.g. nonlinear effects, and have attracted quite some attention as e.g. white light generators.

The very low effective cladding indices that are attainable using PCFs, indicate that fibers with a very large numerical aperture should be feasible. Indeed, it has been found that PCFs with an effective mode area as small as 1 $(\mu m)^2$ are possible [68]. Let us first consider the core-size of PCFs with normal waveguide dispersion.

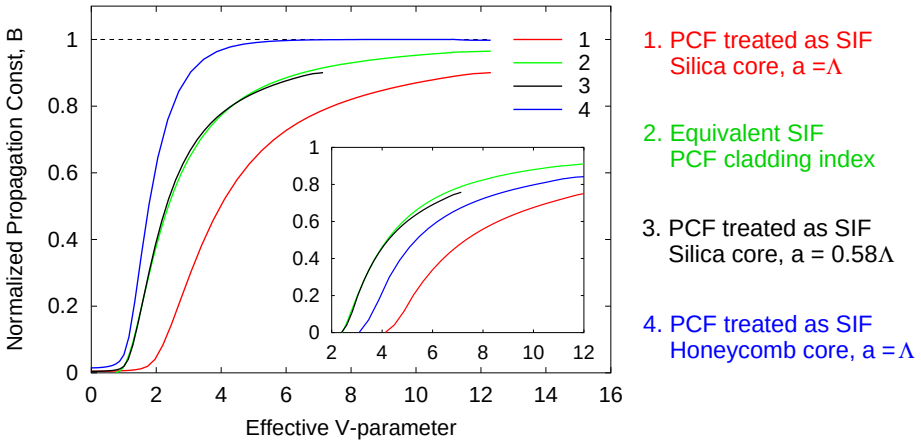

Figure 4.9: B as a function of V_{eff} for different choices of the core index and the core radius. A choice of 0.58Λ for the core radius and n_{si} as the effective core index gives good agreement with the expectations from step index fibers. The inset shows good agreement with the step index analogy for the second order mode as well. Kindly borrowed from [74]

In **Figure 4.10** is shown the mode index for a number of PCFs with different air filling fractions. It is seen that the upward curvature of the mode index curve, corresponding to a negative group velocity dispersion is found at relatively long normalized wavelengths, corresponding to small core-sizes. The strong negative group velocity dispersion is a result of less energy propagating in the cladding air holes as the frequency is increased. This is an effect similar to step index fibers, where the negative group velocity dispersion occurs when an increasing fraction of the energy propagates in the central high index core as the frequency is increased, and thereby causes a decreasing group velocity.

At shorter normalized wavelengths one finds positive group velocity dispersion. As shown earlier (4.3) the effect of a larger fraction of the energy propagating in the high index regions of the fiber, as the frequency is increased, corresponds to a group velocity that increases with the wavelength. This is counteracted by the rising mode-index as the frequency is increased, since this corresponds to an increasing group velocity (4.3). The anomalous waveguide dispersion is a result of the rising mode index having more effect on the group velocity than the extinction of the field from the air holes as the frequency is increased. This occurs when the fraction of the field that

is propagating in air is relatively modest, corresponding to a mode that is propagating almost entirely in the central silica core region.

By comparing **Figure 4.2** and **Figure 4.10** it is seen that the fraction of the modal energy that is propagating in the air holes is modest (typically less than a percent of the energy is propagating in air, when strong anomalous dispersion occurs). This compares to step index fibers, where the field is well localized to the core region, when the fundamental mode has anomalous dispersion.

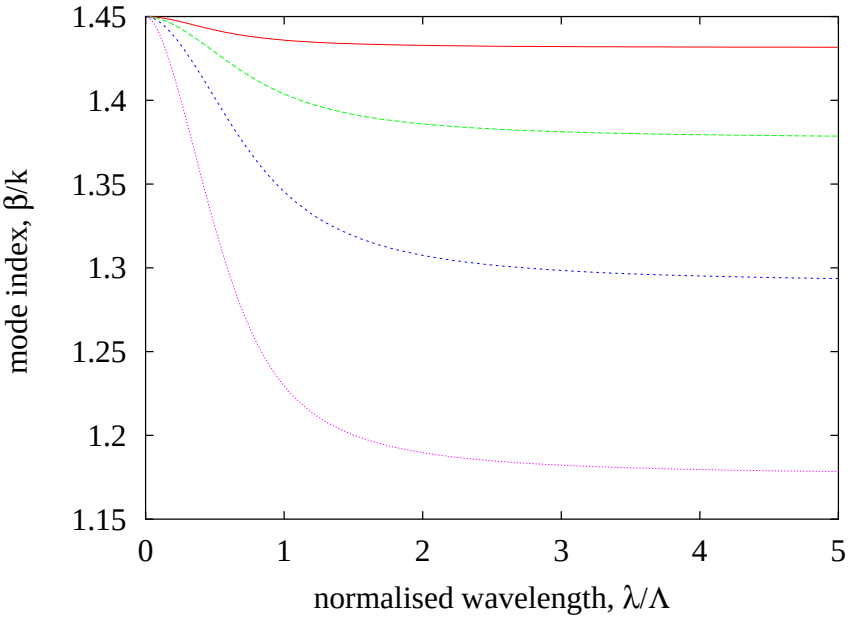

Figure 4.10: The mode index as a function of the normalized wavelength, $\frac{\lambda}{\Lambda}$ for PCFs with air holes on a triangular lattice. The core-region is created by the omission of the central air hole. The cladding air hole diameter is- $D = 0.2\Lambda$ (red curve), $D = 0.4\Lambda$ (green curve), $D = 0.6\Lambda$ (blue curve), $D = 0.8\Lambda$. (purple curve)

Consider the design of a PCF that is intended to guide light at a certain wavelength, λ_0. In the normalized wavelength region where the PCF has anomalous dispersion the field is almost entirely propagating within the central silica core region. The effective mode area is, therefore, proportional to Λ^2, and one may conclude that large values of the interhole distance lead to large effective mode areas. This implies that PCFs with strong anoma-

lous waveguide dispersion also have small cores, and small effective mode areas. This gives the possibility of counteracting the negative group velocity material dispersion at wavelengths shorter than 1300 nm, while having very small effective mode areas. This again offers the possibility of nonlinear fibers with zero dispersion at wavelengths below 1300 nm, even down to 600 nm wavelength. Due to especially self phase modulation and four wave mixing, this makes it possible to generate white light from femtosecond pulses. An example of a nonlinear fiber made for white light generation is shown in **Figure 4.11**. By pumping this fiber with femtosecond pulses, the white light spectrum depicted in **Figure 4.12** is obtained. **Figure 4.13** shows the many-colored light after passing through a prism.

A remark should be made about the need for single mode nonlinear fibers. PCFs with very high numerical aperture combined with strong anomalous waveguide dispersion are often, strictly speaking, multimode. However, the modal index difference between the fundamental and the higher order modes is sufficiently large to ensure that light do not couple from the fundamental mode to higher order modes. Furthermore, the core region (and the effective mode area) is sufficiently small to ensure, that it is unlikely that light will be coupled into the higher order modes by accident. Therefore, one is generally not concerned that these fibers are in fact multimode. Still, it is possible to design micro-structured fibers for white light generation that are truly single mode.

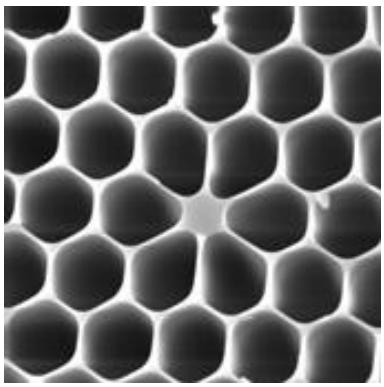

Figure 4.11: A nonlinear fiber manufactured by Crystal Fiber A/S. This fiber is efficient for generating white light from femto second pulses. Kindly borrowed from Crystal Fibre A/S

To illustrate the radical new possibilities micro-structured fibers offer

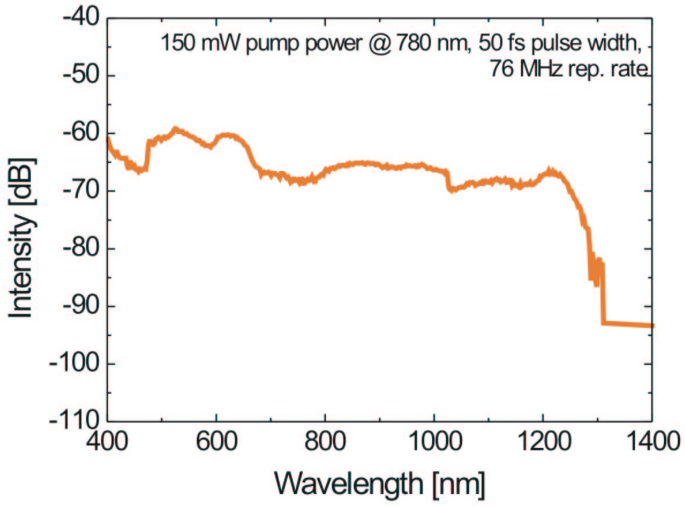

Figure 4.12: The white light spectrum obtained when pumping the fiber from **Figure 4.11** with femtosecond pulses. Measurements by Kakob Juul Larsen, Århus university. Kindly borrowed from Crystal Fibre A/S. Courtesy NKT Research.

within the field of nonlinear optics, the numerical aperture that is possible to obtain is depicted in **Figure 4.14**. The numerical aperture is defined as: $NA = \sqrt{n_{co}^2 - n_{cl}^2}$. Since the refractive index difference between the core and the cladding is rarely larger than 0.02, the numerical aperture of step index fibers is generally below 0.25. However, photonic crystal fibers offer the possibility of a numerical aperture approaching 1, as seen in **Figure 4.14**. Also notice that the numerical aperture may be wavelength dependent in micro-structured fibers, as a result of the wavelength dependent cladding index.

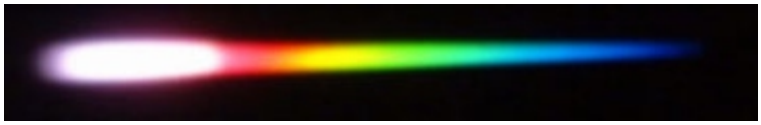

Figure 4.13: The spectrum from **Figure 4.12** visualized by sending it through a prism. Experiment by Erling Riis, Strathclyde university, Glasgow. Kindly borrowed from Crystal Fibre A/S. Courtesy NKT Research.

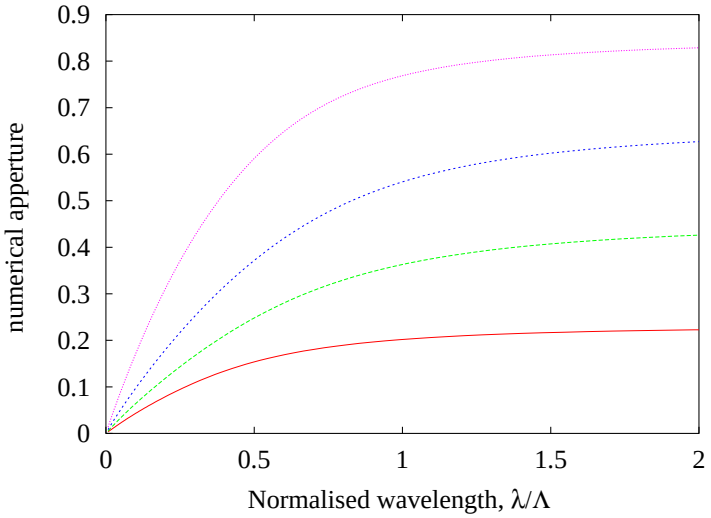

Figure 4.14: The numerical aperture of micro-structured fibers as a function of the normalized wavelength. The diameter of the cladding air holes is parameter, $D = 0.2\Lambda$ (red), $D = 0.4\Lambda$ (green), $D = 0.6\Lambda$ (blue), $D = 0.8\Lambda$ (purple)

4.6 Summary of Chapter 4

Basic properties of index guiding micro-structured fibers may be modeled using a step index fiber analogy. Such a model is capable of predicting that only a finite number of modes will be guided in simple micro-structured fibers, since the effective cladding index approaches the core index at short normalized wavelengths. This is also the reason for the special bending properties of these fibers, since they have increasing bending losses both at wavelengths that are longer and shorter (!) than the wavelength range with acceptable bending losses.

Using the model described in chapter 2, it was found that a substantial portion of the energy can propagate in the air holes, when the interhole distance is small, corresponding to a fiber where the fundamental modes see the cladding structure as an effective refractive index structure. At shorter normalized wavelengths, corresponding to a larger structure scale for a given wavelength, the field is increasingly expelled from the air holes. This is accompanied by a positive group velocity dispersion.

Micro-structured designs may be employed as large core fibers for non-

linear purposes, or alternatively highly nonlinear fibers for continuum generation. Or one may design a fiber with a mode area comparable to standard fibers and obtain new wavelength dependencies. This may be exploited for e.g. fiber amplifiers, especially when lowering the refractive index of the core region.

Chapter 5

Photonic Bandgap Fibers

Micro-structured fibers offer a range of new possibilities. In this chapter, the most radical type of micro-structured fibers- photonic bandgap fibers- will be investigated. The chapter will focus on describing some basic properties and thereby illustrate some new possibilities compared to fibers that are not guiding by the photonic bandgap effect. Also a number of different designs, based on the honeycomb and the kagomé structures, will be shown. The honeycomb and the kagomé lattices may also be used as cladding structures in PCFs that guide light by modified Total internal reflection, however, PCFs based on the honeycomb and the kagomé lattices appear to especially prove their worth as PBG fibers.

One particular photonic bandgap fiber design will not be discussed in detail in this thesis, namely the air guiding fiber [21]. The author recognizes the tremendous potential of being able to guide light almost completely in air, and has also performed work in this field [75, 76], however, the designs discussed for the air-guiding fiber are not fundamentally different from the photonic bandgap designs discussed in this thesis- apart from having photonic bandgaps that extend below the air line. Indeed, a photonic bandgap structure will be presented in the next chapter that allow more than half of the modal energy to propagate in air. The author, therefore, believes that a discussion of the air guiding PBG fiber designs will add little qualitative substance to the discussion presented in this chapter.

5.1 The Honeycomb Fiber Structure

The design of a Honeycomb PBG fiber [19, 77] is shown schematically in **Figure 5.1**. It is noticed that the central core region is formed by adding

an extra air hole [20, 47, 48]. This implies that the core region has a lower effective index than the surrounding cladding region and, therefore, seems to be in contradiction to the principle of total internal reflection, that demands a high index core-region. However, despite the fact that many qualities offered by micro-structured fibers may be understood by using a simple step index analogy, there is one fundamental difference between a homogeneous material and periodic dielectric structures. Any mode will be allowed to propagate through a homogeneous dielectric (of infinite extent), if its effective mode-index (in the direction of propagation) is below the refractive index of the dielectric. This is not the case with two-dimensional periodic dielectrics. If the mode index (in the invariant direction of the periodic dielectric) is within a Photonic Bandgap (PBG) of the dielectric, the mode will not be an extended solution to Maxwell's equations [10, 78].

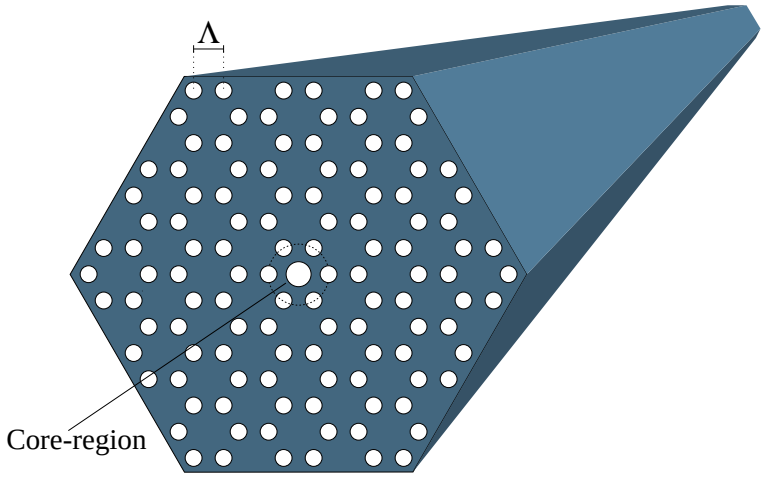

Figure 5.1: Schematic representation of a PBG fiber with cladding air holes on a honeycomb lattice structure. Notice the defect hole at the center of the PCF. The interhole distance, Λ is defined by the Figure.

In PBG fibers light may, therefore, be guided along a core-region with an effective core-index below the effective cladding index, provided the mode index lies within a PBG of the surrounding cladding structure [79, 80, 81, 82]. This is illustrated in **Figure 5.2**, where the effective cladding index as well as the effective mode index below the effective cladding index is shown. However, the effective mode index lies within the PBG boundaries of the fundamental photonic bandgap and, therefore, the mode is a strictly guided

mode (assuming the cladding is of sufficiently large extend).

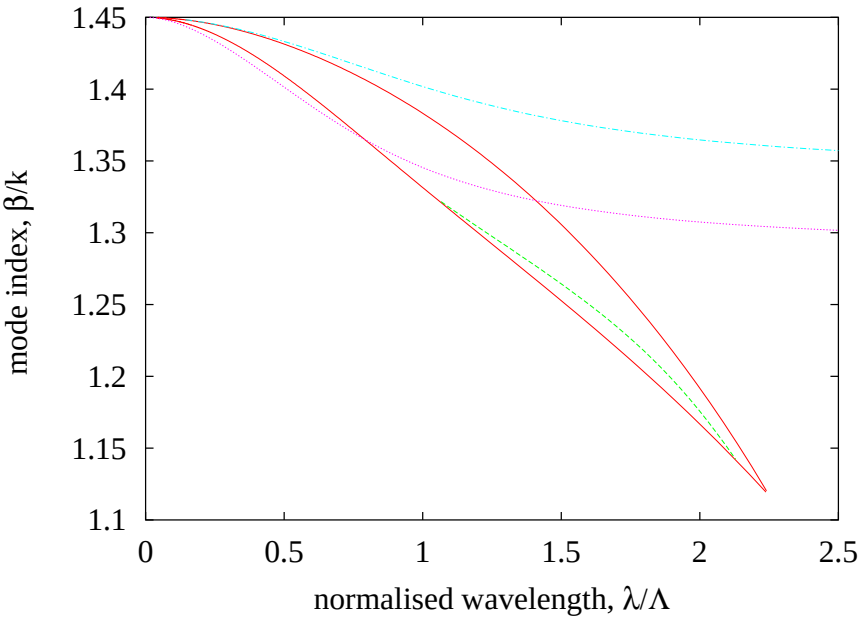

Figure 5.2: The mode index of the guided mode in a honeycomb PBG fiber with air hole sizes $D = 0.6\Lambda$ in both the cladding and the core region. The effective cladding (light blue curve) is above the bandgap edges (red curves). The guided mode with the green mode index curve has a mode index below the core index (purple curve), but above the low index PBG edge.

The core region resembles a periodic triangular dielectric structure. To estimate the effective core-index, the effective index of the fundamental mode of the corresponding triangular dielectric structure is also shown in **Figure 5.2**. It is seen that the mode index is below this effective core index, showing that the effective core index should be above the effective mode index of the photonic bandgap edge with the lowest effective index [65]. A mode index below the effective core index corresponds to step index fibers, which always have mode indices below the refractive index of the core region. That the mode-index should be above the PBG boundary with the lowest index, corresponds to the cladding index of step index fibers, which is below the index of the guided modes. However, in PBG fibers some cladding modes have mode-indices above the effective index of the guided modes, e.g. the PBG boundary with a mode index above the mode index of the guided

mode(s).

Figure 5.3 shows the mode index curves of the guided mode for honeycomb fibers, where the cladding air holes have a diameter of 0.6 times the cladding interhole distance. Three different core hole sizes are shown: $d = 0.3\Lambda$, $d = 0.45\Lambda$ and $d = 0.6\Lambda$, where d is the diameter of the central air hole. It is noticed that a fiber with a large core air hole guides light at long normalized wavelengths, while a smaller central air hole leads to a fiber that guides light a shorter normalized wavelengths. Also notice that the width of the wavelength range where light is guided is increased as the size of the central air hole decreases. This is typical of this design of honeycomb fibers.

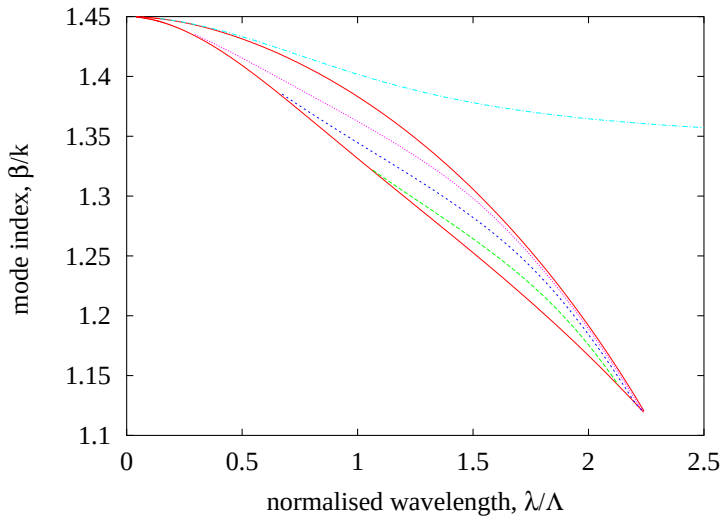

Figure 5.3: The mode index of the guided modes in honeycomb PBG fibers with cladding air hole size $D = 0.6\Lambda$. Three different core hole sizes are represented- 0.3Λ (curve), 0.45Λ (curve) and 0.6Λ (curve)

It is noticed that there is a downward curvature on most of the mode index curves of the guided modes [47]. As the mode index of the guided mode approaches the bandgap edge with the lower index, the guided mode begin to couple to the cladding modes, and a slight upward curvature is seen. This corresponds to a waveguide dispersion that is generally anomalous, however, as the guided mode approaches the low-index bandgap edge the group velocity dispersion becomes slightly negative. It would appear, therefore, that this design is not feasible as standard dispersion compensating fibers, where

a strong negative waveguide dispersion is typically required. The calculated group velocity dispersion (including material dispersion) for fibers with a number of structure sizes (defined in the description of the Figures), based on the designs from **Figure 5.2** is shown in **Figure 5.4**, **Figure 5.5** and **Figure 5.6**

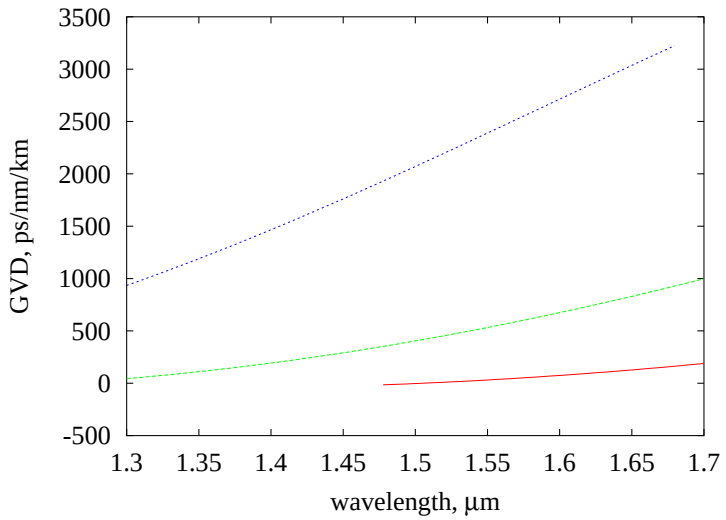

Figure 5.4: The group velocity dispersion for honeycomb fibers with cladding air hole diameters $D = 0.6\Lambda$. The central core air hole has diameter 0.6Λ. $\Lambda = 0.8\mu$m (blue curve), $\Lambda = 1.0\mu$m (green curve), $\Lambda = 1.2\mu$m (red curve)

It is noticed that strong anomalous waveguide dispersion is possible, especially when large central air holes are employed. Strong anomalous dispersion, however, also demands small structural sizes,and may, therefore, seem ideal for nonlinear purposes, where the demand is zero dispersion at short wavelengths. The dispersion curves shown are typical for honeycomb fibers guiding by the PBG effect, however, larger cladding air holes lead to numerically larger dispersion values, while smaller cladding air holes lead to numerically smaller dispersion values.

In **Figure 5.7** is depicted the fraction of the energy of the guided mode that propagates in light for the same three honeycomb fibers. It is noticed that a large central air hole offers the possibility of guiding more light in air, compared to a smaller central air hole. For microstructured fibers with a step index fiber analogy, the fraction of the field that is guided in air was

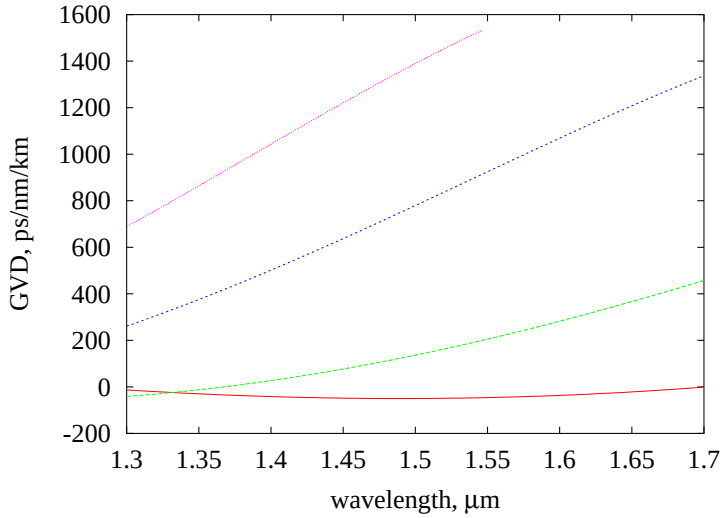

Figure 5.5: The group velocity dispersion for honeycomb fibers with cladding air hole diameters $D = 0.6\Lambda$. The central core air hole has diameter 0.45Λ. $\Lambda = 0.9\mu$m (purple curve), $\Lambda = 1.0\mu$m (blue curve), $\Lambda = 1.2\mu$m (green curve), $\Lambda = 1.5\mu$m (red curve)

found to decrease as the frequency is increased. However, for honeycomb fibers, a more complex behavior is noticed. Moving to shorter normalized wavelengths, the mode initially increases its fraction of energy that is propagating in air. This is caused by the mode being bound to the core by the PBG effect rather than coupling to cladding modes, since the cladding modes near the high index bandgap edge do not have much of the modal energy within the airholes.

At shorter wavelengths, the field become gradually expelled from the air holes by effects similar to the expelling of the field from the airholes as the frequency is increased in index guided micro-structured fibers. Moving to still higher frequencies the guided mode begin to couple to the cladding modes near the low index bandgap edge, and the field become further expelled from the air holes- corresponding to a negative waveguide group velocity dispersion.

Many types of core designs are possible in PBG fibers. **Figure 5.9** shows a design, where the core region is instead formed by enlarging the 6 innermost air holes, again creating a low index core region. **Figure 5.10** shows the calculated mode index curve of the mode guided by this fiber.

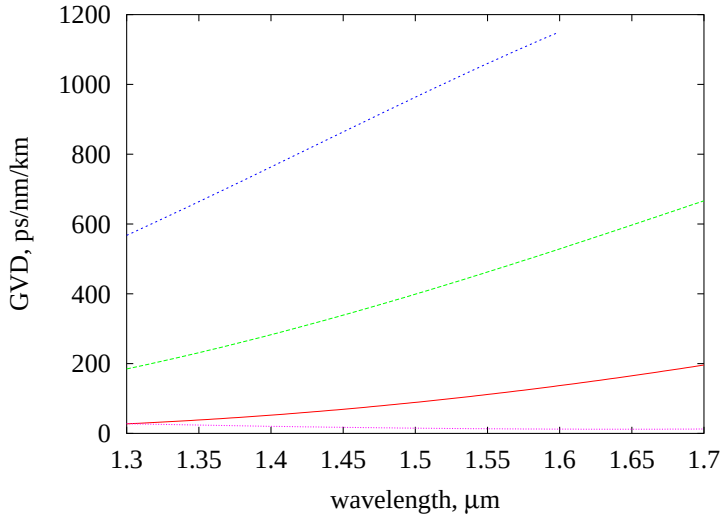

Figure 5.6: The group velocity dispersion for honeycomb fibers with cladding air hole diameters $D = 0.6\Lambda$. The central core air hole has diameter 0.30Λ. $\Lambda = 1.0\mu$m (blue curve), $\Lambda = 1.2\mu$m (green curve), $\Lambda = 1.5\mu$m (red curve), $\Lambda = 2.2\mu$m (purple curve)

Notice that this mode index curve does not bend as strongly as the former honeycomb mode index curves, indicating that this design is more suitable for applications, where near zero group velocity dispersion is desired, such as four wave mixing processes near 1500 nm wavelength. This is an example of a structure, where near zero flat dispersion may be obtained at 1550 nm wavelength of light [47]. In general, more work need to be performed on e.g. the polarization properties of honeycomb PBG fibers [83, 84]

In general, honeycomb fibers tend to demand small structure sizes if a significant portion of the energy is to propagate in air. Also the simple core designs shown in this thesis tend to be single mode. Multimode PBG fibers are possible by enlarging the area of the core region (by e.g. introducing a number of extra air holes to create a core-region with a structure resembling a triangular cladding structure of finite size).

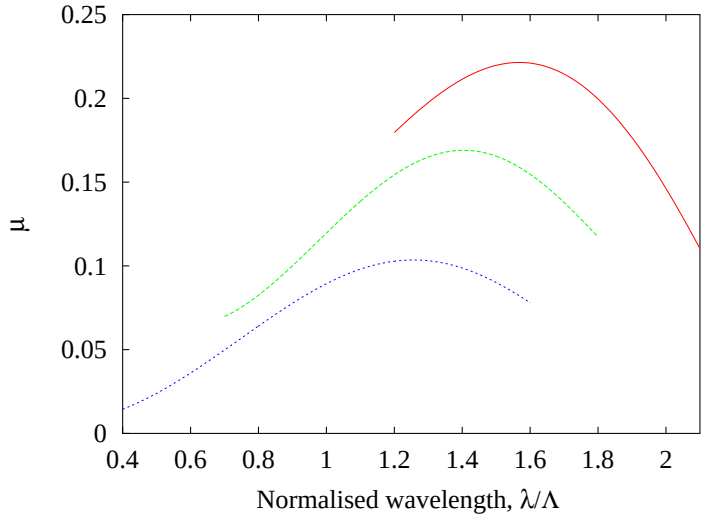

Figure 5.7: The fraction of the energy of the guided mode that is propagating in air. The design is honeycomb fibers with cladding air hole diameters $D = 0.6\Lambda$. The central core air hole has diameter 0.3Λ, 0.45Λ, 0.6Λ

5.2 The Kagomé Structure

The principal design of a PBG fiber with cladding air holes on a kagomé lattice, is shown in Figure 5.11 [85, 86]. Important parameters, such as the inter-hole distance, Λ, the cladding-hole diameter, D, and the defect-hole diameter, d, are also defined here. The extra air hole introduced to create the core-region is also indicated. The kagomé structure is interesting, since it constitutes the third basic hexagonal lattice structure (the other two are the honeycomb structure and the triangular structure). The author has, therefore, made calculations upon a kagomé fiber that is guiding light by the photonic bandgap effect.

The kagomé lattice looks similar to the honeycomb lattice. Both lattices may be described by repetitious use of hexagonals. However, in the honeycomb fiber, the cladding air holes are situated on the corners of the hexagonals, whereas the air holes are situated mid-corners in the kagomé PBG fiber as indicated by **Fig 5.11**. Compared with the triangular lattice cladding design [17], one notices that every third air hole is omitted in the honeycomb design, while only every fourth air hole is omitted in the kagomé cladding structure. The kagomé cladding design, therefore, has an

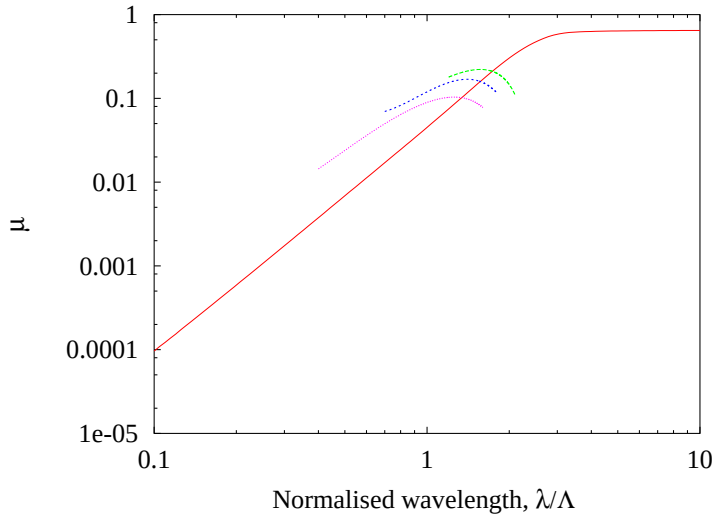

Figure 5.8: The curves from the former plot. The curve showing the fraction of the energy guided in air for the fundamental mode of a silica fiber with cladding air hole diameter 0.6Λ is included for comparison.

inherently larger air filling fraction, than the honeycomb cladding structure.

One of the attractive qualities of the honeycomb lattice structure is that the interstitial holes, which can appear during the fabrication process of the fiber, enlarge the low order bandgaps [19] in the cladding structure of the final fiber. Calculations reveal that a similar beneficial effect result from interstitial holes in the kagomé lattice cladding structure. Further, the two lowest order PBGs of the kagomé cladding structure are found above band number 2 and above band number 6, as is the case for the honeycomb cladding structure. Another similarity is that, compared to the triangular cladding structure, only small air filling fractions are required before PBGs are found in the kagomé and the honeycomb cladding structure.

In **Figure 5.12** is shown the electric field squared for a guided mode in the kagomé optical fiber. Notice that the fiber guides light along the air-core. The electric field squared is chosen to emphasize the fact that an appreciable amount of the field is guided in the six innermost interstitial air-holes. The diameter of the cladding and core air holes is 0.4Λ, which should be relatively simple to obtain in real fibers.

In **Figure 5.13** is shown the mode index (full line), $\frac{\beta}{k}$, of the guided

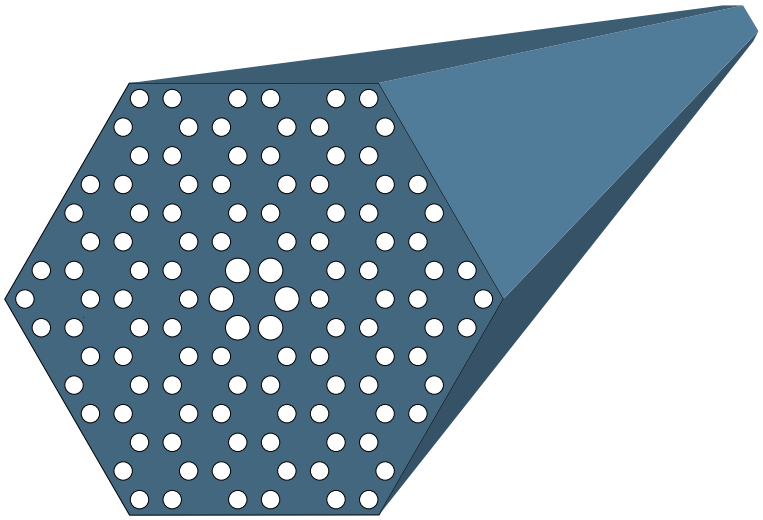

Figure 5.9: Schematic representation of a PBG fiber with cladding air holes on a honeycomb lattice structure. Notice the 6 innermost enlarged air holes at the center of the PCF that forms the low index core region.

mode depicted in Figure 5.12 as a function of the normalized wavelength $\frac{\lambda}{\Lambda}$, where λ is the free space wavelength, while Λ is the interhole distance defined in Figure 5.11. As with the honeycomb PBG fiber it is noticed that the mode index is below the index of silica (1.45 in the calculations), which is possible, since the guided mode has a mode index that is not allowed in the cladding region because of the fundamental bandgap of the kagomé cladding structure. The boundaries of the fundamental PBG of the cladding structure is also depicted in Figure 5.13.

The confinement to the core region is strongest, when the guided mode is approximately at the center of the photonic bandgap in **Figure 5.13**. Even though the mode index of the guided mode is not exactly in the center for $\frac{\lambda}{\Lambda} \approx 0.88$, the mode is still well localized, as indicated by **Figure 5.12**. At longer wavelengths, a larger portion of the field is within the central air hole, while the field is almost completely able to avoid the air holes at short wavelengths.

For the group velocity dispersion of a guided mode in a optical fiber, the following relation exist:

$$GVD = -\frac{\lambda}{c}\frac{d^2n}{d\lambda^2} \tag{5.1}$$

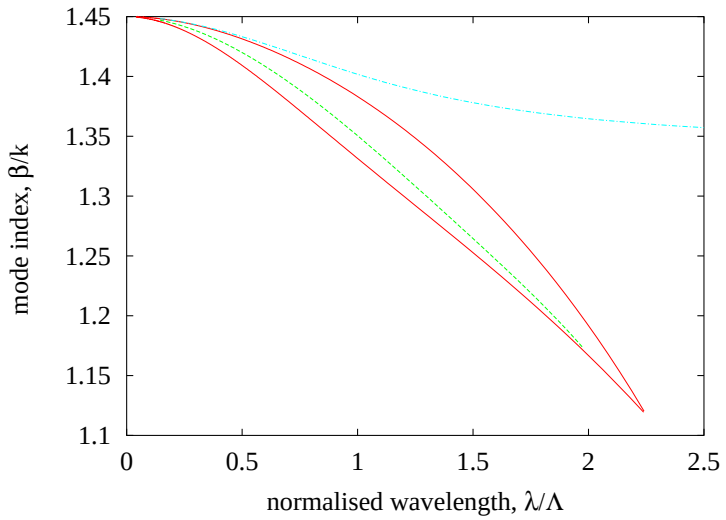

Figure 5.10: The mode index of the guided mode (green) of a PBG fiber with the design from **Figure 5.9**. The cladding hole size is $D = 0.6\Lambda$ while the diameter of the six innermost air holes is $D = 0.9\Lambda$. The red curves identify the fundamental PBG, while the light blue curve shows the effective cladding index.

In (5.1) GVD is the group velocity dispersion, while n is the mode index, $\frac{\beta}{k}$, of the guided mode. Comparing with **Figure 5.13**, where the normalized wavelength, $\frac{\lambda}{\Lambda}$ is proportional to the free space wavelength, we conclude that a downward curvature in Figure 5.13 corresponds to a positive waveguide dispersion (material dispersion is not included in the calculations), while an upward curvature corresponds to a negative waveguide dispersion. We conclude that the fiber has positive waveguide dispersion for long normalized wavelengths, while the waveguide dispersion is negative for short normalized wavelengths. The waveguide dispersion can therefore be tuned by simply changing Λ (Corresponding to changing the final size of the fiber).

In **Figure 5.14** is shown the calculated group velocity dispersion, with the size of the fiber as parameter. It is noticed that a relatively large fiber with $\Lambda = 2.0\mu m$ has negative waveguide GVD at 1550 nm wavelength. Also notice that the bandpass effect of the fiber is clearly illustrated here- the fiber only guides over a limited wavelength range. Pulling the fiber to smaller sizes has the effect of lowering the zero dispersion wavelength. Also notice that it is possible to obtain very large positive dispersion below $1.3\mu m$

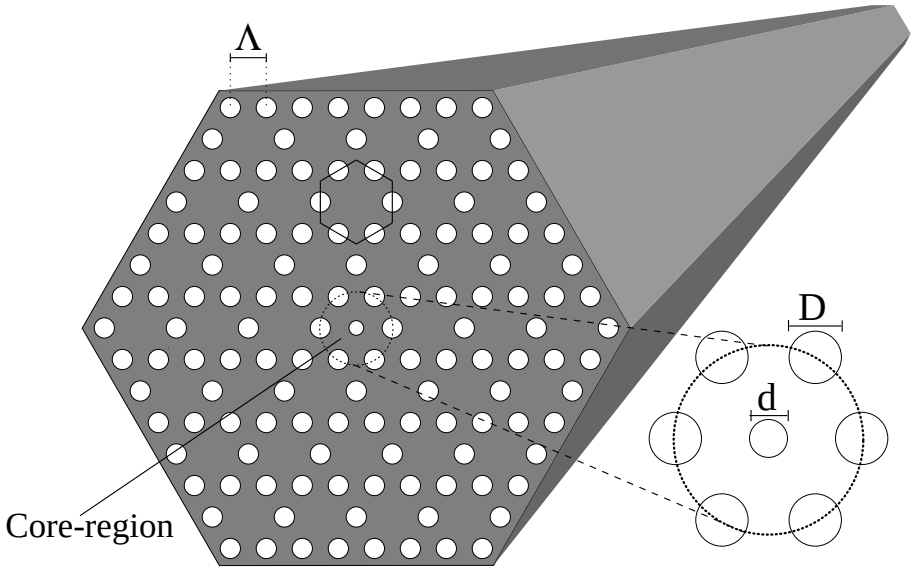

Figure 5.11: Schematic representation of a PBG fiber with cladding air holes on a kagomé lattice structure. Notice the defect hole at the center of the PCF. The periodicity of the cladding structure is defined by the hexagonal unit cell shown. The interhole distance, Λ, the defect hole diameter, d, and the cladding hole diameter, D, are also defined by the Figure.

wavelength, making it possible to use the fibers for e.g. efficient continuum generation at short wavelengths.

Changing the size or the geometry of the fiber core will also influence the dispersion properties of the fiber. Finally, the size of the air holes in the cladding structure also affect the group velocity of the final fiber. In these fibers not only the core, but also the cladding structure influences the group velocity dispersion.

Finally, it should be noticed that the confinement of light can be quite strong in the kagomé fiber. As an example, the effective mode area for the field plot in **Figure 5.12** corresponds to an effective mode area of less than 9 μm^2 when the structure scale is chosen as $\Lambda \approx 1760$ nm corresponding to a free space wavelength of 1550 nm. Tighter confinement of the field is possible by employing a smaller air core, by choosing a smaller Λ, or by using larger cladding holes.

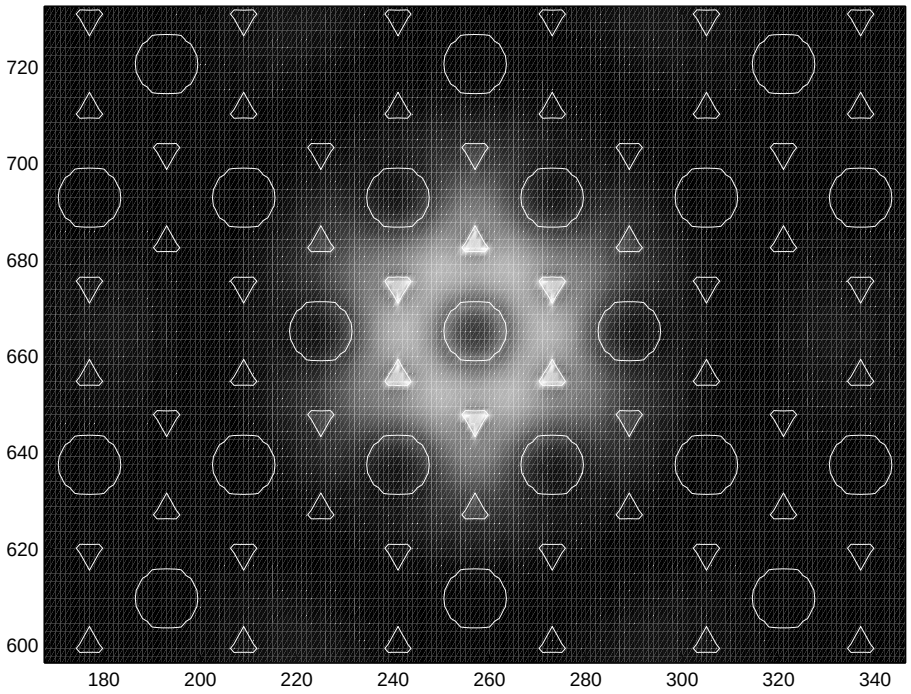

Figure 5.12: The electric field squared for the guided mode in the kagomé fiber structure with interstitial holes. The normalized wavelength is approximately 0.88. For a free space wavelength of 1550 nm this corresponds to an interhole distance of approximately 1760 nm. The diameter of the air holes is 40 % of the interhole distance, Λ.

5.3 Summary of Chapter 5

PBG fibers allow guidance of light within a low index core, if the mode index of the guided mode is within a photonic bandgap. Despite the novel guiding principle of multiple reflections, many known principles from standard fiber technology still hold true, including a mode index that is below the effective core index, yet above the low index bandgap edge. PBG modes are found capable of having very high positive group velocity values, a phenomenon that co-exist with small core regions. Such fibers may find use as future non-linear fibers.

The structural size that guide light at a particular wavelength may be tuned by changing the size of the central air hole, or by changing the cladding

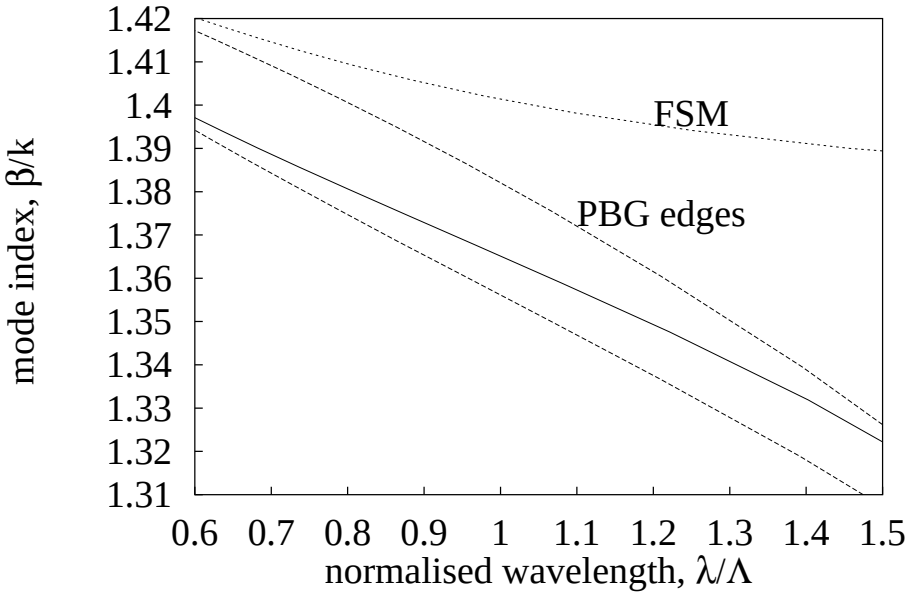

Figure 5.13: The full line shows the calculated mode index of the guided mode as a function of the normalized wavelength, for the structure shown in Figure 5.12. The mode index is lower than the mode index of the fundamental space filling mode, FSM. However it does not couple to any cladding modes, since cladding modes are strictly forbidden within the photonic bandgap, illustrated by the PBG edges in the figure.

air hole diameters.

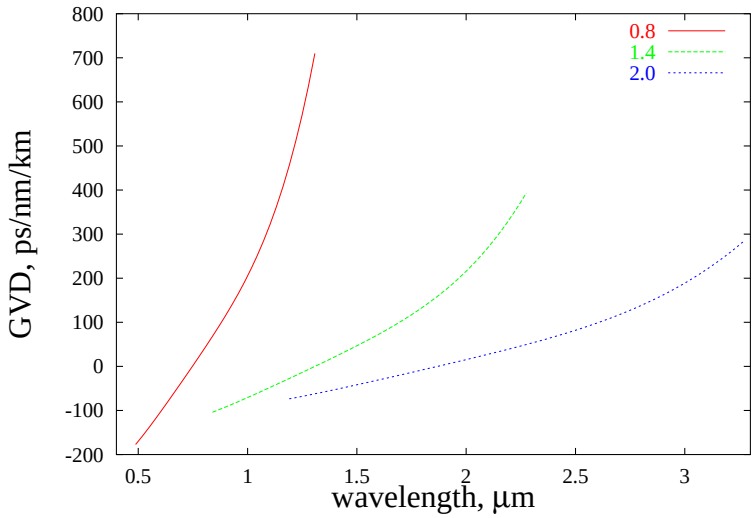

Figure 5.14: The waveguide group velocity dispersion as a function of the wavelength. The curve to the left corresponds to $\Lambda = 0.8\mu m$, the curve in the center corresponds to $\Lambda = 1.4\mu m$, while the curve to the right corresponds to $\Lambda = 2.0\mu m$

Chapter 6

Group Velocity Dispersion Compensation

In the preceding chapters examples of group velocity dispersion in micro-structured fibers have been shown to illustrate some basic qualities in PCFs. In this chapter, micro-structured fibers designed specifically for the purpose of group velocity dispersion will be described. Because of the protection of IP and patenting rights, only a few examples will be shown. Still, some of the physics employed to identify possible design routes will be given, as well as examples of some of the new properties that may be obtained.

6.1 Different Schemes for Group Velocity Dispersion Compensation

The need for dispersion compensating fibers in optical links is caused by anomalous dispersion at 1550 nm wavelength in standard step-index fibers. One could design optical fibers with near zero dispersion at 1550 nm wavelength this, however, would greatly facilitate undesired nonlinear effects in the fibers [59]- a serious concern as still higher bit-rates, and still more channels are carried by each optical fiber. For high capacity optical links it will, therefore, be advantageous to employ optical links with non zero dispersion, thus enforcing the need for distributing dispersion compensating fibers along the optical link.

As indicated by the examples of group velocity dispersion in micro-structured fibers, PBG fibers generally have a positive group velocity dispersion. It would, therefore, seem that the designs shown will not offer any advantages in most optical links, since one generally need to compensate

anomalous dispersion. However, one should not forget the important possibility of designing new optical links with negative group velocity dispersion, thereby creating a market for fibers with strong anomalous dispersion as group velocity dispersion compensating fibers. Since single-mode step-index fibers do not offer the possibility of strong anomalous dispersion this possibility has never existed until the advent of micro-structured fibers.

Micro-structured fibers that do not guide light by the PBG effect but by modified Total internal reflection have the possibility of offering both positive (up to +600 ps/nm/km) and negative (down to approximately -2000 ps/nm/km) group velocity dispersion with the simple triangular fiber designs shown this far. If one can accept new optical links, where the dispersion compensating fibers should have anomalous dispersion, then PBG fibers have the potential of high dispersion values. However, all the fibers discussed so far have combined high dispersion with small mode areas, leading to potential problems with nonlinearities within the fibers, as well as poor coupling between fiber links.

6.2 Group Velocity and Refractive Index Contrast

A typical optical fiber designed for dispersion compensating purposes will have a group velocity dispersion of approximately -100 ps/nm/km. This is a quite modest value, compared to the group velocity dispersion values that are attainable with micro-structured fibers. It is advantageous to investigate why PCFs offer the possibility of more negative group velocity dispersion than -100 ps/nm/km.

The starting point of the analysis is the expression for the group velocity for a guided mode:

$$v_g = c_0 \frac{\beta}{k} \frac{\int_A (\mathbf{H} \times \mathbf{E}^*) \cdot \mathbf{z} dA}{\int_A (\epsilon \mathbf{H} \times \mathbf{E}^*) \cdot \mathbf{z} dA} \tag{6.1}$$

For simplicity we will assume that the mode index does not change significantly in the wavelength region with negative group velocity dispersion (corresponding to an abrupt upward curvature on a curve showing the mode index as a function of the wavelength). Since the group velocity dispersion is defined as $\frac{\partial \frac{1}{v_g}}{\partial \lambda}$ strong negative group velocity dispersion at a given mode-index corresponds to a significant change in the value of the integral $\int_A (\epsilon \mathbf{H} \times \mathbf{E}^*) \cdot \mathbf{z} dA$ in (6.1). This again corresponds to a significant change in the value of the average geometrical refractive index (evaluated from the spatial field distribution) as the frequency is altered.

One, therefore, see the reason underlying the numerically large group velocity values found in PCFs, compared to step index fibers. Since the refractive index change between air and silica is significantly larger than the index difference between the core and cladding in step index fibers, this leads to more powerful group velocity dispersion in micro-structured fibers, especially when the air filling fraction of the cladding is large. **Figure 4.10** also shows that the normalized wavelength region with strong group velocity dispersion increases with the air filling fraction of the cladding. It, therefore, appears that strong negative group velocity dispersion corresponds to a smaller mode area than the corresponding mode area of fibers designed to exhibit numerically large positive group velocity dispersion at a desired wavelength.

For micro-structured fibers to be successful as dispersion compensating fibers, one must design fibers with a numerically large negative group velocity dispersion while ensuring an effective mode area that is compatible with the high bit rates expected in the communication links of the future. A design route for such a fiber will be the topic of two subsequent sections.

6.3 Positive Group Velocity Dispersion

According to **Figure 4.10**, the positive group velocity dispersion occur at a smaller normalized wavelength region than the negative group velocity dispersion. Micro-structured fibers designed for compensating communication links with negative group velocity dispersion will, therefore, have larger core sizes, than PCFs designed to exhibit strong negative group velocity dispersion. Unfortunately, the numerical dispersion values of PCFs designed for strong positive group velocity dispersion are smaller than those that may be obtained with fibers designed to have large negative group velocity dispersion.

According to the derivation in the preceding section, the dominating reason for the numerically large negative group velocity dispersion made possible in PCFs, is caused by an abrupt change in the fraction of the modes energy that is propagating in air (cf. **Figure 5.7**). However, for fibers exhibiting strong positive group velocity dispersion the dispersion is largely caused by another phenomenom. Equation (6.1) shows that group velocity dispersion may also be caused by a change in the effective mode index, even though no significant changes occur in the integral $\int_A \epsilon \mathbf{H} \times \mathbf{E}^* \cdot \mathbf{z} dA$. The positive group velocity dispersion is to a large extent the result of the increase in the effective mode index as the frequency is increased (the

slight decrease in the fraction of the field that is propagating in air as the frequency is increased, actually lead to negative group velocity dispersion and, therefore, counteracts the anomalous dispersion created by the increase of the effective mode index).

One may conclude that more positive group velocity dispersion would be possible if one could design a fiber with an increasing fraction of the field propagating in air with increasing frequency. This is exactly the possibility offered by PBG fibers with a low index core region (cf. **Figure 5.8**) and this is, therefore, the main reason why PBG fibers offer more positive group velocity dispersion than PCFs with a simple step index analogy, as seen in e.g. **Figure 5.4**.

6.3.1 The Coupled Core Photonic Crystal Fiber

Micro-structured fibers offer the possibility of numerically large negative group velocity dispersion, however, this is coupled with small core regions and small effective mode areas in the basic micro-structured fiber designs. We now turn to the topic of designing a fiber with strong dispersion, while maintaining a reasonable core-size.

The basic idea underlying the design may also be applied to standard optical fibers. **Figure 6.1** shows the radial variation of the refractive index of a standard optical fiber designed for strong negative group velocity dispersion. In the center is a central core-region with a relatively high dopant level. Outside this inner core is a cladding region circumscribed by a core with a ring-like shape. Outside this ring shaped core (the outer core) is the outer cladding.

The refractive index of the inner core is chosen to be higher than the refractive index of the outer core. Both cores would guide a fundamental guided mode in the absence of the other core. However, since the area of the inner core is smaller than the area of the outer core, the effective mode index of the mode supported by the inner core is lower than the effective mode index of the mode supported by the outer core at wavelengths that are longer than the wavelength region where strong numerical group velocity dispersion is observed. At shorter wavelengths, the mode index of the mode supported by the inner core is higher than the effective mode index of the mode supported by the outer core, because of the larger refractive index of the inner core.

As in quantum physics, the dispersion curves cannot cross each other. Therefore, the mode index of the inner core cannot cross the mode index of the outer core. Instead avoided crossing occurs- the modes supported by

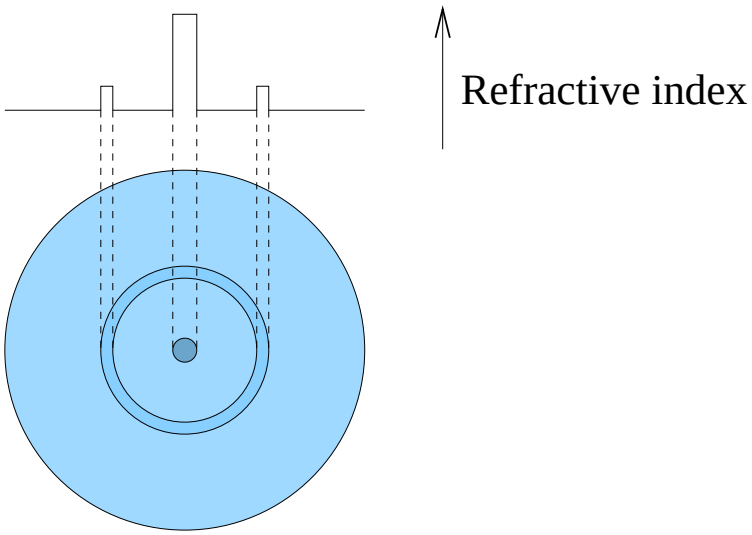

Figure 6.1: Schematic representation of the refractive index of coupled core fibers. Both the central core region, and the outer 'ring' core can guide light

the two core-regions couple to each other leading to a 'supermode'- as the wavelength is decreased one mode with a relatively higher index increases its portion of the energy within the inner core region (while decreasing its energy within the outer core), leading to a negative group velocity dispersion. At the same time another mode of the supermode (with a relatively lower mode index) increases its portion of the field in the outer core, corresponding to a positive group velocity dispersion.

This design is not the typical design of a dispersion compensating fiber today (despite its ability of yielding group velocity dispersion values in excess of -5000 ps/nm/km), since it has some weaknesses. To obtain a numerically large dispersion values, the modes supported by the outer core should be physically well separated from the mode supported by the inner core. Therefore, the radial distance between the outer core and the inner core must be relatively large. If the refractive index step between the outer core and the cladding is small (which is necessary to ensure single-mode guidance) the fiber, therefore, exhibits macro-bending losses because of the large radius of the outer core. This can be avoided by choosing a larger refractive index step between the outer core and the cladding at the cost of the fiber becoming multimode. Therefore, one is forced to choose between a multimode fiber or

a fiber that is bending nonresistant, if such large group velocity dispersion values are desired using step index fiber technology.

The reason for the large radius of the outer core-region is the need of a good spatial separation between the modes supported by the outer and the inner core. However, employing micro-structured fibers a good separation between the modes supported by the inner and the outer core can be obtained, while choosing a reasonable (smaller) radial distance between the two core regions. By separating the two core regions with air holes a much lower effective cladding index can be obtained between the two cores, thereby limiting the necessary radial size of the inner cladding region. This again lead to the possibility of a smaller radius of the outer core that may be employed to obtain reasonable bending losses while keeping the fiber single mode.

Because of the need of protecting IP and patenting rights, this important and novel fiber design will not be described in detail. Instead a simple design idea will be shown, along with an example of the group velocity dispersion values that are attainable. The basic design is shown in **Figure 6.2** which shows a high index inner core region (doped with e.g. germanium). The cladding consist of air holes (small air filling fraction) on a triangular lattice. The outer core region is created by omitting some of the cladding air holes (six air holes are removed in the example structure, creating a honeycomb like outer core region). The inner core and the outer core is separated from each other by the six enlarged innermost air holes. Because of these air holes the outer core size can be made smaller than when designing this type of fiber using step index fiber technology through doping of silica, however, the physical principles ensuring large negative group velocity values are the same.

As an example **Figure 6.3** shows the calculated mode index of the guided mode that light is coupled into (red curve), as well as the cladding index (blue curve). Here the diameter of the outer holes is 0.3Λ, the diameter of the six enlarged inner air holes is 0.6Λ while the refractive index of the inner core is raised by 0.03. Below the cladding index curve is shown the mode index of the second order mode guided by the outer core-region, however, for the normalized wavelength region depicted this mode is not guided since its mode index is below the effective cladding index. Combined with the green curve, the red curve shows the mode-index of the super-mode guided by the fiber. At long wavelengths the mode corresponding to the red curve is guided in the outer core (corresponding to the more horizontal part of the red curve), while the mode guided by the inner core is represented by the green curve. At short wavelengths the modes have 'switched' cores,

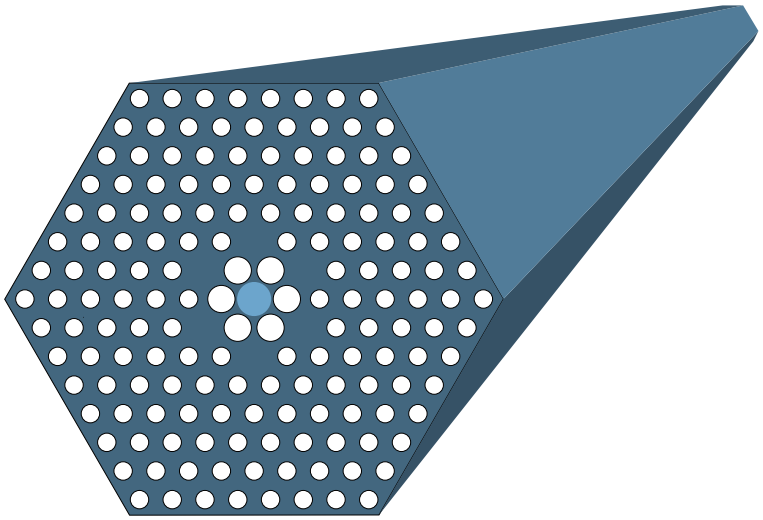

Figure 6.2: Schematic representation of a dispersion compensating microstructured fiber with coupled cores. The outer core region is the six honeycomb-like silica regions, surrounding the 6 innermost enlarged airholes. The enlarged air holes prevent the mode propagating at the up-doped inner core region from coupling to the mode guided by the outer core, at wavelengths that are different from the wavelength region with numerically large dispersion values.

implying that the green curve now represents a mode guided in the outer core region while the red curve represents a mode guided in the inner core region. **Figure 6.3** shows the normalized wavelength region, where the two modes couple strongly to each other (and 'swap place'), corresponding to the wavelength region with numerically large dispersion values.

The calculated group velocity dispersion for an example design corresponding to **Figure 6.3** is shown in **Figure 6.4**. Notice that the wavelength range with strong dispersion is fairly narrow. More negative group velocity dispersion may be obtained at the cost of the wavelength span with negative group velocity dispersion becoming even more narrow, or the wavelength window with dispersion compensating qualities may be enlarged at the cost of smaller dispersion values. The limitation on the wavelength span that can be obtained for a desired minimum group velocity dispersion value is the limited difference in the group velocities for modes guided by the inner and the outer core regions, respectively. The difference in group velocities is

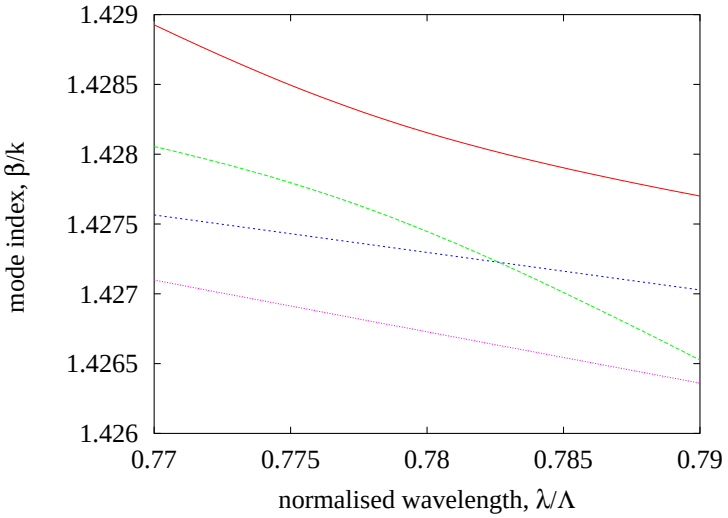

Figure 6.3: The guided mode index of the mode used for dispersion compensation (red curve) as well as the mode with positive waveguide dispersion (green). Notice the strong curvature resulting from a coupling between the inner and the outer core regions. The cladding index is shown with blue, while the second order outer core cladding mode is shown with purple, indicating a truly singlemode fiber

limited by the refractive index difference that can be obtained between the two core regions through the doping of the inner core.

By designing properly, one can obtain that the light guided by the outer core (with anomalous dispersion) leak to the cladding because of the small index difference between the green curve and the cladding index. At the same time the light guided in the outer core region couples poorly to Gaussian shaped modes, so that combined these two efforts ensure that light is only transmitted by the mode represented by the red curve. This design idea indeed appear promising as a future dispersion compensating fiber.

6.3.2 The PBG Coupled Core Fiber

We now move to another more radical design for dispersion compensating micro-structured fibers. This time, the cladding is a honeycomb structure ($D = 0.8\Lambda$) with photonic bandgaps. By designing the fiber in a way that ensures that the outer and the inner core modes couple to each other while

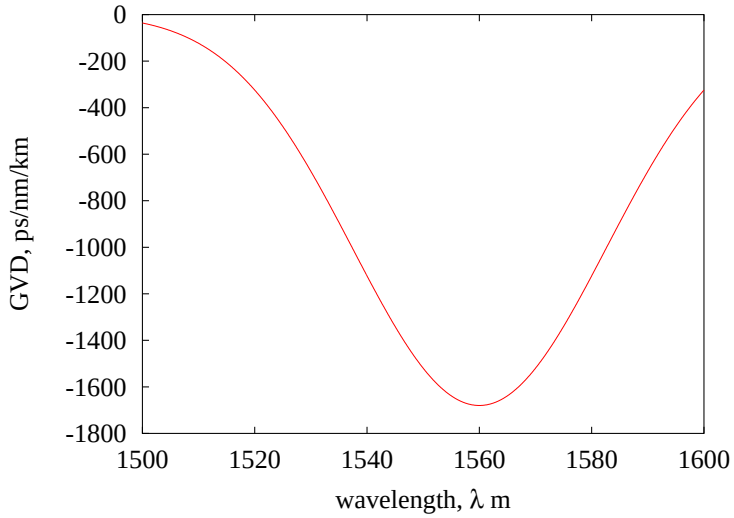

Figure 6.4: The group velocity dispersion of a coupled core fiber. Large negative group velocity values are found, however, the wavelength span with strong dispersion is limited, compared to the example shown in the next section

the mode-index is within a photonic bandgap, it becomes possible to exploit the large refractive index difference between silica and air. The basic design is shown in **Figure 6.5**. For the calculations in this section, the inner (silica) core has a diameter equal to Λ, while the air-ring with the small silica 'bridges' has a diameter of 2.5Λ. Notice that the 'triangular' outer core has a substantial air filling fraction, and therefore makes it possible for light to be guided in air, when it is situated in the outer core region.

Figure 6.6 shows the PBG boundaries (red curves) and the estimated effective outer core index (blue curve). The purple curve shows the mode index of the mode to ensure a dispersion compensating fiber. Notice the large slope difference when the purple mode index is below respectively above the outer core index. This ensures very strong dispersion values or alternatively wide wavelength regions with large negative group velocity dispersion values. Also notice that no index curves corresponding to positive group velocity dispersion is shown, since none are found in this calculated example. This is caused by the inner and the outer core being isolated less from each other than in the example shown in the former section. Therefore, one should expect negative dispersion over a wide wavelength range with this design,

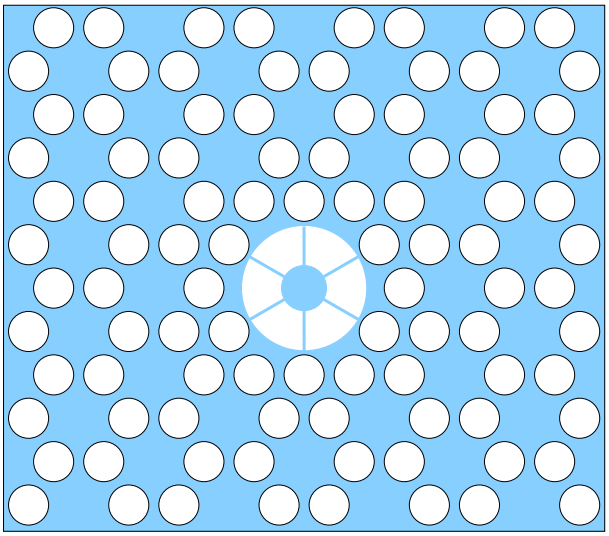

Figure 6.5: Schematic of a photonic bandgap fiber designed for dispersion compensating purposes.

compared to the design shown in the former section.

The green curve in **Figure 6.6** shows the mode index of the second order mode guided by the outer core region. It is noticed that the fiber is truly single-mode when the strong upward bending of the purple curve occurs, implying that this is a singlemode dispersion compensating fiber. Still, the index difference between the guided mode and the PBG boundaries is large (approximately 0.02) indicating a very bending resistant fiber (no satisfactory macro bending loss model has been developed for PBG fibers, however, it appears reasonable to assume that such a large index difference corresponds to modes that couple poorly to each other, even when the fiber is bended).

The calculated dispersion values are shown in **Figure 6.7**. Despite the very wide window with negative dispersion, one still finds dispersion values below -1300 ps/nm/km. Very impressive figures indeed, especially considering the expected bending loss resistance of the fiber. **Figure 6.8** shows the mode index and the group index of the guided mode. A very large group index variation is seen, in accordance with the large wavelength region with strong negative dispersion. Notice that the group index is approaching the theoretical limit of the mode index at a normalized wavelength of approximately 1.9. This ensures a large variation in the group velocity.

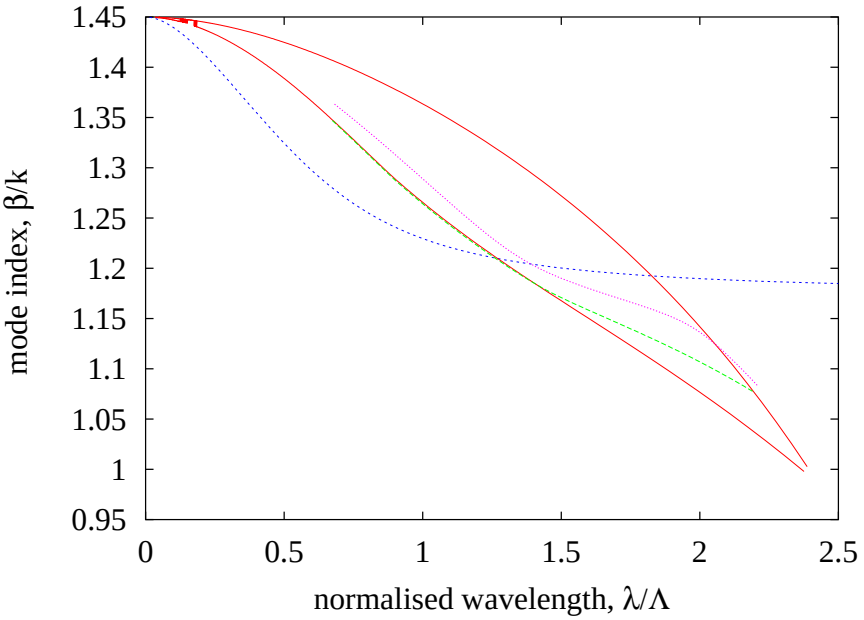

Figure 6.6: The photonic bandgap edges (red) and the effective outer core index (blue) of a coupled core PBG fiber. The purple curve shows the mode index of the mode providing negative group velocity dispersion. The green curve shows the effective mode index of second order outer core mode, indicating a truly singlemode fiber

The fraction of light that is propagating in air at different wavelengths is shown in **Figure 6.9**. Notice that almost 70% of the light is guided in the air holes of the outer core, when the strong variation of the group index begins. At short wavelengths almost all the energy is propagating in silica. Combined it can be concluded that this fiber exploits the possibilities of moving the energy from air to silica in a way that gives large dispersion values. For a more systematic study, the design may be sought exploited to compensate a standard fiber over wide wavelength regions. This design idea will be investigated heavily in the near future since it offers such large variation of the group index.

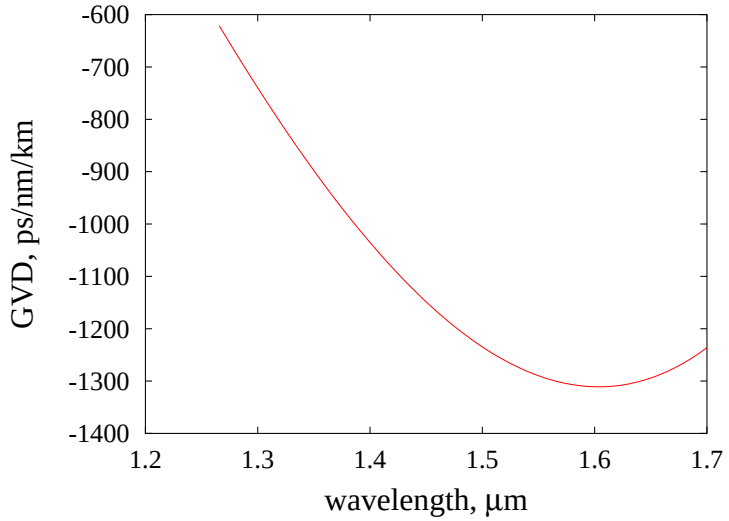

Figure 6.7: The calculated group velocity dispersion of a PBG coupled core fiber. Notice the wide wavelength span with negative group velocity dispersion

6.4 Summary of Chapter 6

To obtain efficient group velocity dispersion one must design a fiber, where the cross-section of the electromagnetic light changes strongly with the wavelength. This makes it possible for the group velocity to change significantly as a function of the wavelength. It was found that micro-structured fibers are ideal for this purpose, since they allow the design of fibers with a inner and a outer core region that is optically separated, except at wavelengths with near mode index matching between the modes of the two cores. If this is sought accomplished with standard step index technology, one is forced to choose between accepting macro bending losses or multimode behavior.

Even more impressive group velocity dispersion values may be obtained by employing photonic bandgap guidance of light. This makes it possible to construct fibers that guide a significant portion of the modal energy in the air holes at long wavelengths, yet guide almost all of the field in silica at shorter wavelengths. This offers the possibility of combining dispersion compensation over wide wavelength regions and numerically large group velocity dispersion values. This design needs to be investigated further, but seems very impressive for dispersion compensating purposes.

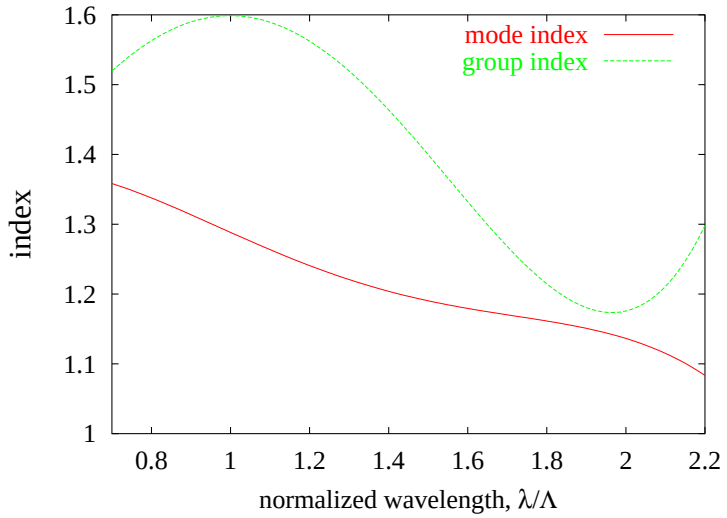

Figure 6.8: The mode index and the group index of the fundamental mode of a PBG dispersion compensating fiber. Notice that both positive and negative group velocity is present, depending on the wavelength. Also notice the large group index span.

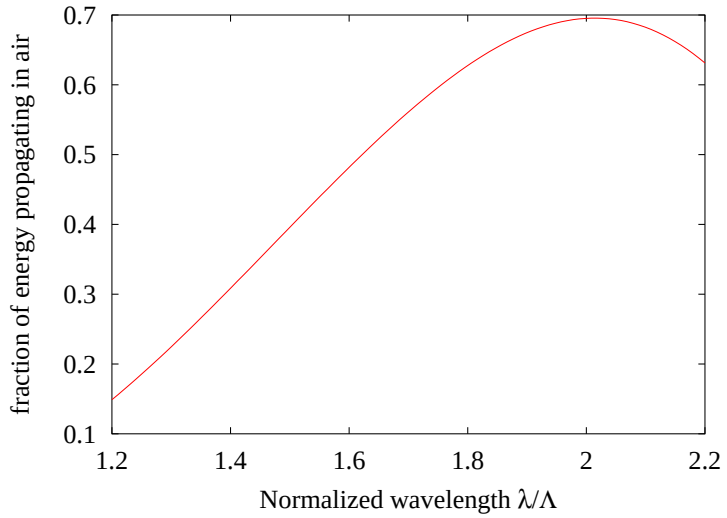

Figure 6.9: The fraction of the energy that is guided in air. Strong negative group velocity dispersion is a result of the exclusion of modal energy from the air holes as the frequency is increased

Chapter 7

Summary

Photonic crystal fiber technology is emerging as an interesting complementary technology to step index fibers. This is caused by a number of new possibilities. The most renown are probably the ability to guide light in air as well as the possibility of using nonlinear micro-structured fibers as white light generators. However, the possibilities of micro-structured fibers extend far beyond the present applications.

In this thesis micro-structured fibers have been analyzed assuming that index guiding photonic crystal fibers have a close analogy to step index fibers. The novel behavior of micro-structured fibers, compared to standard optical fibers, may thus be seen as a result of the effective cladding index varying with the wavelength of light.

Thus, the possibility of singlemode guidance of light at all frequencies is a direct result of the varying cladding index, at the same time leading to increased bending losses at short wavelengths (step index fibers have decreasing bending losses as the frequency is increased at the cost of becoming multimode)

The possibility of singlemode guidance at all frequencies is a result of the effective cladding index approaching the refractive index of the silica core -region. This was shown to correspond to the effective frequency, V_{eff} reaching only finite values. This is interesting because V_{eff} is a measure of the degree of localization of the mode to the core region. Apart from energy being expelled from the air holes as the frequency is increased, one would therefore expect a modal field cross section that is almost invariant with the wavelength, in the wavelength region with almost constant V_{eff}-values.

By decreasing the refractive index of the core region, through the usage of dopant material, the overlap between a mode at 980 nm wavelength and a

mode at 1550 nm wavelength may be as large as 99.87%. This is particularly interesting, since one may design fibers with constant V_{eff}-values at a desired core size, through the technique of decreasing the refractive index of the silica core region. Using this technique, important new designs within the area of fiber amplifiers may be realized.

The possibility of a positive waveguide dispersion has enabled nonlinear micro-structured fibers with a zero dispersion wavelength below 1300 nm wavelength. The combination of zero dispersion and small effective mode areas ensures the possibility of using the fibers as white light generators. Such fibers have reached a level of maturity, where they are commercially available- partly as a result of the work of the present author.

Photonic bandgap fibers offer even more radical possibilities, including the possibility of guiding light within a low index core region. These fibers are particularly interesting because they combine the possibility of very small effective mode areas with large positive waveguide dispersion. This large positive waveguide dispersion is the result of a larger portion of the modal energy propagating in air as the frequency is increased- a possibility that is unique to photonic bandgap fibers. But photonic bandgap fibers may also be designed to have flat near zero dispersion near 1550 nm wavelength of light.

The concept of dispersion compensating fibers is important to any optical fiber manufacturer, since long haul optical fiber transmission is only possible, by including links with negative group velocity dispersion. Photonic crystal fibers appear promising as dispersion compensating fibers, since they allow the combination of large negative group velocity dispersion values and reasonably large effective mode areas in fibers that are singlemode and have reasonably low macro bending losses. It is the present authors expectation, that such fibers will in time become the most important application of photonic crystal fibers, despite the current status of no papers being published on the issue. However, a long maturity process must be undertaken, before photonic crystal fibers will find effective usage in optical fiber links.

7.1 Future Work

This thesis has put emphasis on understanding the basic ability of micro-structured fibers to act as optical waveguides. This has made it possible to recognize important novel possibilities within the field of photonic crystal fibers. However, one should not be led to the conclusion that all there is to be said concerning photonic crystal fibers may be understood from a simple

analysis of the waveguiding properties. Important qualities still need to be understood.

A model for the bending losses of photonic bandgap fibers is very much needed for the correct evaluation of the qualities of a given photonic bandgap fibers. Further, a number of models concerning the applications of micro-structured fibers should be developed. This include models of the nonlinear processes in photonic crystal fibers, models of the polarization mode dispersion as well as models for particular applications of the fibers, such as fiber amplifier models.

But first and foremost an excessive amount of progress needs to be made. Photonic crystal fibers are still relatively lossy compared to standard fibers, and the control of the cross-section of the final fiber structure is relatively modest. The present author believes that considerable progress will be made in this field, partly as a result of the desire to realize some of the promises of the dispersion compensating micro-structured fiber designs.

The work on designing micro-structured fibers with specific waveguiding properties will continue. The design freedom with micro-structured fibers is enormous, and the future is likely to see fibers with completely novel waveguiding properties. This work will be driven by the search for new fiber components, and will therefore be performed alongside the attempts to produce more traditional fiber components, such as fiber amplifiers, dispersion compensating modules and fiber lasers.

7.2 Closing Remarks

In closing I would like to express some of my more personal feelings concerning this work. I have been working with photonic crystal fibers since 1997 and have often felt great excitement about the novel possibilities made possible with photonic crystal fibers. The excitement has been spiced with moments of anxiety and disbelief concerning the possibility of realizing the at times complicated dielectric structures, necessary to exploit some of the more subtle qualities of micro-structured fibers. However, this 'journey' has seemed ever more promising as other research groups realized still better micro-structured fibers.

One particular exciting development was the authors co-foundation of the company Crystal Fibre A/S. It was very touching to see the work I had been part of, develop into a company committed to the development and exploitation of micro-structured fibers. This excitement has since then grown into a maturing confidence, that photonic crystal fibers will indeed become

an important supplement to the commercial fiber technology of tomorrow. I hope that this excitement has shone through the present thesis, and trust that this work, among others may initiate more interest and research in the area of photonic crystal fibers.

References

[1] A. Bjarklev. *Optical Fiber Amplifiers: Design and System Application.* Boston-London:Artech House, August 1993.

[2] J. Dakin and B. Culshaw. *Optical fiber sensors*, volume 4 of *Applications, analysis, and future trends.* Boston: Artech house, 1997.

[3] S. Takahashi, M. Futamata, and I. Kojima. Spectroscopy with scanning near-field optical microscopy using tunneling mode. *Journal of Microscopy*, 194(2-3):519–22, 1999.

[4] Biomedical sensors, fibers, and optical delivery systems.

[5] Abraham. Katzir. *Lasers and optical Fibers in medicine.* Academic press, inc, 1993.

[6] E. Yablonovitch. Inhibited spontaneous emission in solid-state physics and electronics. *Physical Review Letters*, 58(20):2059–62, May 1987.

[7] S. John. Strong localization of photons in certain disordered dielectric superlattices. *Physical Review Letters*, 58(23):2486–9, 1987.

[8] Best bets for 1999. *Science*, 1998.

[9] Science & technology: New-age crystals. *The Economist*, 349:89–90, 21 Nov 1998.

[10] J.D. Joannopoulos, J.N. Winn, and R.D. Meade. *Photonic Crystals: Molding the Flow of Light.* Princeton University Press, 1995.

[11] J.D. Joannopoulos, P.R. Villeneuve, and S. Fan. Photonic crystals: putting a new twist on light. *Nature*, 386(13):143–9, March 1997.

[12] Attila Mekis, Chen J.C, Kurland I., Shanhui Fan, Pierre R. Villeneuve, and Joannopoulos J.D. High transmission through sharp bends in photonic crystal waveguides. *Physical Review Letters*, 77(18), oct. 1996.

[13] S.-Y. Lin, E. Chow, V. Hietala, P. Villeneuve, and J. Joannopoulos. Experimental demonstration of guiding and bending of electromagnetic waves in photonic crystal. *Science*, 1998.

[14] Broeng J., Barkou S.E., Søndegaard T., and Bjarklev A. Analysis of air-guiding photonic band gap fibers. *Optics Letters*, 25(2):96–98, Januar 2000.

[15] Knight J.C., Birks T.A., and Russell P.St.J. Properties of photonic crystal fiber and the effective index model. *J. Opt. Soc. Am. A*, 15(3), March 1998.

[16] S.E. Barkou, J. Broeng, and A. Bjarklev. Novel silica/air photonic crystal fiber allowing waveguiding by the true photonic bandgap effect. *Optics Letters*, 21:1547–1549, 1999.

[17] T.A. Birks, P.J. Roberts, P.S.J. Russell, D.M. Atkin, and T.J. Shepherd. Full 2-d photonic bandgaps in silica/air structures. *Electronics Letters*, 31(22):1941–3, Oct. 1995.

[18] T. Birks, D. Atkin, G. Wylangowski, P. Russell, and P Roberts. *2D photonic band gap structures in fibre form.* Kluwer, 1996.

[19] J. Broeng, S.E. Barkou, A. Bjarklev, J.C. Knight, T.A. Birks, and P.St.J. Russell . Highly increased photonic band gaps in silica/air structures. *Optical Letters*, 21(19):1547–9, Oct. 1997.

[20] Knight J.C., Broeng J., Birks T.A., and Russell P.St.J. Photonic band gap optical fiber: a new class of light guide. *Science*, 282(5393):1476–78, 1998.

[21] Cregan R.F., Mangan B.J., Knight J.C., Birks T.A., Russell P.St.J., Roberts P.J., and Allan D.C. *Science*, 285:1537–9, 1999.

[22] E. Yablonovitch. Photonic band-gap structures. *Journal of the Optical Society of America B*, 10(2):283–95, Feb. 1993.

[23] S. John and Tran Quang. Optical bistability and phase transitions in a doped photonic band-gap material. *Physical Review A (Atomic, Molecular, and Optical Physics)*, 54(5):4479–88, Nov. 1996.

[24] *Journal of the Optical Society of America B*, 10, Feb 1993.

[25] C. Soukoulis. *Proceedings of the NATO advanced research workshop, Heraklion 1992*, chapter Photonic band gaps and localization. NATO ASI series. Series B, Physics. Dordrecht : Kluwer, 1993.

[26] E. Burstein and C. Weissbuch. *Confined electrons and photons New physics and applications*, volume 340 of *Proceedings of the NATO advanced study institute, Erice 1993NATO ASI series, series B.* New York, N.Y.: Plenum Press, 1995.

[27] ed. Soukoulis, C. *Photonic band gap materials, Proceedings of the NATO advanced study institute, Elounda 1995.* NATO ASI series. Series E, applied sciences. Dordrecht: Kluwer, 1996.

[28] J. Rarity and C. ed. Weisbuch. *Microcavities and photonic bandgaps Physics and applications*, volume 324 of *NATO Asi series. Series E, applied sciences.* Dordrecht: Kluwer, 1996.

[29] Steven. G. Johnson and J.D. Joannopoulos. *Photonic Crystals: The Road from theory to Practice.* Kluwer Academic Publishers, 2002.

[30] H. Benisty. Modal analysis of optical guides with two-dimensional photonic band-gap boundaries. *Journal of Applied Physics*, 79(10):7483–92, May 1996.

[31] T. Krauss and R.M. DelaRue. Two-dimensional photonic bandgap structures at 850 nm. *Optics and Photonics News*, page 26, Dec. 1996.

[32] T. Baba and T. Matsuzaki. Polarization changes in spontaneous emission from gainasp/inp two-dimensional photonic crystals. *Electronics Letters*, 31:1776–8, Sept 1995.

[33] O. Painter, Lee R., A. Scherer, A. Yariv, P. O'Brien, J.D. Dapkus, and I. Kim. Two-dimensional photonic band-gap defect mode laser. *Science*, 284:1819–21, June 1999.

[34] M. Plihal and A.A. Maradudin. Photonic band structure of two-dimensional systems: The triangular lattice. *Physical Review B*, 44(16):8565–71, Oct. 1991.

[35] A. VanBlaaderen. Materials science - opals in a new light. *Science*, 282:887–8, Oct 1998.

[36] B. Goss-Levi. Search & discovery: Visible progress made in 3d photonic crystals. *Physics Today*, 52(17-9), Jan 1999.

[37] E. Yablonovitch, T. Gmitter, G. Tuttle, and K. Leung. Photonic band structure: the face-centered-cubic case employing nonsperical atoms. *Physical Review Letters*, 67:2295–8, Oct 1991.

[38] A.R. Baughman, Z.A, Z. Iqbal, C. Cui, I. Khayrullin, S. Dantas, J. Marti, and V. Ralchenko. Carbon structures with three-dimensional eriodicity at optical wavelengths. *Science*, 5390:897–901, 1998.

[39] S. Kawakami. Fabrication of submicrometer 3d periodic structures composed of si/sio2. *Electonics Letters*, 24:49–51, Jan 1999.

[40] J. Fleming and S. Lin. Three-dimensional photonic crystal with a stop band from 1.35 to 1.95 mum. *Optics letters*, 1999.

[41] J.C. Knight, T.A. Birks, D.M. Atkin, and P.St.J. Russell. Pure silica single-mode fibre with hexagonal photonic crystal cladding. In *OFC'96*, volume 2, page CH35901, 1996.

[42] J.C. Knight, T.A. Birks, P. St.J. Russell, and D.M. Atkin. All-silica single-mode optical fiber with photonic crystal cladding. *Optics Letters*, 21(19):1547–9, Oct. 1996.

[43] J.K. Ranka, R.S. Windeler, and A.J. Stentz. Visible continuum generation in air silica microstructure optical fibers with anomalous dispersion at 800 nm wavelength. *Optics Letters*, 25(1):25–7, 2000.

[44] J.K. Ranka, R.S. Windeler, and a.J. Stentz. Optical properties of high delta air-silica microstructure optical fibers. *Optics Letters*, 25(11):796–8, 2000.

[45] J.K. Ranka and R.S. Windeler. Nonlinear interactions in air-silica microstructure optical fibers. *Optics & photonics News*, 11(8):20–5, 2000.

[46] Tanya. Monro, D. Richardson, and N. Broderick. Holey fibres: an efficient modal model. *Journal of Lightwave technology*, 17:1093–1102, june 1999.

[47] S. E. Barkou, J. Broeng, and A. Bjarklev. Dispersion properties of photonic bandgap guiding fibers. In *OFC99 Friday*, pages 117–9, 1999.

[48] J. Broeng, D. Mogilevstev, Stig. E. Barkou, and A. Bjerklev. Photonic crystal fibers: A new class of optical waveguides. *Optical fiber technology*, 5:305–30, 1998.

[49] T. A. Birks, J. C. Knight, and P. St. J. Russell. Endlessly single-mode photonic crystal fiber. *Optics Letters*, 22(13):961–3, July 1997.

[50] A. Bjarklev, J. Broeng, S. Barkou, and K. Dridi. Dispersion properties of photonic crystal fibers. In *European Conference on optical communications*, pages 135–6, Madrid, September 1998.

[51] T.A. Birks, D. Mogilevtsev, J.C. Knight, P.St.J. Russell, P.J. Broeng, J. adn Roberts, J.A. West, D.C. Allan, and J.C. Fajardo. The analogy between photonic crystal fibres and step index fibres. In *OFC99 Friday*, volume friday, pages 114–16, 1999.

[52] Tanya. M. Monro, D.J. Richardson, and N.G. Broderick. Efficient modelling of holey fibers. In *OFC99 friday*, pages 111–113, 1999.

[53] F. Brerchet, J. Marcou, and D. Pagnoux. Accurate computation of the chromatic dispersion in unimodal photonic crystal fibres. In *ECOC99*, pages I–26–27, 1999.

[54] R.D. Meade, A.M. Rappe, K.D. Brommer, J.D. Joannopoulos, and O.L. Alerhand. Accurate theoretical analysis of photonic band-gap materials. *Physical Review B*, 48(11):8434–7, Sept. 1993.

[55] A.A. Maradudin and A.R. McGurn. Photonic band structure of a truncated, two-dimensional, periodic dielectric medium. *Journal of the Optical Society of America B*, 10(2):307–13, Feb. 1993.

[56] K.M. Ho, C.T. Chan, and C.M. Soukoulis. Existence of a photonic gap in periodic dielectric structures. *Physical Review Letters*, 65(25):3152–5, Dec. 1990.

[57] S.E. Barkou, J. Broeng, and A. Bjarklev. Guidance of light along an air column in a new class of optical fibers. *Dops-Nyt*, pages 16–21, 1999.

[58] J.C. Knight, T.A. Birks, R.F. Cregan, St.J.P. Russell "Photonic crystals as optical fibres: physics, and applications". Photonic crystals as optical fibres - physics and applications. *submitted to Optical Materials*, 21(19):1547–9, Oct. 1997.

[59] Govind. P Agraval. *Fiber-Optic Communication Systems, 2. edition.* John Wiley & Sons, 1997.

[60] The coupled core photonic bandgap fiber introduced in the last chapter may be seen as a fiber that exploits both pbg effects and more traditionel effective index effects.

[61] B. Scaife. *Principles of dielectrics.* Clarendon Press, 1989.

[62] A. W. Snyder and J. D. Love. *Optical Waveguide Theory.* Kluwer Academic Publishers, 2000.

[63] T. M. Monro, P. J. Bennett, N. G. R. Brodrick, and D. J. Richardson. Holey fibers with random cladding distributions. *Optics letters*, 25(4):206–8, 2000.

[64] S.E.Barkou. Libori, J. Broeng, E. Knudsen, A. Bjarklev, and H.R. Simonsen. High-birefringent photonic crystal fiber. In *OFC01 tuesday*, Anaheim, CA, USA, 2001.

[65] Jes. Broeng. *Photonic crystal fibres.* PhD thesis, Technical university of denmark, September 1999.

[66] J. Riishede, S.E.Barkou. Libori, A. Bjarklev, J. Broeng, and E. Knudsen. Photonic crystal fibres and effective index approaches. In *European Conference on Optical Communication*, page paper no. Th.A.1.5, 2001.

[67] Kristian Hougaard. Rare-earth-doped photonic crystal fibres. Master's thesis, University of Denmark, 2002.

[68] Tanya M. Monro, Walter Belardi, Kentaro Furusawa, N.G.R. Broderick, and D.J. Richardson. Microstructured optical fibres: new opportunities for sensing. *Proceedings of SPIE - The International Society for Optical Engineering*, 4185:895–899, 2000.

[69] T. Sørensen, J. Broeng, A. Bjarklev, E. Knudsen, and S.E.Barkou Libori. Macro-bending loss preoperties of photonic crystal fibre. *IEEE Electronics Letters*, 37(5):287–9, 2001.

[70] T. Sørensen, J. Broeng, A. Bjarklev, E. Knudsen, S.E.Barkou Libori, H. Simonsen, and J.R. Jensen. Macrobending loss properties of photonic crystal fibres with different air filling fractions. In *ECOC'2001*, page paper no. We.P.1, 2001.

[71] A. Bjarklev, T.P. Hansen, K. Hougaard, S.E.Barkou. Libori, E. Knudsen, and J. Broeng. Microbending in photonic crystal fibres - an ultimate loss limit? In *ECOC'2001*, page paper no. We.L.2.4.

[72] B.J. Mangan, J. Arriaga, T.A. Birks, J.C. Knight, and P. St.J. Russell. Photonic crystal fibre with a shortwavelength cutoff. *Lasers and Electro-Optics, 2000. (CLEO 2000). Conference on*, pages 606 –607, 2000.

[73] B.J. Mangan, J. Arriaga, T.A. Birks, J.C. Knight, and P.S.J. Russell. Fundamental-mode cutoff in a photonic crystal fiber with a depressed-index core. *Optics Letters*, 26(19):1469–71, 2001.

[74] Jesper. Riishede. Bragg-gratings in photonic crystal fibres. Master's thesis, Research Center COM, Technical University of Denmark, 2002.

[75] J. Broeng, S. E. Barkou, T. Søndergarrd, and A. Bjarklev. Analysis of air-guiding photonic band gap fibers. *Optics Letters*, 2000.

[76] S.E. Barkou, J. Broeng, and A. Bjarklev. Leakage-free, guidance of light in hollow core optical fibers. In *CLEO'2000*, pages 319–320, Paper CWK40, San Francisco, CA, USA, May 7-12 2000.

[77] S.E. Barkou, J. Broeng, and A. Bjarklev. Silica-air photonic crystal fiber design that permits waveguiding by a true photonic bandgap effect. *Optics Letter*, 24(1):46–8, January 1999.

[78] S. Barkou, J. Broeng, and A. Bjarklev. Photonic bandgap fibers. In *LEOS'99*, pages 615–6 Paper WAA1, San Francisco, CA, USA, Nov.8-11 1999.

[79] J. Broeng, T. Søndergaard, S.E. Barkou, P.M. Barbeito, and A. Bjarklev. Waveguidance by the photonic bandgap effect in optical fibres. *J.Opt.A: Pure Appl. Opt.*, 1:477–82, 1999.

[80] A. Bjarklev, J. Broeng, and S.E. Barkou. New developments in photonic crystal fibres. In *NORTHERN OPTICS 2000*, page 31, Uppsala, Sweden, June 6-8, Invited Paper 2000.

[81] J. Broeng, S.E. Barkou, and A. Bjarklev. Waveguiding by the photonic band gap effect. In *19th Topical Meeting of The EOS*, Marseilles, France, Sept 1998.

[82] A. Bjarklev, J. Broeng, S. Barkou, and T. Søndergaard. Fundamenatlly new microstructured fiber waveguides for potential sensor applications. In *LIGHT FOR LIFE 99*, page Paper W4.4, Cancun Q.R., Mexico, July 27-30 1999.

[83] T.W. Berg, A. Bjarklev, J. Broeng, S.E.Barkou. Libori, E. Knudsen, T. Søndergaard, and M.G. Dyndgaard. Polarization properties of honeycomb-structured photonic bandgap fibres. *J.Opt.A: Pure Appl. Opt.*, 2:584–8, 2000.

[84] J. Broeng, D. Mogilevtsev, S.E.Barkou. Libori, A. Bjarklev, and J.R. Jensen. Birefringence in photonic crystal fibers. In *OEEC/IOOC'2001*, pages paper no. TuG–3, Sydney, Australia, July 1-5 2001.

[85] S.E. Barkou, J. Broeng, and A. Bjarklev. Photonic bandgap fibers. In *LEOS'99*, pages 615–6, San Francisco, CA, USA 1999 Invited.

[86] J.B. Nielsen, T. Søndergaard, S.E. Barkou, A. Bjarklev, and J. Broeng. Two-dimensional kagomé photonic bandgap waveguide. *Photonics Technology Letters*, 12(6):630–32, 2000.